Design, Development, and Analysis of a Tactile Display Based on Composite Magnetorheological Elastomers

Ali Alkhalaf

A Thesis

in

The Department

of

Mechanical, Industrial, and Aerospace Engineering

Presented in Partial Fulfillment of the Requirements

for the Degree of

Master of Applied Science (Mechanical Engineering) at

Concordia University

Montréal, Québec, Canada

August 2019

CONCORDIA UNIVERSITY

School of Graduate Studies

This is to certify that the thesis prepared

By: **Ali Alkhalaf**

Entitled: **Design, Development, and Analysis of a Tactile Display Based on Composite Magnetorheological Elastomers**

and submitted in partial fulfillment of the requirements for the degree of

Master of Applied Science (Mechanical Engineering)

complies with the regulations of this University and meets the accepted standards with respect to originality and quality.

Signed by the Final Examining Committee:

______________________________ Chair
Dr. Tsz Ho Kwok

______________________________ External Examiner
Dr. Mojtaba Kahrizi

______________________________ Examiner
Dr. Ramin Sedaghati

______________________________ Supervisor
Dr. Javad Dargahi

Approved by ______________________________
Martin D. Pugh, Chair
Department of Mechanical, Industrial, and Aerospace Engineering

__________ 2019 __________
Amir Asif, Dean
Faculty of Engineering and Computer Science

Abstract

Design, Development, and Analysis of a Tactile Display Based on Composite Magnetorheological Elastomers

Ali Alkhalaf

In minimally invasive surgery, surgeons carry out the operations by employing small tools and viewing equipment into the patient's body by means of small incisions. In manual and robotic minimally invasive surgery, surgeons do not have direct touch and natural sense of touch, due to utilization of long and often flexible instruments, and palpation is a necessity to provide perfect diagnoses. As a potential candidate, magnetorheological elastomers were investigated as a stiffness display for surgical application. To this end, three different samples of magnetorheological elastomers with various volume fraction of iron particles and one non-MRE rubber sample were fabricated. Six composite MREs were made by combining two layers of different fabricated samples. The samples were characterized under compression test and perpendicular to the applied magnetic field (MF). The compression test was carried out with the strain range of $(5 - 25\%)$ at magnetic field densities of 0, 143, 162, 198, 238, 287, 365 mT. It was observed that the elastic modulus of one-layered MREs and bi-layered MREs increase with increasing the magnetic fields. Moreover, MR-effect was enhanced via bi-layer composition, e.g. mono-layered 45%vol iron particles: 211% , bi-layered 45%vol iron particles: 253%. Afterward, a solution for the medical need of the tactile display during minimally invasive surgeries was proposed. To this end, a tactile display based on the composite magnetorheological elastomers, *MiTouch* , was designed and prototyped. Also, the electromechanical parameters of *MiTouch* were identified through a transfer function optimization and a PID controller was fine-tuned to achieve a desired stiffness. Later, validation experiments were carried out to showcase the feasibility of *MiTouch* for pulse examinations and maintaining a desired stiffness. The results revealed that *MiTouch* applied a pulsed contact force of 0.6N to the phantom finger. The results were within the range of reported pulse examination forces, i.e. 0.5-2N. In addition, the system was capable of following a desired stiffness of $4 N/mm$ and maintaining it within a range of $4.07 \pm 0.41 N/mm$. In the end, results confirmed the hypothesis of the feasibility of the suggested solution for surgical applications.

This thesis is dedicated to my parents Mahdi Alkhalaf and Fatima Alquaism as well as my beloved wife and daughters, Sukyna Alkhalifa, Zainab Alkhalaf, and Maria Alkhalaf for their endless love, support, and encouragement

Acknowledgments

I would like to express my intense gratitude to my supervisor Professor Javad Dargahi for his constant support and critical supervision.

I would also take the opportunity to thank my mentor at our Robotic Surgery Lab, Mr. Amir Hooshiar, for his precious and valuable advice and guidance through my research work. My thanks go to all my lab-mates: Naghmeh Bandari, Amir Molaei, Mohammad Jolaei, Masoud Razban, Majid Roshanfar, Saman Namvarrechi, Hamid Reza Nourani, and Nima Amooye for their motivation and support.

Warm and heartfelt gratitude goes to my brother, Mr. Abdullah Alkhalaf who endlessly supported me in all the stages of master's studies. I would also extend the gratitude to all my brothers and sisters. No words can express my love to my family.

Last, but not least, special sincere thanks go to my friends: Mr. Ibrahim Alhaji and Mr. Mesfer Alkhathami who persistently were by my side during my studies. Truly, I could not have had better friends.

Contents

List of Figures

List of Tables

Chapter 1

Introduction and Problem Definition

1.1 Introduction

Open surgeries, where surgeons make large incisions in patients, are gradually evanescing since the invention of minimally invasive surgeries (MISs) [1, 2]. Minimally invasive technologies allow surgeons to carry out the operations by employing small tools and viewing equipment into the patient's body by means of very small incisions. Moreover, MIS is also reducing the time stay at hospitals and the healing time because of the small cuts [3, 4]. The MIS is further developed by the implementation of robots, which is known as a robotic minimally invasive surgery (RMIS). Surgeons remotely utilize robots to perform the surgery and to precisely operate the slender instruments and cameras into the body through small holes [1]. With all these advantages of MIS and RMIS, there is still a gap that needs to be filled. During MIS and RMIS, surgeons are missing the sense of touch, which is a very important aspect to make the right diagnosis.

Researchers have made a tremendous effort to alleviate the loss of palpation and sense of touch by developing a tactile display, which is simply known as a physical structure with the utility of adjustable stiffness that can mimic the softness of biological tissues during MIS or RMIS. Although the concept of the tactile display is the same in all the available studies, different structures and various materials have been investigated. For instance, distinct approaches have been suggested for tactile displays like the use of magnetorheological fluids (MRF), DC motors, and pneumatic balloons.

This research work focuses on designing, developing, and analyzing of a composite magnetorheological elastomers-based tactile display. Based on the author's knowledge, this is the first time to investigate MREs to be based for tactile display devices. Moreover, this is the maiden attempt to investigate multi-layer MREs in compression with a horizontal applied magnetic field.

The first objective of this research is to compensate the lost MR effect caused by non-parallel magnetic field with compression test. For this approach, ten different samples were fabricated including: a non-MRE rubber sample, three mono-layered MREs that have different volume fraction of iron particles, three bi-layered MRE-MRE samples that have two layers of MREs with different contents of iron particles, and three bi-layered MRE-non-MRE samples that are constructed from one layer of MRE with another layer of non-MRE rubber. All the ten samples were experienced a quasi-static compression test with varying magnetic field. The results were analyzed to calculate the MR effect of both mono-layered and bi-layered samples. Later, a comparison between the elastic moduli of human tissues and the best MRE candidate to resemble the elastic modulus was demonstrated.

The second objective of this dissertation is to suggest a solution for stiffness display during minimally invasive surgeries. The steps for this objective started by designing and developing a tactile display system. Then, the sample that demonstrated high magnetorheological effect during the first objective experiments was selected for the proposed tactile display. After that, electromechanical parameters were identified by the utilization of a transfer function optimization. Then, a PID controller was suggested to follow a desired stiffness. At the end, the validity of the proposed tactile system was examined by validation experiments.

In this chapter, a review of the application of tactile display is presented in section 1.2, followed by methods of fabricating magnetorheological elastomers in section 1.3. Later in section 1.4, a study concerning the characterization of MREs is demonstrated. Finally, the research objective and dissertation layouts are demonstrated in sections 1.5 and 1.6, respectively.

1.2 Review of Recent Softness Display Devices and Their Feasibility in Minimally Invasive Surgeries

Beside sight and hearing, sense of palpation is a very important feature for the human interaction with computers. It enables the computer users to feel and recognize the softness of a projected material. In minimally invasive surgeries, surgeons are missing this precious sense of touch, which could lead to a misevaluation of the exact disease. Researchers have spent the time and effort to come up with a softness display device that can provide surgeons with the softness of human tissues. They have utilized different ways to build softness display devices in particular for minimally invasive surgeries. In the following subsections, five different types of tactile displays are discussed based on their working principle. In addition, at the end of each type, a statement about the feasibility of using that particular type of tactile display in minimally invasive surgeries is provided.

1.2.1 Rheological fluid softness displays

The Rheological fluids are classified into two groups, magneto-rheological fluid (MRF) and electrorheological fluid (ERF). MRFs are composited of micro-ferromagnetic particles suspended in a fluid like oils[5, 6, 7, 8], while ERFs are constructed from very tiny electro-active particles (0.1 - 100 μm in size) immersed in insulating fluids [9, 10]. Both groups have the same working concept, which is changing its physical state from Newtonian fluids to semi-solid or gel in a fraction of seconds upon the existence of an external magnetic field for MRFs and electrical field for ERFs. In the coming subsections, a brief example of both type is discussed.

1.2.1.1 Magnetorheological Fluid

A recent study by Seung-Woo Cha *et al.* implemented the use of MRF in a sponge. In their study, the tactile display device based on MRF and a sponge is designed and created to recognize the softness of human-like tissues that can be used in robot-assisted minimally invasive surgeries. They fabricated 3 samples to reproduce the softness of porcine heart, liver, and lung. The MRF sponge sample was placed on an electro magnet, which provides the magnetic field through the sample, and below an ATI 6-axis force sensor as presented in the experimental setup shown in Figure 1.1. The displacement was measured using the laser sensor positioned above the moving arm holding the end-effector with force sensor. The test was carried out in a quasi-static process. The porcine tissues were also tested under the same procedure. Consequently, the force and displacement curves for both the MRF sponge and porcine tissues were compared. A model was generated to predict the force displacement behavior of the MRF sponge, which was then compared to the measured data. The authors of this study concluded that MRF sponge can reproduce the softness of targeted materials like human tissues [11]. More studies about using magnetorheological fluid in haptic feedback devices can be found in [12, 13].

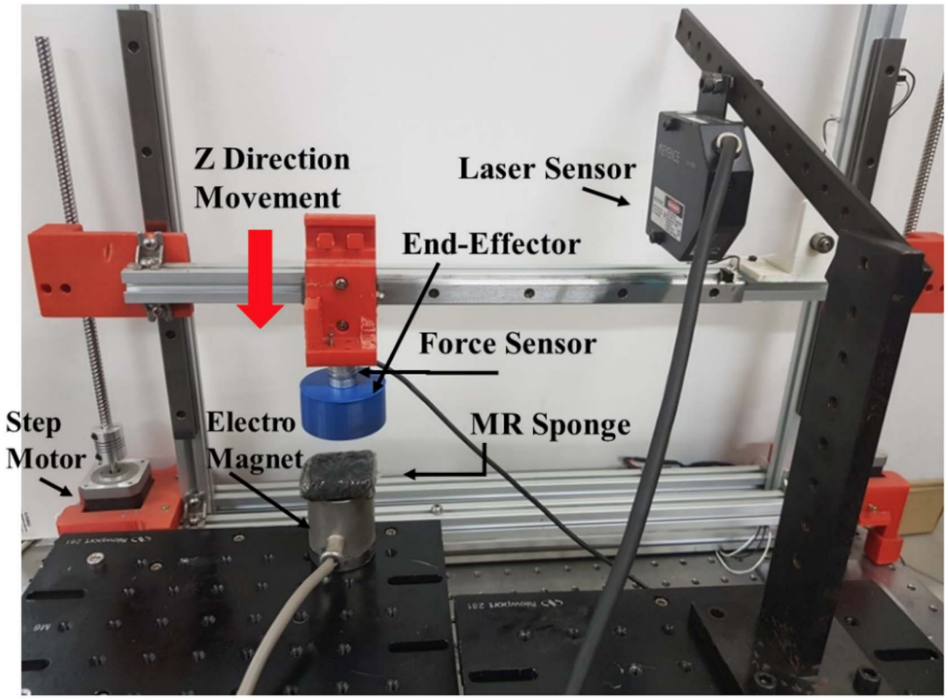

Figure 1.1: Magnetorheological foam tactile display [11]

1.2.1.2 Electrorheological Fluid

Figure 1.2 illustrates the working principle for a study done by Alex Mazursky *et al.* [14] on using ERFs in tactile display actuator. Once the user pushes down the actuator, it forces the ERF to flow out to the two-sided chambers that moves the two thin silicone membranes up. Upon the release of the pressure created by the user, the two membranes push down the ERF to go back to the equilibrium level. They controlled the flow of ERF using two sets of electrodes as shown in Figure 1.2. The components of the actuator are presented in Figure 1.3 and they are a plastic cover, one silicone membrane, one plastic spacer and O-ring, a high voltage printed circuit board (HV PCB), and grounding printed circuit board (GND PCB). Figure 1.4 demonstrates the experimental setup for the study, in which they used a voltage amplifier, a function generator, oscilloscope, RSA3 Ta instrument, and a computer. The authors calculated the force-depth relationship under variable loading frequency and input voltage. Then, they compared the result with the data given from a mathematical model. They concluded that ERFs could generate a range of softness and can be used in haptic feedback applications [14].

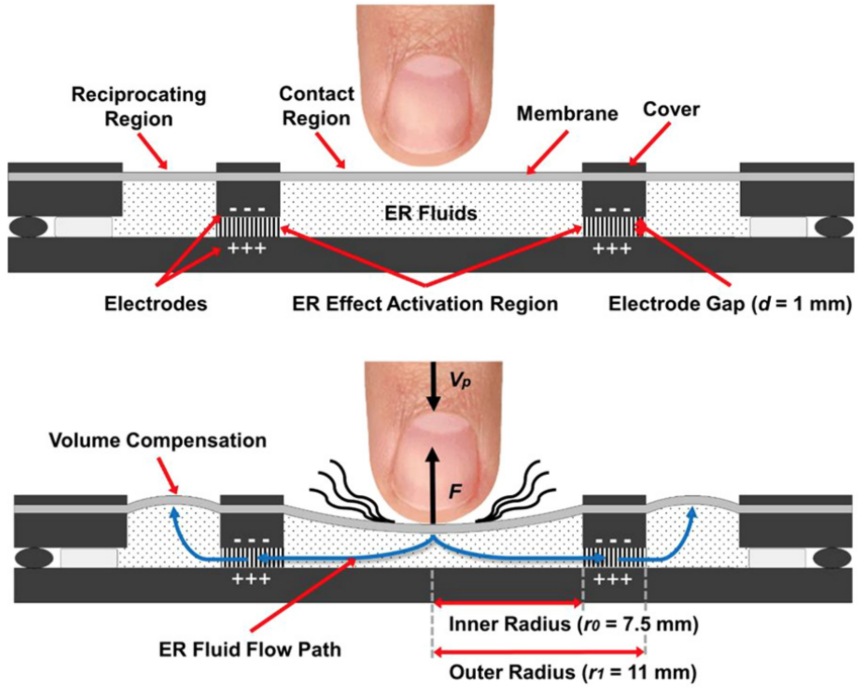

Figure 1.2: Electrorheological fluid tactile display [14]

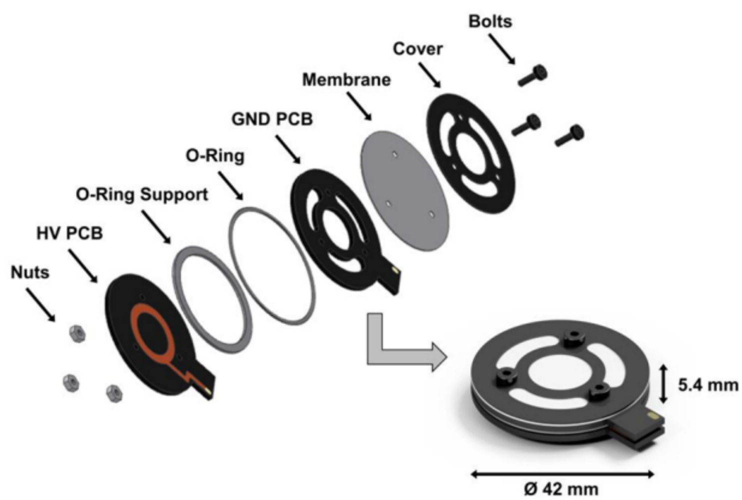

Figure 1.3: Components of ERF actuator proposed by [14]

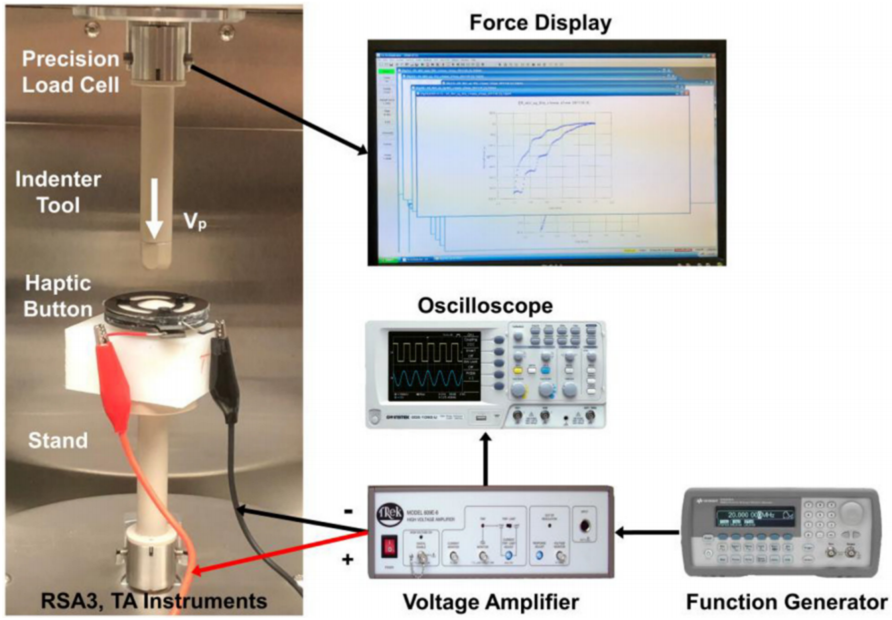

Figure 1.4: Experimental setup of ERF tactile display actuator designed by [14]

The downsides of using rheological fluids in softness displays and especially in the operating room (OR) for MIS can be listed as follows. One of them is that these are fluids that are considered hazardous substances in the OR since they might be spilled out from their devices. Moreover, suspended particles might tend to get complete settlement in time [9]. One more point that is particularly for ERFs, these fluids are driven by electromagnetic field that could affect other electronic devices available in the operating theater.

1.2.2 Shape memory alloy (SMA) tactile displays

SMAs are simply alloys that can be shaped while they are cold and once they are heated, the SMAs return to its original shape [15]. It was shown in literature that SMAs demonstrate hysteresis cycles during the transformation process [16, 17]. An example of tactile display actuator based on SMAs is studied by Parris S. Wellman *et al.* [18] and demonstrated in Figure 1.5. They utilized a V-shaped SMA wire to actuate a single pin that can be touched by a person. The SMA wire was heated beyond its transition temperature by supplying electrical current and cooled down using water. The authors concluded that this SMA tactile display has some level of difficulty to perceive the curvature of the pin line during sweeping the user's finger on the line. However, the curvature along the line was easily perceived.

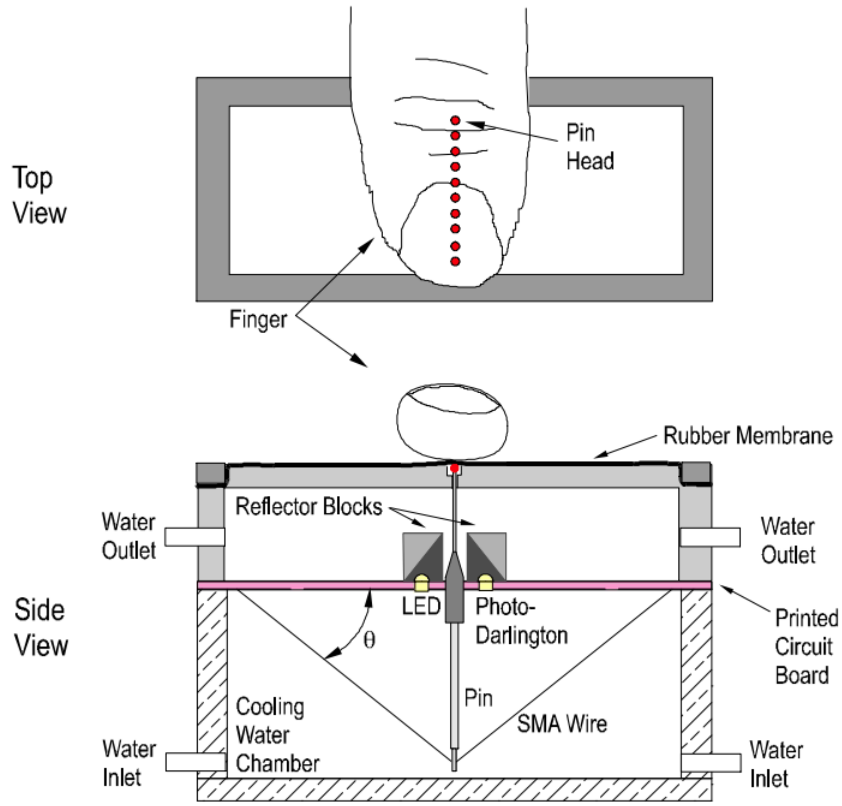

Figure 1.5: Shape memory alloy tactile display suggested by [18]

The negative side about SMAs is that the dynamic range is very low, which shortens the range of softness that can SMAs reproduce. Furthermore, SMAs could take a long period of time to get cold [9].

1.2.3 DC motor tactile display

Alternative way to replicate the softness of materials is to use DC motors. Fuminobu Kimura *et al.* [19] have focused on creating 2-DOF softness display by using 2 DC motors to control the contact area between a human finger and a sheet. A schematic diagram in Figure 1.6. delineates their proposed 2-DOF softness display. The two DC motors were attached to flexible sheet at one end and to laser displacement sensors at the other end as shown in Figure 1.6. Using a force sensor placed underneath the Acryl stage, the force applied by human finger was measured. The over all operational principle is depicted in Figure 1.7. When a user pushes down the sheet, the sensed force goes to a voice-coil motor (VCM) that presses an object. Cameras were utilized to calculate the contact width. Consequently, the measured widths are transmitted to the softness controller.

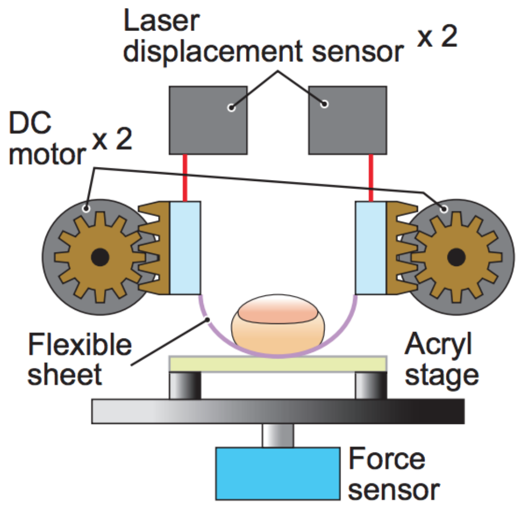

Figure 1.6: A schematic illustration of the propsed 2-DOF softness display by [19]

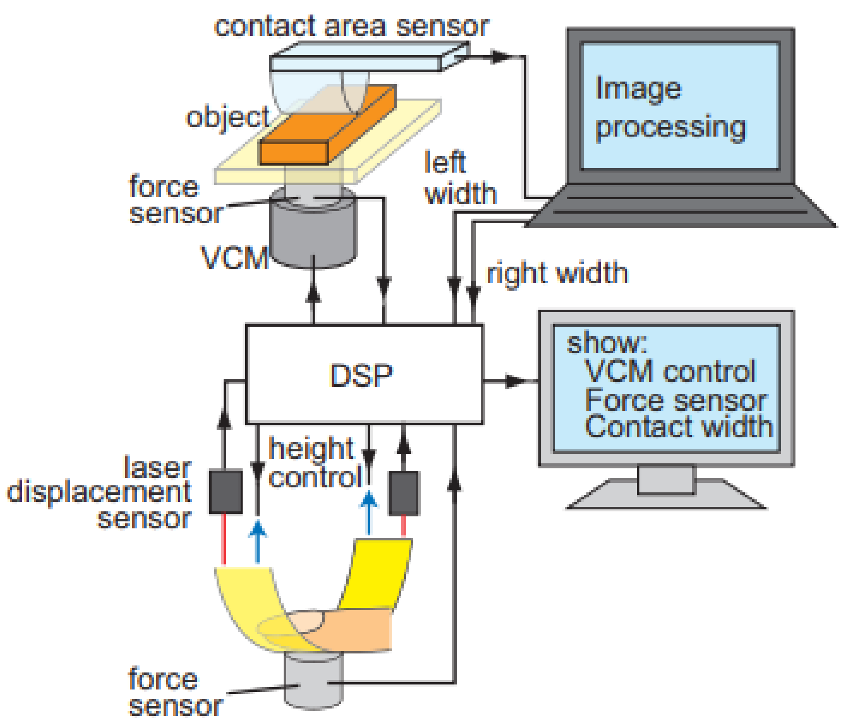

Figure 1.7: A prototype of the 2-DOF softness display by [19]

Using the laser displacement sensors, the heights at the two sides of the sheet were calculated. After that, these heights were modified using a PID controller to insure that both the contact width between the finger and the sheet and the measured widths provided by the cameras are equivalent.

The authors claimed that this 2-DOF softness display is feasible by adjusting both the contact area and contact force. Other DC motor softness display can be found in [20].

There are some disadvantages of using DC motors in softness display inside the OR. For instance, the DC motors need cables to operate and the operating room should be cleared from cables to provide more rooms to physicians to move. In addition, according to Kinya Fujita and Hisayuki Ohmori, although using DC motors for a softness display is applicable, it does not provide the exact softness of a required material, which could lead to a major misdiagnosis by physicians.

1.2.4 Pneumatic tactile display

Several studies have investigated pneumatic balloon based systems for tactile feedback applications [21, 22]. Martin Culjat *et al.* have designed an actuator of 3 mm balloons that can be used in pneumatic balloon tactile display. Authors intended to use three stages for the pneumatic tactile feedback including sensors mounted on graspers, a control system, and actuator placed on the master controls. The sensors send the measured force to the control system that transforms these signals into the actuators and subsequently to the pneumatic balloons as demonstrated in Figure 1.8.

The actuator is composed of pneumatic channels, which are made from polydimethylsiloxane (PDMS), and a thin silicone film. The design of the pneumatic balloon actuator is presented in an array of 3 x 2 as captured in Figure 1.9, and has the dimensions of 1.0 cm x 1.8 cm x 0.4 cm. A pressure regulator was employed to control the pressure inside the balloons based on the information received from the control system. By controlling the pressure inside the balloons, a desired softness can be felt by surgeons. Martin Culjat *et al.* claimed that this tactile display is very effective for providing tactile sensations to the surgeon's fingers [21].

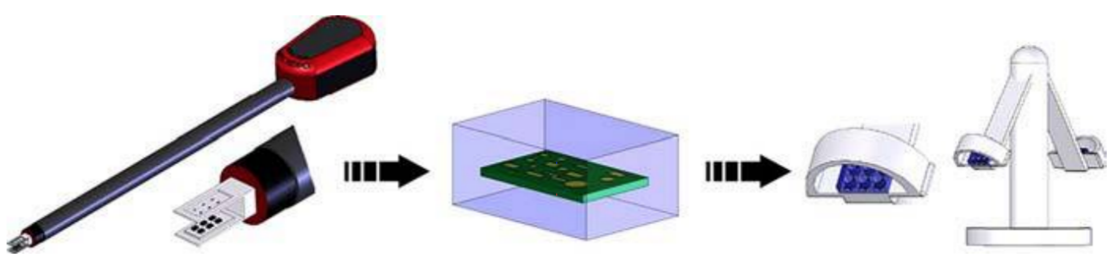

Note: The control system translates the sensed force from the robotic grasper into proportional inflation pressures provided to the fingers

Figure 1.8: Conceptual demonstration of pneumatic ballons tactile display [21]

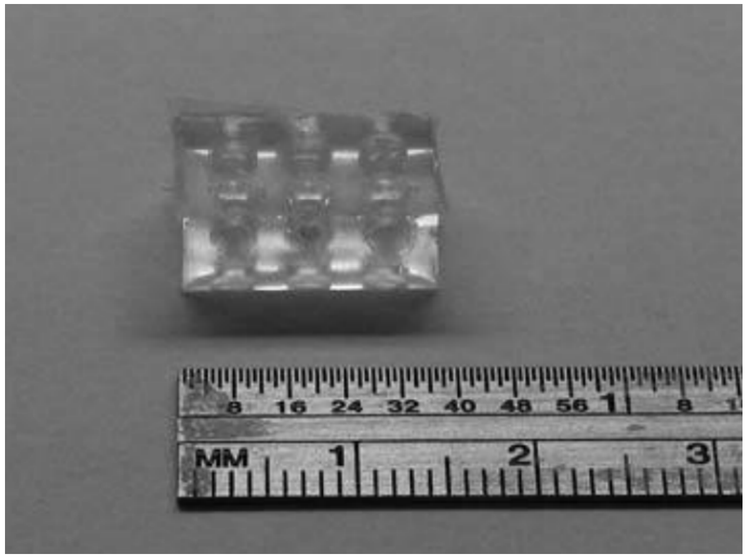

(a)

(b)

Figure 1.9: Pneumatic balloons tactile display [21]

Softness displays based on pneumatic balloons are not suitable for minimally invasive surgeries because of their high power consumption. In addition, the response time is very high, which could increase the time of the minimally invasive surgeries.

1.2.5 Electro-active polymers (EAPs)

Electro-active polymers are materials that change their sizes or shapes upon the exposure to an electric field [23]. A tactile display based on electro-active polymers was studied by Amy Kyungwon Han *et al.* in 2018 [24]. They considered multilayer EAP films to display softness to fingertips. Figure 1.10 illustrates the six layers and dimensions for the proposed EAPs actuators for tactile displays. Next Figure 1.11 shows the EAP actuator connected to a muscle lever though a lever arm, in which force and displacement are measured in part (A), and part (B) presents the EAP actuator attached to a load cell by means of a compression spring to predict the behavior once it is pressed by fingertips. Amy Kyungwon Han *et al.* concluded that the tactile display is capable of providing more than 98% similar softness of targeted materials [24].

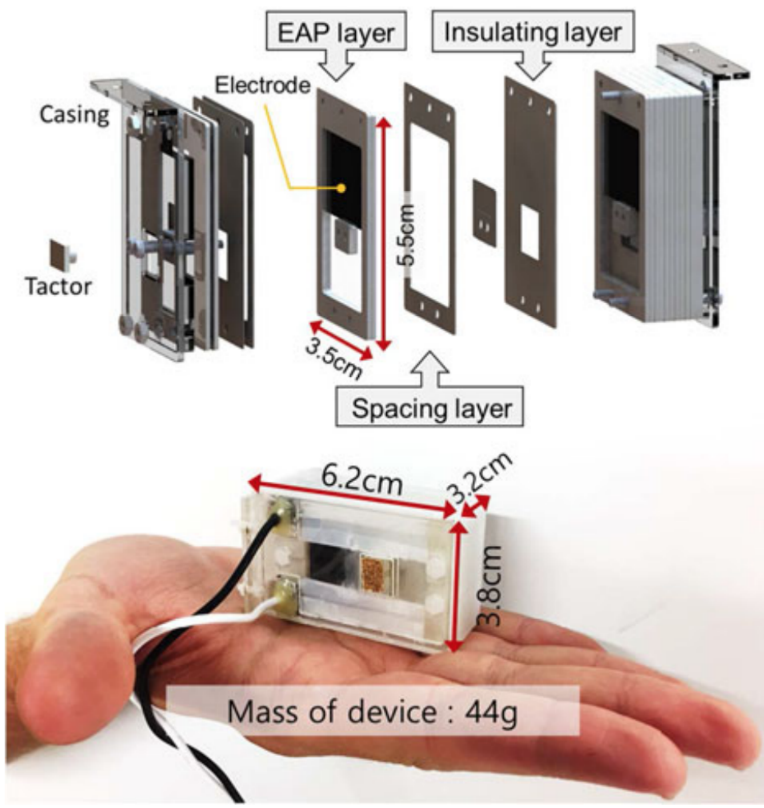

Figure 1.10: Dimensions of six-layer EAP actuators compared to a human hand [24]

Just like the tactile displays based on DC-motors, EAPs have very limited range of stiffness. Moreover, EAPs are also similar to the ERFs in terms of dependency on an electrical field; therefore, they could damage electronic devices in the operating room.

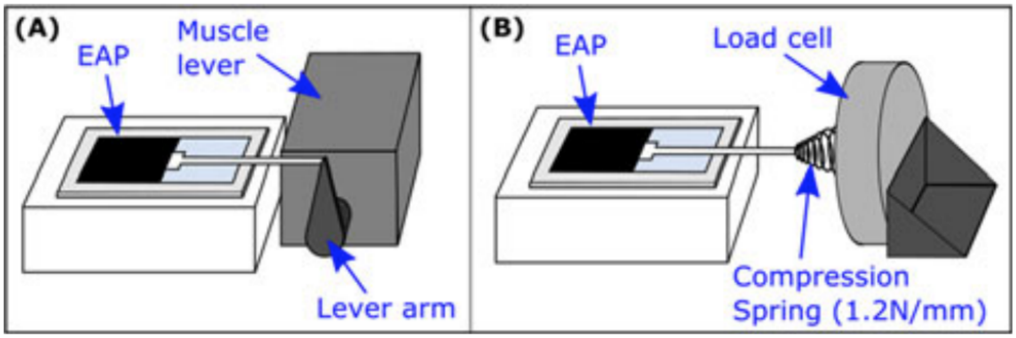

Figure 1.11: Testing apparatus. (A) EAP actuator is attached to a muscle lever (B) EAP actuator is attached to a compression coil spring and a load cell [24]

1.3 Fabrication of Magneto-Rheological Elastomer

Magnetorheological elastomers, simply – MREs, are magneto-sensitive materials that regulate their mechanical properties in a fraction of seconds once they are presented in a region around a magnetic material [25, 26]. Due to this great feature of MREs, they have attracted many researchers to employ them in a wide range of engineering applications like adaptive noise canceling, vibration neutralizer, and automobile suspensions [27]. Magnetorheological elastomers are mainly made from an elastomeric medium, like silicone rubber and ferromagnetic particles. Some studies have suggested the use of additive materials, such as silicone oil and silicone thinner to enhance the mechanical properties of MREs [25, 28].

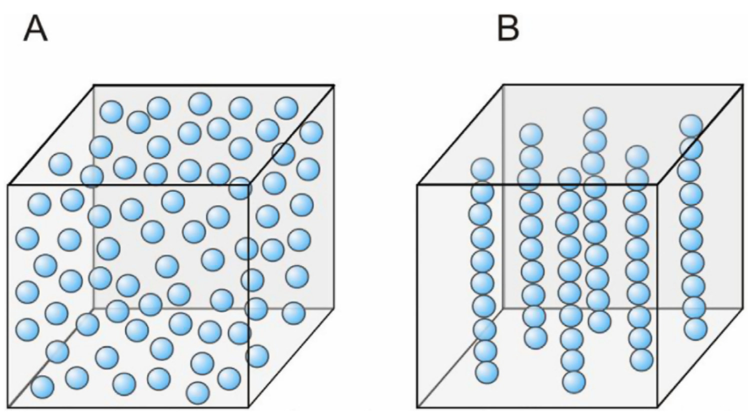

Figure 1.12: A schematic illustration of the alignment of iron particles for (A) isotropic MREs (B) anisotropic MREs [29]

There are two types of MREs based on their fabrication process [29]. The first type is known as isotropic MREs that is when the fabrication of MRE samples is completed away from any external magnetic field, which causes the iron particles to scattered though the rubber medium as seen in the schematic Figure 1.12 (A). On the other hand, anisotropic MREs are those MREs in which there was a magnetic field applied directly on the molds casing the MRE samples during the production time that causes the iron particles to align themselves in the direction of the applied magnetic field, which can be seen in Figure 1.12 (B). Owing to the alignment of iron particles inside the anisotropic MREs, the mechanical properties measured in the aligned direction are stronger and tougher from the ones calculated in the direction with no magnetic field applied. On the other hand, the random distribution of ferromagnetic particles in isotropic MREs causes no difference for the calculation of the mechanical properties in any direction, i.e., in X-axis, Y-axis, and Z-axis [30]. Based on the literature review, researchers have fabricated MREs considering different factors like changing rubber matrix, supplementary materials, size of iron particles and type of MRE. However, they all follow the same fabrication process for either isotropic MREs or anisotropic MREs. Researchers start by preparing the aimed amounts of rubbers and carbonyl iron particles (CIPs) with or without additive materials. It is recommended to start by stirring well each ingredient. Once the aimed amounts are ready, if there are some additive substances like slackers, silicone thinners, or silicone oils, they are poured on the rubber material and mixed until the solution gets a complete homogeneity. After that, the CIPs are added to the homogeneous mixture and stirred for about 5 minutes. It is highly suggested to place the solution in a vacuum chamber for around 5 minutes to degas the air bubbles and get clear MRE samples. Consequently, the MRE samples are exposed to magnetic field for regular alignment of iron particles or placed away from the magnetic field for irregular alignment. To reduce the curing time, MRE samples are heated in an oven for more than 100°C. Table 1.1 summarizes some of the available studies for fabricated MREs considering the aforementioned factors.

Table 1.1: Summary of the literature review of MREs

Author	Rubber matrix	Additives contents	Iron Particles	Type of MRE
Sapouna *et al.* [30]	SR 70%wt.	-	Small particles (4-6μm) Large particles (<220 μm) 30 %wt.**	Iso. and Aniso.
Deng *et al.* [28]	SR	silicone oil	CIP (3 - 5 μm) 70%vol.*	Aniso.
Chen *et al.* [31]	NR and SR	Dimethyl-silicon oil, vaseline, and paraffine	CIP (3, 6, and 11 μm) 60%wt., 70%wt., 80%wt., and 90%wt.	Aniso.
Bica *et al.* [32]	SR 60%vol.	-	CIP (4.5 - 5.4 μm) 40%vol.	Iso.
Boczkowska *et al.* [33]	PUG	-	CIP (6-9 μm) 11.5%vol. and 33%vol.	Aniso.
Bose *et al.* [34]	SR 70%vol.	-	CIP (5 μm) 30%vol.	Iso. and Aniso.
Hu *et al.* [35]	SR 20%wt.	Silicone oil 10%wt.	CIP (4.5 - 5.2 μm) 70%wt.	Iso.
Norouzi *et al.* [36]	SR	Silicone oil 10%wt.	CIP (3 - 5 μm) 70%wt.	Iso.
Song *et al.* [37]	NR and TPE	Stearic acid Zinc oxide	CIP (3 - 4μm) 60%wt.	Iso.
Yang *et al.* [38]	NR	-	CIP (3μm)	Aniso.
Dargahi *et al.* [25]	SR	Silicone thinner 10%vol. Slacker 10, 15, and 20 %vol.	CIP (3.9 - 5μm) 12.5%vol., 17.5%vol., 25%vol., 30%vol. and 40%vol.	Iso.
Ngoc Thien Lai [29]	NR	Paraffin oil 1.0%wt. Zinc oxide 5%wt.	CIP (4 μm)70%wt.	Iso. and Aniso.
	* : percent of volume, ** : percent of weight.	Iso. : Isotropic Aniso. : Anisotropic	SR : Silicone rubber TPE : Theromplastic elastomer	NR : Natural rubber PUG : Polyurethane gel

1.4 Characterization of Magneto-Rheological Elastomer

In this section, the characterization of MREs is divided in two groups; one is characterization in compression mode, and the other is characterization in shear mode.

1.4.1 Characterization in Compression Mode

Some studies characterized MREs under compression test. Sapouna *et al.* [30] measured the MR effect of single layer of MREs and composite MREs. The composite MREs have two layers of MREs that can be two isotropic MRE layers, two anisotropic MRE layers, or one anisotropic with isotropic MRE layers in series and parallel configurations as depicted in Figure 1.13. The MRE samples have 70% per weight silicone rubber and 30% per weight CIPs. Two sizes of CIPs were equipped in the study, small that is $4-6\mu m$ and large that is $< 220\mu m$. The MRE samples were placed between two aluminum plates for the zero magnetic field and between two magnets for the magnetic field density of 0.5 T.

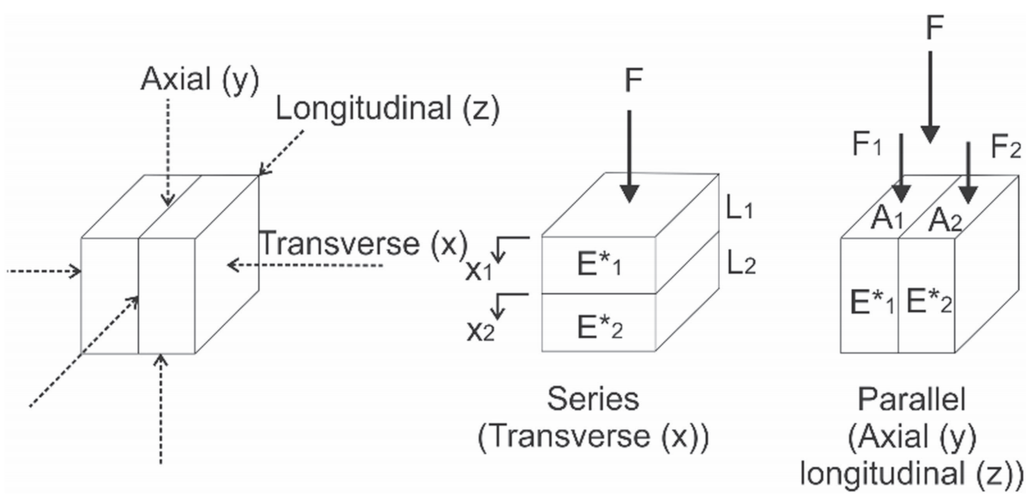

Figure 1.13: Series and Parallel alignments of composite MREs; $E_1^*, E_2^*, x_1, x_2, F_1, F_2, A_1$, and A_2 are the elastic modulus of layer 1, elastic modulus of layer 2, displacement of of layer 1, displacement of of layer 2, force on layer 1, force on layer 2, area of layer 1, and area of layer 2 respectively [30]

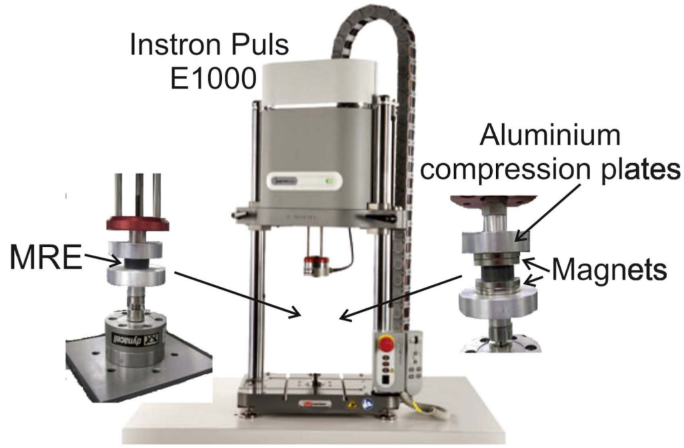

Figure 1.14: Experimental setup for compression test [30]

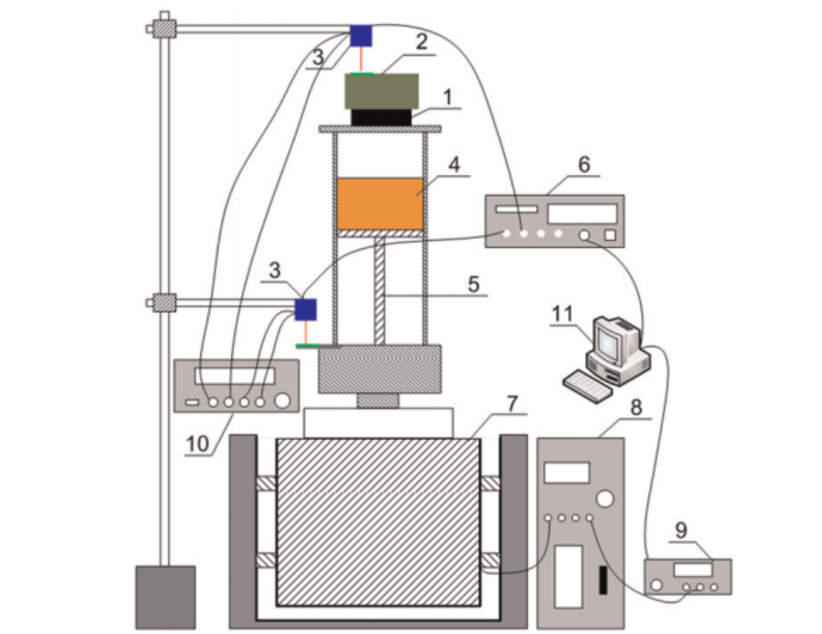

1. MRE 2. Mass 3. Laser displacement sensor 4. NdFeB permanent-magnet
5. Guide rails 6. Data acquisition instrument 7. Electromagnetic vibration table
8. Power amplifier 9. Controller 10. Agilent power 11. Computer

Figure 1.15: A schematic diagram of the compression test setup by Yang *et al.* [39]

The researchers utilized the Instron Puls E1000 for the compression test. Figure 1.14 demonstrates the experimental setup including the equipped machine and MRE samples with and without the magnets. The authors tested the samples under a small range of strain amplitude 0.0% - 1.5% and at two magnetic field densities, 0.0 T and 0.5 T. They investigated the mechanical properties in the axial, transverse and longitudinal directions as shown in Figure 1.13. They concluded that the composite MREs have higher magnetorheological (MR) effect compared to single layer MREs. They also found that isotropic MRE samples with small and large iron particles have almost the same dynamic properties at 0.0 T with some minor changes in the MR effect. On the other hand, anisotropic MREs containing large CIPs get stiffer and have higher MR effect compared to their equivalent samples with small CIPs. Yang *et al.* [39] characterized the MRE in compression mode and their schematic diagram and test arrangement are illustrated in Figure 1.15 and 1.16, respectively. They prepared two MRE samples with dimensions 62.8 mm x 4 mm x 4 mm and ϕ 20 mm x 4 mm. As shown in Figure 1.15, the MRE sample, labeled as (1), was situated between a mass, labeled as (2) and a permanent magnet, labeled as (4). The mass was attached to a displacement sensor to measure the displacement and consequently the strain. The compression test was carried out with a strain amplitude of about 0.025%, frequency of 30 Hz, and magnetic field densities from 0.0 mT up to 500 mT.

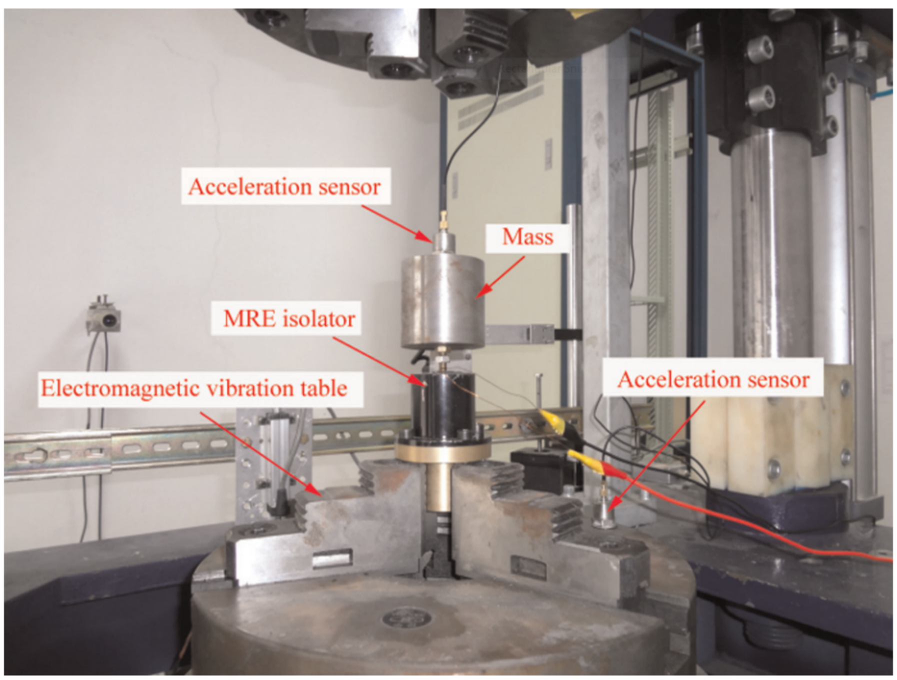

Figure 1.16: Compression test arrangement by Yang *et al.* [39]

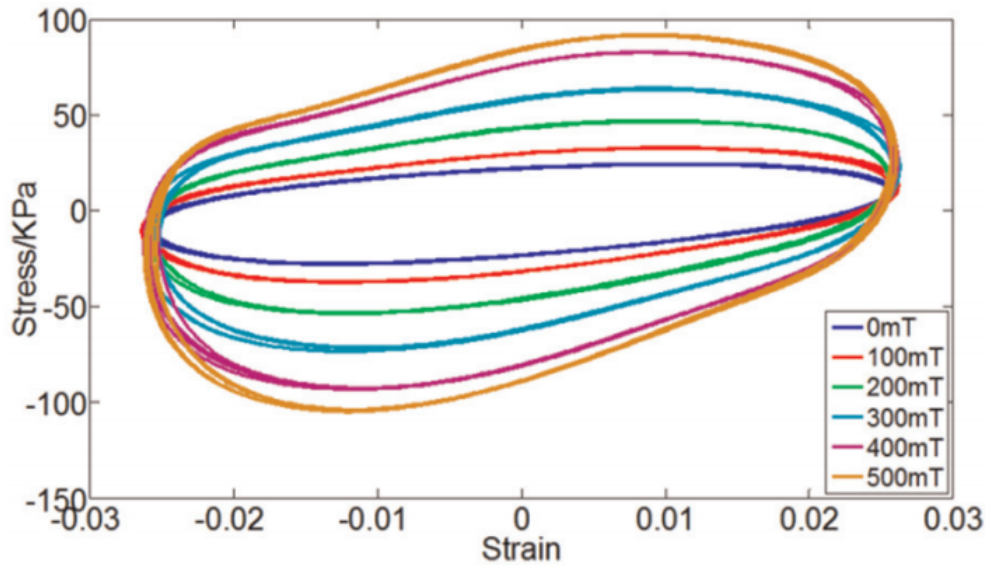

Figure 1.17: Stress-strain relationships of MREs at 6 different magnetic field intensities done by [39].

The results of the stress strain behavior is depicted in Figure 1.17. It is apparent from the results that the hysteresis of MREs increases by raising the magnetic field density. The author concluded that the MR effect could reach up to 200% with a magnetic field below 500 mT. They also found that the zero field elastic modulus increases from 1.5 MPa to 3.05 MPa at 500 mT.

1.4.2 Characterization in Shear Mode

Dargahi *et al.* [25] characterized MRE samples in sandwich shear test with an external magnetic field generated by two sets of three permanent magnets as shown in Figure 1.18. In their study, they fabricated different types of MREs with varying CIPs and additives. The volume fraction of silicone rubber was selected from 40% to 87.5% corresponding to the volume fraction of CIPs from 40% to 12.5%. The selected additive materials were silicone thinner that had a volume fraction of 10% and slacker that had a varying volume fraction from 10% to 20%. In their shear test, they calculated the MR effect of MRE samples with the dimension of 25 mm x 20 mm x 5 mm by employing different magnetic field up to 450 mT, strain amplitudes from 2.5% to 20%, and frequencies between 0.1 Hz and 50 Hz.

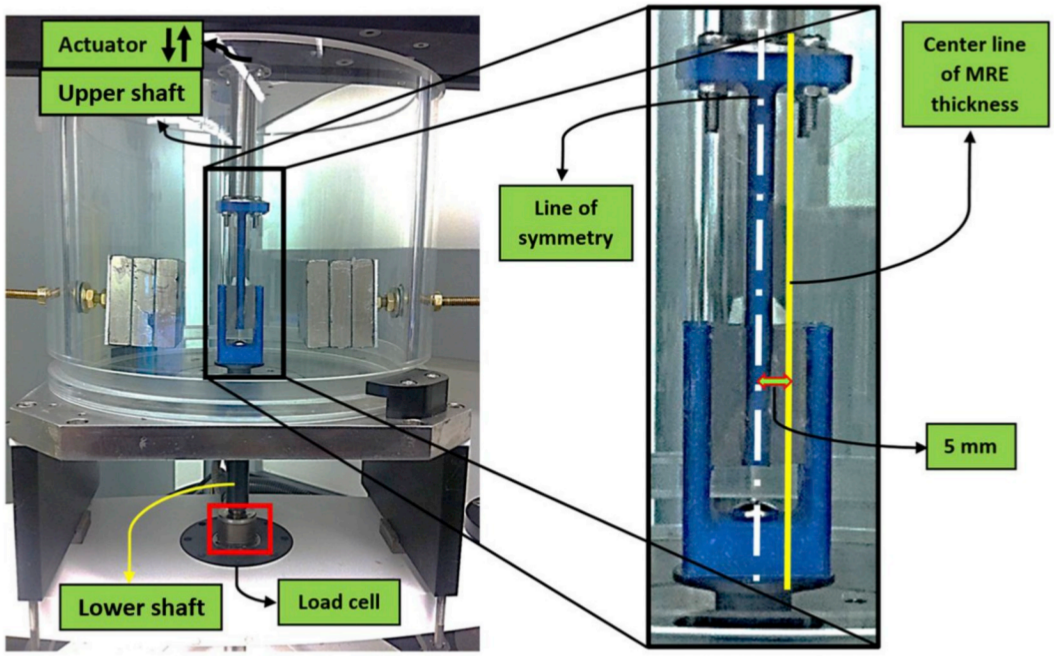

Figure 1.18: Experimental layout of MRE in shear created by Dargahi *et al.* [25]

The stress-strain curves of MRE that has 40% volume fraction of CIPs at 450 mT and different frequencies is demonstrated in Figure 1.19. The curves for other types of MREs and different loading conditions can be found in [25]. It is clear in Figure 1.19 that MREs have different hysteresis loops with distinct loading frequencies. The authors illustrated that the use of additive materials enhances the MR effect. In addition, the results demonstrated that the MR effect is dependent on the strain rate and strain amplitude. They also found out that the MRE with 40%vol of iron particles revealed a considerable MR effect of 555% at 450 mT, related to an increase of 1672% in the shear modulus.

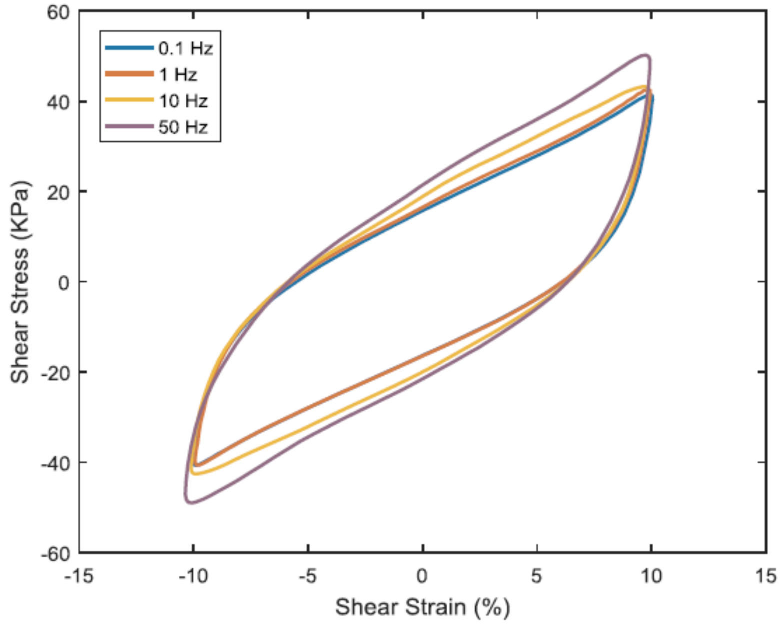

Figure 1.19: Shear stress versus shear strain for MRE with 40%vol iron particles at 450 mT don by Dargahi *et al.* [25]

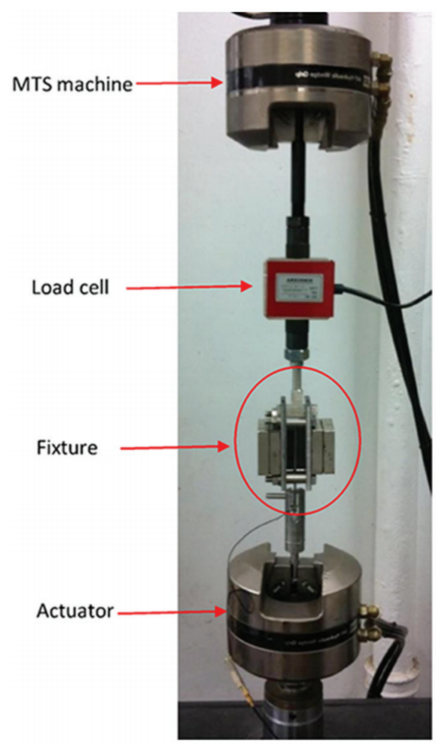

Figure 1.20: A double lap shear test of MRE suggested by Norouzi *et al.* [36]

Another shear test on MRE was carried out by Norouzi *et al.* [36] during which they use 50 mm x 12 mm x 9.5mm isotropic MRE samples. The MRE consisted of 70% CIPs, 20% silicone rubber, and 10% silicone oil, in which all percentages were calculated in weight fraction. The diameter of CIPs is between 3 μm and 5 μm. The authors conducted their research with a servo-hydraulic machine that can be seen in Figure 1.20. The MRE sample was placed between two steel plates and permanent magnets that can magnetically saturate the MRE samples during the shear test. They considered the range of strain amplitudes between 2% to 16% and a wide set of frequencies starting by 0.1 Hz to 8 Hz. The applied magnetic field varies from 100 mT to 272 mT. The output-input relationship of MRE at 16% strain amplitude and different frequencies is demonstrated in Figure 1.21 (a) for 0 mT and Figure 1.21 (b) for 272 mT. It is evident from Figure 1.21 that area and the slope of the hysteresis curves are raised up dramatically by magnifying both the loading frequency and magnetic field intensity, i.e., the shear modulus has a dependency on magnetic field intensity and loading frequency.

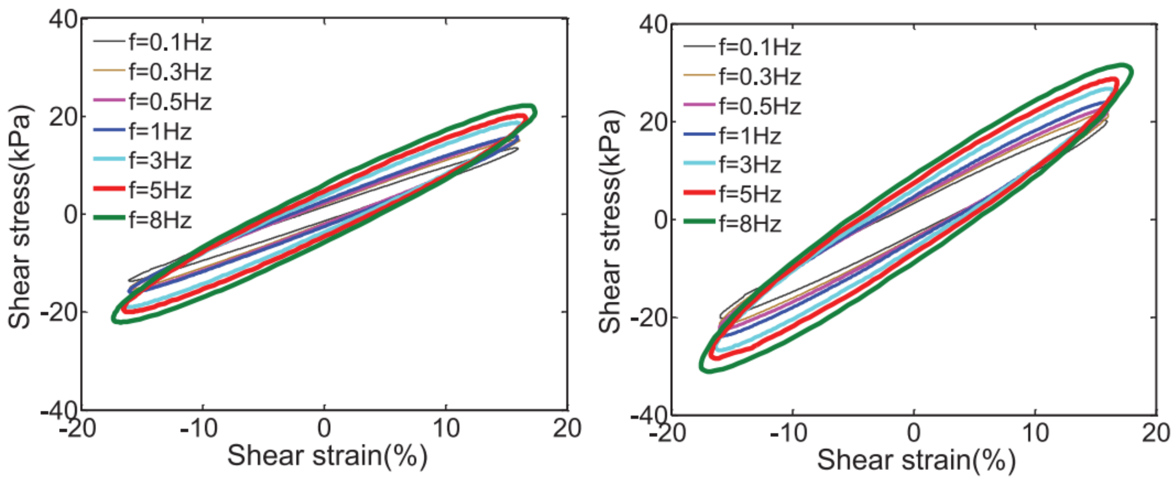

(a) (b)

Figure 1.21: Stress-strain relationship of MRE at 16% strain amplitudes and (a) 0 mT, (b) 272 mT done by [36]

1.5 Research objectives

The long-term objective of the dissertation research is to present a tactile display based on composite magneto-rheological elastomers. The short-term objectives of the study can be listed as follows:

(i) Fabricate mono-layered and bi-layered MREs with different ingredients of iron particles using a dependable process.

(ii) Characterize the output-input response of the mono-layered and bi-layered MREs under a compression test and wide range of magnetic field.

(iii) Designing and developing a tactile display system based composite magnetorheological elastomers.

(iv) Controlling the stiffness of composite MRE samples in the proposed tactile system by adjusting external magnetic field.

1.6 Dissertation layout

This thesis is structured in manuscript form and consists of the following four chapters:

Chapter 1: This chapter provides the main introduction for the studied topic along with literature review. It has a manuscript titled as *"Review of Magnetorheological Elastomers Fabrication, Characterization, and Modeling."* This paper was accepted in the International Conference on Engineering and Technology (ICET-19) that will be held in Toronto, Canada, on August 15th, 2019.

Chapter 2: This chapter includes the fabrication of the isotropic MRE and non-MRE samples. In addition, it provides the proposed tactile display based on MRE samples. This chapter also presents the magnetic analysis of the two sets of neodymium magnets used in this research. At the end of this chapter, an investigation of the magneto rheological effects of a broad range of transverse magnetic field on the mechanical properties of mono-layered and bi-layered MREs is discussed. This chapter is based on a manuscript entitled as *"Composite Magnetorheological Elastomers for Tactile Display: Enhanced MR-effect Through Bilayer Composition"*, submitted to and under-review in *Journal of Composites Part B: Engineering*.

Chapter 3: In this chapter, the proposed tactile system is presented. Afterwards, electromechanical parameters are identified through a transfer function optimization. In addition, it shows the applicability of the proposed system in medical applications like pulse examination. Moreover, it demonstrates the stiffness control of MREs via controlling the magnetic field in the tactile display system. This chapter is based on a manuscript entitled as *"Development and Assessment of* *a Stiffness Display System for Minimally Invasive Surgery based on Smart Magneto-rheological Elastomers"*, submitted to and under-review in *Journal of Materials Science and Engineering: C*.

Chapter 4: This chapter demonstrates the conclusions and proposed extensions for the future works, which can be carried by referring to the current study.

Figure 1.22 presents the thesis layout.

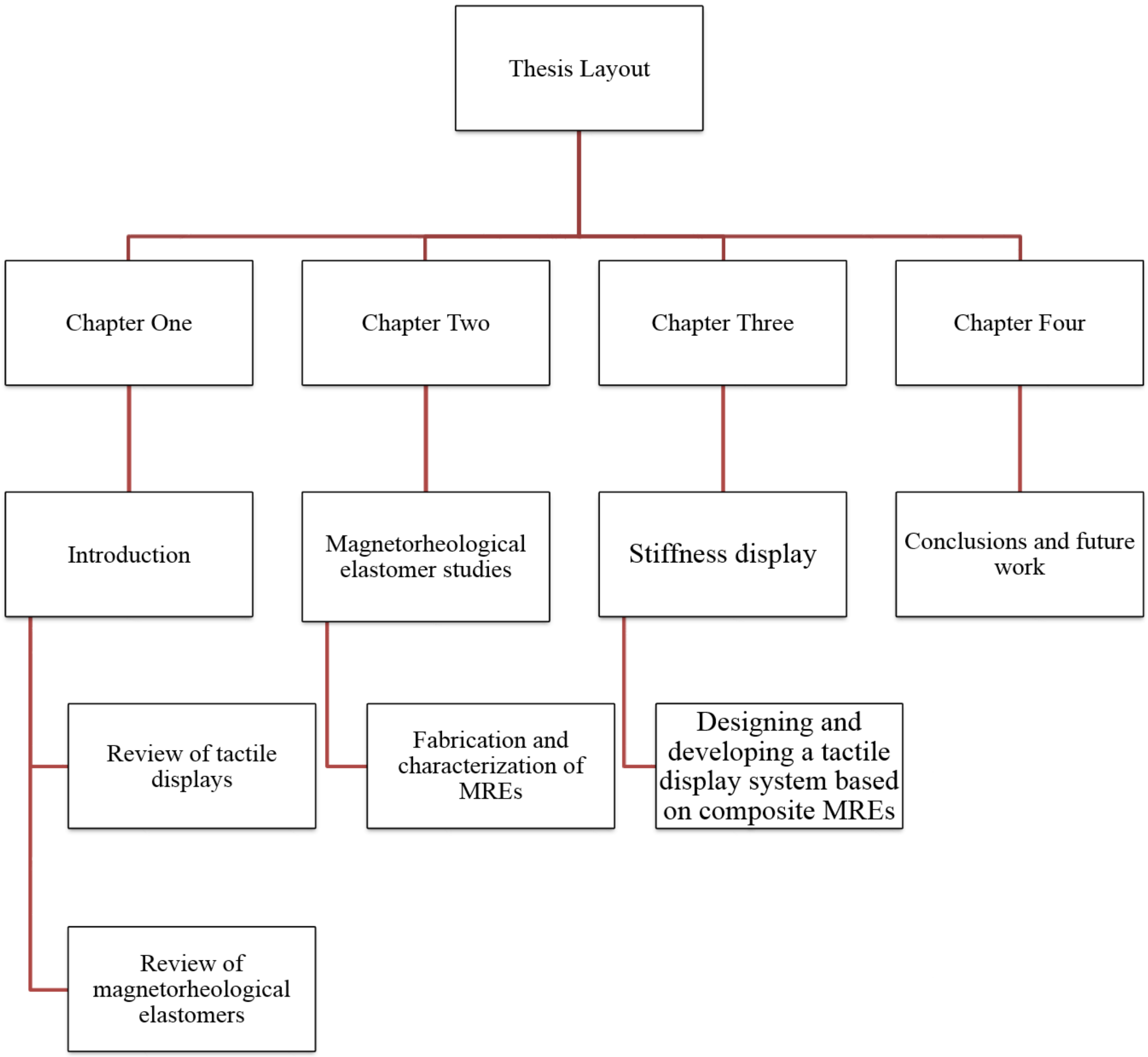

Figure 1.22: Thesis layout

Chapter 2

Composite Magnetorheological Elastomers for Tactile Display: Enhanced Properties Through Bi-layer Composition

Abstract

In this study the feasibility of a novel tactile display based on the magnetorheological elastomers (MREs) was studied. To this end, initially a survey on various requirements of tactile displays for surgical applications was performed. The survey showed that MREs would make a good fit for tactile displays. To further study the MREs, initially the samples were characterized perpendicular to the magnetic field, similar to the actual use-cases. Also, to compensate for the loss of MR-effect due to non-parallel application of compression and magnetic field, MREs were composited in bi-layer configuration with a non-MRE elastomer. The results of mechanical characterization showed that bi-layer composition increased the MR-effect in MREs by 42%. This study showed that further enhancement of MR-effect in MREs is possible through bi-layer composition with a non-MRE elastoemr. Also, it was shown that development of an MRE-based tactile display is feasible using the proposed enhanced MRE composites.

2.1 Introduction

2.1.1 Background

Magnetorheological elastomers (MREs) are a class of novel composite materials with realtime tunable mechanical properties under a magnetic field [40, 25]. Researchers have utilized the controllability of MREs for adaptive vibration absorbers and isolators [41, 38, 42], noise reduction [43], and actuation applications [43, 44].

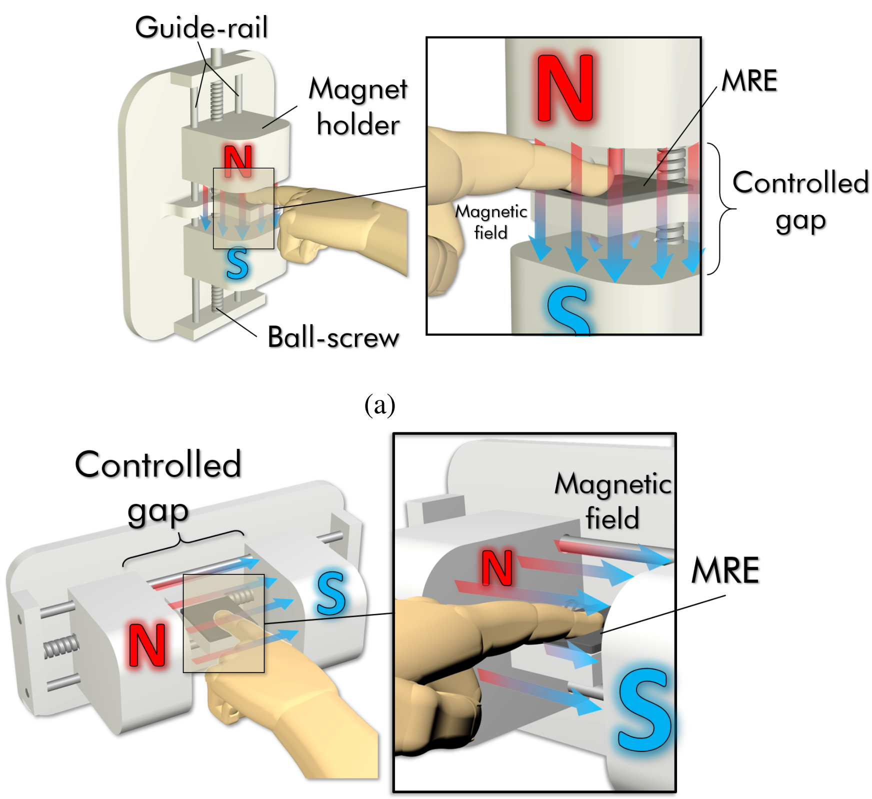

(a)

(b)

Figure 2.1: Proposed MRE-based tactile display with the magnetic field applied (a) in the direction of surgeon's palpation and (b) perpendicular to the direction of surgeon's palpation.

MREs are composed of two main components: elastomeric matrix and filler. Different elastomeric matrices such as silicone rubber and natural rubber have been used as the matrix. Specifically for medical applications, silicon-rubber is well-suited due to the availability of its medical-grade form. Also, iron and carbonyl iron particles (CIP) have been investigated as the fillers. Considering its high magnetic saturation, CIPs are suggested for enhanced magnetic effect [45].

Mechanical properties of MREs change upon application of a magnetic field [46, 40, 47]. This phenomenon is known associated with the reformation of the ferromagnetic particles inside the matrix to align with the magnetic field. Such reformation changes the distribution of internal stress in the MRE and leads to a different strain energy; thus, causes a different force-displacement behavior [46]. To quantize this effect, *'MR-effect'* indicator is defined as the change in mechanical properties of MRE in response to the magnetic field. This indicator is expressed either in the form of absolute effect (absolute difference) or relative effect (percentage of the change) compared to the MRE's non-magnetized state.

MREs, in contrast to MR fluids, are considered environmentally friendly, and inexpensive. Also, because of their solid state, utilization of MREs in MR devices is more convenient compared to the MR fluids [48, 25].

Fabrication of MREs involves three steps: mixture, addition, and curing. In the mixture step, the constituents of the matrix, i.e. the base and hardener components, are thoroughly mixed with a prescribed proportion. Based on the literature, the proportion of the components are either reported based on the weight-fraction or volume-fraction. In the second step, the additives, e.g. slacker, thinner, and iron particles, are added to the mixture. Softness (shore-hardness) of an MRE depends on the fraction of slacker in the mixture. Also, adding a thinner results in more fluidity of the mixture and easier injection into a mold. Furthermore, the fraction of iron particles determines the maximum MR-effect exhibited by the MRE before magnetic saturation. The maximum reported volume fraction of iron particles in the reviewed literature was 40% [25]. Experimental evidence suggests that for the silicon-rubber-based MREs, volume fraction of 40% to 45% would result in saturation of the emulsion [49], agglomeration of particles [50], and non-homogeneous dispersion of particles in the MRE [51]. Homogeneity of the particle dispersion is crucial to achieve repeatable mechanical properties [50, 51]. To have more MR-effect in an MRE, it is suggested that the particle should be large enough to contain multiple magnetic domains [45]. On the other hand, studies have shown that the use of small-diameter magnetic particles, $1 - 10\mu m$ facilitates the homogeneous dispersion in the emulsion, which is crucial to have repeatable properties. Therefore, there is a balance between the particle size, homogeneity, and the maximum MR-effect of MRE.

To free the air bubbles entrapped in the mixture during stirring, placing the mixture in a vacuum chamber before curing (5 min., 29inHg) was recommended in a recent study [25]. Such air bubbles form voids inside the MRE and adversely affect the MRE performance. Elastomeric polymerization starts upon the mixture of base and hardener components and natural curing happens in the scale of hours for silicon-rubber-based MREs. Nevertheless to accelerate the process, curing in an oven (e.g. more than 100°C) reduces the curing time to 1-3 hours.

MREs cured in the absence of a magnetic field show isotropic MR-effect, i.e. similar MR-effect along X, Y, and Z-axes. Researchers have fabricated anisotropic MREs by curing the MREs in a magnetic field upto 1T [52, 53, 54]. The magnetic field aligns the particle while the mixture cures. Anisotropic MREs exhibit enhanced MR-effects in the direction of particle alignment [54]. Although, a *'preferred'* direction in an MRE might be desirable for unidirectional applications, e.g. compressive dampers, it results in weaker mechanical properties in the perpendicular plane, which could compromise the long-term durability of the MRE [54, 30].

MREs have been widely investigated under various modes of mechanical testing, i.e. shear, torsion, tension, and compression [55, 48, 56, 25, 57]. Mechanical properties of sample MREs have been characterized in the same direction as the magnetic field. The reason might be due to the researchers' interest in the maximum MR-effect, which occurs in the same direction as the magnetic field. The main independent variables considered in magnetorheological characterization of MREs are: particle content, particle size, and the applied magnetic field. Also, depending on the application of an MRE, its quasi-static or dynamic properties have been investigated. Shore-hardness [58], elastic modulus [25, 58, 59, 60], creep [61] and relaxation [62] for quasi-static, and loss-modulus, storage-modulus, and phase-lag ($\tan \delta$) for dynamic tests, are the investigated properties [63, 25]. Owing to the intrinsic large-deformation of the elastomeric matrix, MREs have been modeled as hyperelastic (quasi-static) [64] or viscoelastic (dynamic loading) [65, 55] nonlinear materials.

Table 2.2 summarizes the reviewed literature for silicon-rubber-based MREs along with the corresponding mechanical test mode, percentage of particles, magnetic field variations, and maximum MR-effect.

2.1.2 Rationale and hypothesis

In this study, a tactile display is suggested for surgical applications based on silicon-rubber-MRE (Fig. 2.1). Tactile display is a physical medium with controllable apparent stiffness. Haptic displays are used for replicating the stiffness of a biologic tissue during a remote robotic surgery, e.g. laparoscopy [9], cardiac surgery [66]. Loss of sense of touch and direct palpation have been reported as the prime limitations of the state-of-the-art in robotic surgery [9, 66]. To this end, various tactile displays have been proposed based on utilization of DC motors [9], pneumatic balloons [22, 21], electro-active polymers (EAPs) [24], shape-memory-alloys (SMAs) [67] and MR-fluids [13, 12, 9, 14]. Considering the availability of medical-grade silicon-rubbers, this study was scoped to evaluate the feasibility of an MRE-based tactile display. With the proposed designs, mechanical properties of the MRE could be controlled through controlling the applied magnetic field. Based on the literature review, the utilization of MREs for this application has not been exploited. Table 2.1 lists the main functional requirements for tactile displays and compares different technologies accordingly.

Table 2.1: Comparison of different modalities for tactile display based on the functional requirements.

Requirement	DC-motor	Pneumatic balloon	EAPs	SMAs	MRFs	MREs
Design simplicity	×	✓	✓	×	✓	✓
Dynamic range	Low	High	Low	Low	High	High
Response-time	✓	×	✓	✓	✓	✓
Passive stability	×	×	✓	✓	×	✓
Repeatability	✓	○	✓	✓	○	✓
Electrical passivity	×	✓	×	✓	✓	✓
Easy handling	✓	×	×	○	×	○
Low power consumption	✓	×	✓	×	✓	✓
Disinfectability	×	✓	×	✓	×	✓

✓: Pass ○: Marginally-pass ×: Fail

Based on the comparison, it was inferred that MREs are a well-suited candidate for the tactile display application. To this end, two design options were conceptualized in Fig. 2.1. In the proposed tactile display, two permanent magnets were used to generate a homogeneous magnetic field. Compared to the use of coils for generating magnetic field, permanent magnets have zero power-consumption (passive elements), provide more stability, and are less sensitivity to the thermal effects, e.g. associated with the heat generation in coils. In order to control the magnetic field strength, ball-screw and guide mechanism was proposed to control the gap between the two magnets.

In design (a), the magnetic field was applied in the same direction as surgeon's palpation, i.e. direction of compression on the MRE. With such alignment of magnetic field and compression, maximal MR-effect would be expected. However, design (a) would provide a limited space for the user's access to MRE. Also, interference of the surgeon's hand with the field would compromise the homogeneity and MR-effect.

On the other hand in design (b), magnetic field is applied perpendicular to the palpation direction. Such configuration would resolve the access-space limitation and provide the desirable user access; however, it would lead to less MR-effect compared to design (a). Consequently, design (b) would provide less control over the achievable elastic modulus of MRE. Therefore, the initial objective of this study was to quantify the effect of magnetic field on the elastic modulus in the perpendicular plane.

Secondly, a bi-layer MRE structure was suggested to enhance the MR-effects on MREs. To this end, elastic moduli of various MREs ($25\%, 35\%, 45\%$vol. of CIP) in single and bi-layer MRE-MRE and MRE-non-MRE combinations were studied. Finally in order to verify the feasibility of design (b) for the tactile display application, the elastic moduli of composites were compared with biologic tissues.

In the following, Sec. 2.2 describes the MRE and composite fabrications, test protocol, and data analysis. Sec. 2.3 presents the test results and discussions. In the end, the remarks and future works of this study are provided in Sec. 2.4.

Table 2.2: Selected studies investigating the magnetorheological mechanical properties of the silicon-rubber-based MREs.

Authors	Particle content	Mechanical Test	Strain (%)	Magnetic Field (mT)
Deng *et al.* [28] (2006)	70.0 %wt.**	Shear	-	0 - 900
Chen *et al.* [31] (2006)	60.0-90.0 %wt.	Shear	0.03 - 0.70	0 - 900
Böse *et al.* [68] (2009)	0.0, 35.0 %vol.*	Rheometry	-	0 - 700
Hu *et al.* [35] (2011)	70.0%wt.	Shear	0 - 100	0 - 95
Gordaninejad *et al.* [53] (2012)	30.0, 70.0 %wt.	Compression, Shear	0 - 20	0 - 1600
Bica *et al.* [32] (2014)	40.0%vol.	Compression	-	0 - 82
Norouzi *et al.* [36] (2016)	70.0 %wt.	Shear	0 - 16	0 - 272
Sapouna *et al.* [30] (2017)	30.0 %vol.	Compression	0 - 1.5	0, 350, 500
Vatandoost *et al.* [50] (2017)	70 %wt.	Compression, tension	0 - 14	0 - 260
Song *et al.* [37] (2018)	60.0%wt.	Rheometry	0 - 1	0 - 750
Dargahi *et al.* [69] (2019)	12.5-40 %vol.	Shear	2.5 - 20	0 - 450

* : percent of volume, ** : percent of weight.

2.2 Material and Methods

2.2.1 Magnetic field

In Sec. 2.1.2 magnetic field was proposed to be controlled by adjusting the gap distance between the magnets. Recently, Dargahi *et al.* reported magnetic fields of up to 450mT utilizing a similar mechanism [25] and achieved unprecedented MR-effects of up to 1672% for similar MREs [25].

In this study, four Neodymium N52 magnets ($2'' \times 2'' \times 1''$, CMS Magnetics, Inc., Texas, USA) were coupled in two couples of two magnets. The gap distance was adjusted manually using nuts and bolts. To avoid the magnetic field leakage, the holding elements, nuts and bolts were non-ferrous.

To obtain the range of the average magnetic field across the gap, magnet couples and air-gap were modeled in the Finite Element Method Magnetics package (FEMM v4.0, open-source, [70]). Simulation was performed for gap distances of 45mm to 95mm with 5mm increment (n=11). Magnetic properties provided by the manufacturer were coercive force as $875 \, {}^{kA}\!/\!_{m}$, and remanence as 1.45T. Fig. 2.2 (a) depicts the distribution of magnetic field around and between the magnets.

Furthermore, the gap distance was changed from 45mm to 95mm and the magnetic field was measured using a gauss-meter for five readings(GM2, AlphaLab Inc., PA, USA). A minimum of 45mm gap distance was selected to provide enough space for the MRE sample (Fig. 2.2 (c)). Results showed a fair agreement between FEMM and experiment (Fig. 2.2 (b)). The average magnetic field decreased from 365mT to 143mT with increasing the gap from 45mm to 95mm.

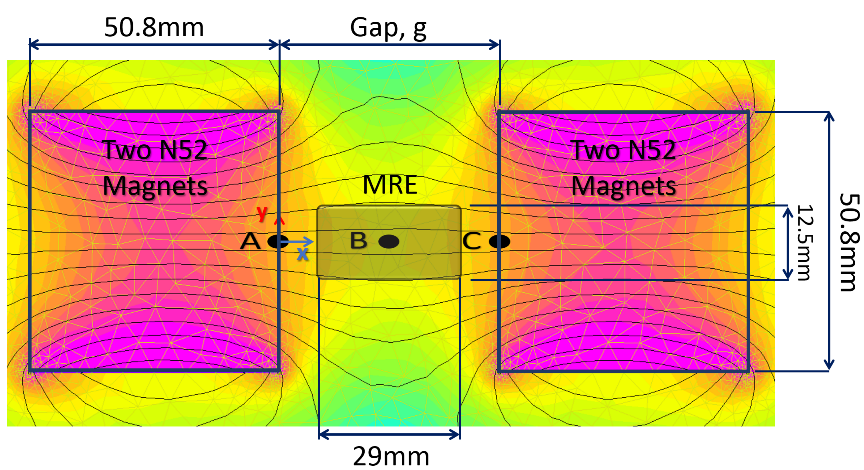

(a)

Figure 2.2: (a) Distribution of the magnetic field generated by two N52 magnets from FEMM, (b) average magnetic field along the x-axis with different separations, (c) magnetic field along the x-axis for the minimum separation between the two magnets, i.e. 45mm *(cont.)*.

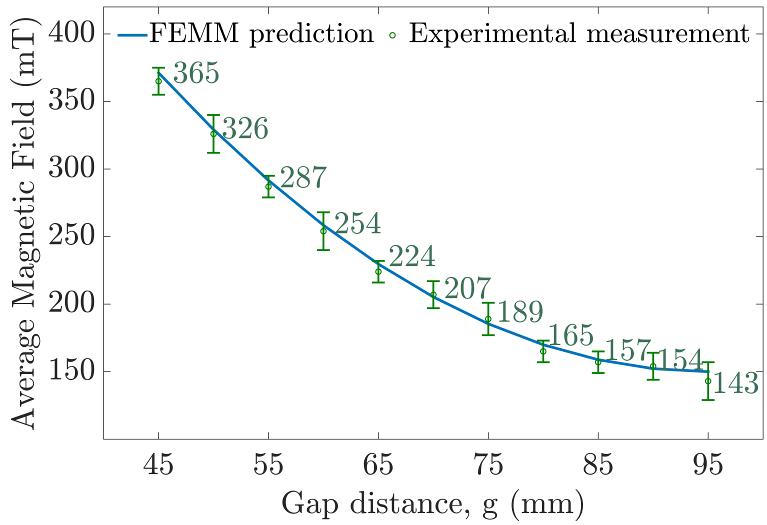

(b)

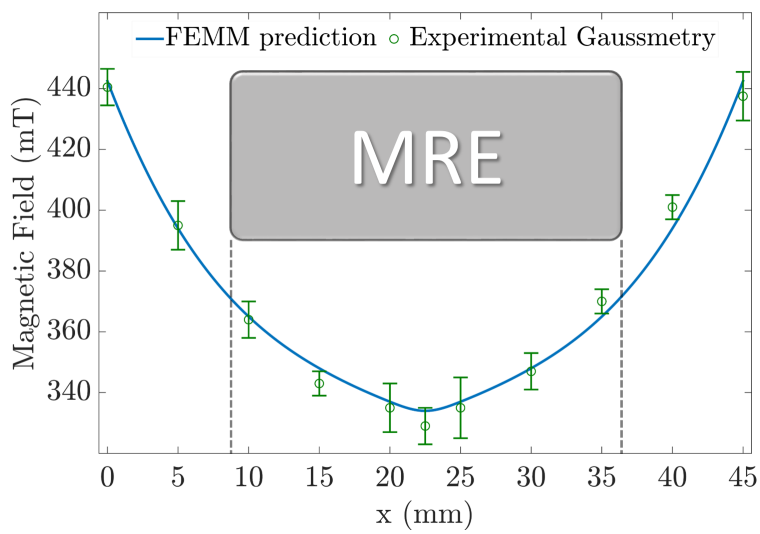

(c)

Figure 2.2: (a) Distribution of the magnetic field generated by two N52 magnets from FEMM, (b) average magnetic field along the x-axis with different separations, (c) magnetic field along the x-axis for the minimum separation between the two magnets, i.e. 45mm.

Also to evaluate the longitudinal homogeneity of the field, the gap distance of 45mm was selected as the gap distance decreases, homogeneity diminishes. At this distance, magnetic field decreased from 440mT at points A and C to 335mT at point B (24% variation). However, since the MRE samples were only 29mm in diameter, the actual variation of magnetic field inside the MRE was from 370mT at $x = 8$mm to 335mT at $x = 22.5$mm (9.5% variation). Similar level of variations have been reported in other studies [71].

2.2.2 Material selection

Following the protocol described in [25, 72, 28], three types of MREs, i.e. MRE A, B, and C, with 25%, 35%, and 45% volume fractions of CIPs, and one non-MRE Dragon Skin (Material D) were fabricated. The CIPs (AC-325, Sculpture Supply Canada, Ontario, Canada) had a nominal mean diameter of 45μm with variation of less than 5%. The matrix elastomer for MREs was EcoFlex™ $00-20$ (Smooth On Inc., PA, USA) as suggested in [25, 69]. Components of MRE A, B and C were adopted from [25] and are summarized in Table 2.3. Also for choosing material D, the following analysis was performed.

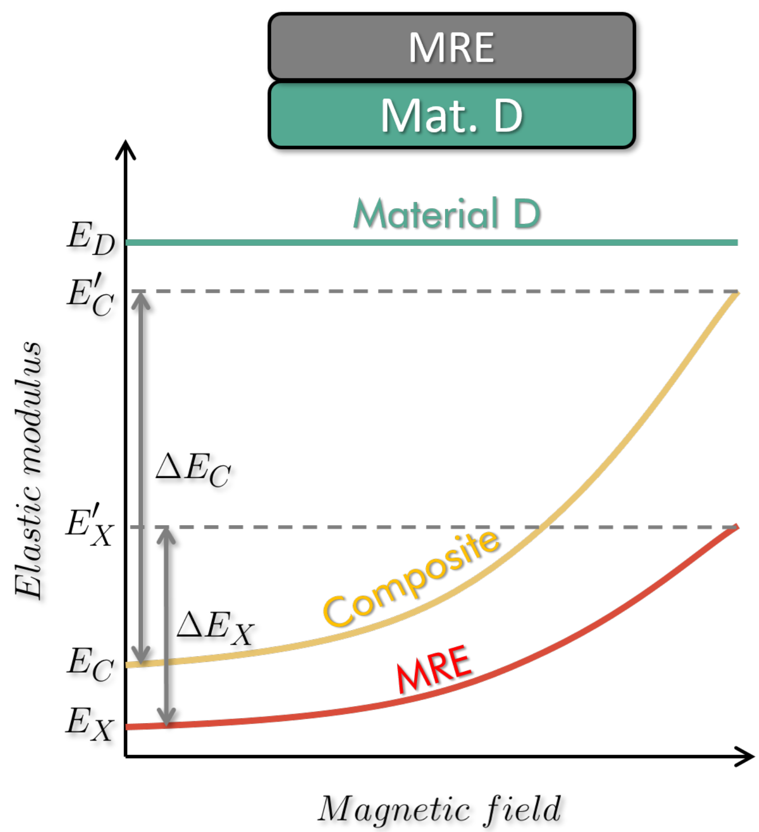

Figure 2.3: Schematic view of changes in the elastic modulus of an arbitrary bi-layer composite X compared to its components MRE X, and Material D.

As stated in the hypotheses, the objective of fabricating bi-layer MREs was to have higher MR-effect compared to the single-layer structure. Based on the literature, it was assumed that the elastic modulus of any arbitrary MRE X, increases non-linearly but monotonically from its initial value, E_X to a higher value, E'_X as magnetic field increases. On the other hand, material D was non-MRE, thus its modulus would remain at a value of E_D. As depicted in Fig. 2.3 and without losing generality, a composite C composed of a layer of X and a layer D, with the same size, was desirable if and only if its demonstrated MR-effect was more than MRE X. This condition necessitated that:

$$\Delta E_C > \Delta E_X, \tag{1}$$

where ΔE denotes the absolute MR-effect. Therefore:

$$E'_C - E_C > E'_X - E_X. \tag{2}$$

A generalized one-term power-law constitutive equation for the elastomers X and D was assumed [73]. The power-law form was selected as a simplifying assumption so that the existence of a necessary condition could be justified analytically.

$$\sigma_X = \mu_X \lambda^{\alpha}, \tag{3}$$

$$\sigma_D = \mu_D \lambda^{\alpha}, \tag{4}$$

where μ was the shear modulus, α was the non-linearity fitting parameter, and λ was the stretch ratio . Therefore, based on the conservation of mass and momentum principles, the shear modulus of the composite [74] was obtained as:

$$\mu_C = 2^{\alpha} \left(\mu_D^{\frac{-1}{\alpha}} + \mu_X^{\frac{-1}{\alpha}} \right)^{-\alpha}, \tag{5}$$

and similarly,

$$\mu'_C = 2^{\alpha} \left(\mu_D^{\frac{-1}{\alpha}} + {\mu'}_X^{\frac{-1}{\alpha}} \right)^{-\alpha}, \tag{6}$$

Also, considering the MRE as near fully-incompressible, its poisson's ratio,ν would be approximately 0.5; therefore,

$$E_X = 2(1+\nu)\mu_X \approx 3\mu_X. \tag{7}$$

Thus, by substituting Eq. 5-7 in Eq. 2 the necessary condition reformed as:

$$\left(\mu_X^{\frac{-1}{\alpha}} + \mu_D^{\frac{-1}{\alpha}}\right)^{\alpha} - \left({\mu'}_X^{\frac{-1}{\alpha}} + \mu_D^{\frac{-1}{\alpha}}\right)^{\alpha} - (\mu'_X - \mu_X) \times \left(\frac{\left({\mu'}_X^{\frac{-1}{\alpha}} + \mu_D^{\frac{-1}{\alpha}}\right)\left(\mu_X^{\frac{-1}{\alpha}} + \mu_D^{\frac{-1}{\alpha}}\right)}{2}\right)^{\alpha} > 0 \tag{8}$$

Further analysis showed that Eq. 8 tends to $-\infty$ if $\mu_D \rightarrow 0^+$ and tends to 0.0057 if $\mu_D \rightarrow +\infty$. Therefore, due to its continuity in $\mathbb{R}^+$, there must necessarily be a μ_D at which Eq.8 turns positive and the bi-layer composite would show more MR-effect than its constituent MRE X.

Solving Eq. 8 by substituting $\alpha = 1.3$ [75], $\mu_X = 75$kPa, and $\mu'_X = 270$kPa [25, 69] for Ecoflex 00-20, the minimum μ_D was determined as 165.63kPa. Therefore, Dragon Skin™30 (Smooth On Inc., PA, USA), as a common material in practice, was selected as the material D. Previous studies have reported the Ogden shear modulus of 1114kPa for the Dragon Skin™30 under quasi-static loading [76].

2.2.3 MRE fabrication

The weight composition of silicon-rubber, CIPs, slacker, and thinner per $100cc$ of total volume of each material were calculated using the mass-volume mixture formula:

$$m_{_Y} = \rho_{_Y} \nu_{_Y} V_{_{total}}, \tag{9}$$

where, Y is a dummy replaced by CIP, silicon-rubber (SR), slacker (SL), and thinner (TH), m is the required mass, ν is the volume fraction, ρ is the density, and $V_{_{total}}$ was $100cc$. Table 2.3 summarizes the estimated required mass of each component for the fabricated elastomers.

Table 2.3: Density, ρ_X, volume fraction, ν_X and mass, m_X of the contents in the fabricated elastomers.

Material	Contents ν_Y, m_Y				
	Silicone rubber	Dragon Skin	Slacker	Silicone thinner	CIPs
	$\rho_{SR} = 1.04\frac{gr}{cc}$	$\rho_{DS} = 1.08\frac{gr}{cc}$	$\rho_{SL} = 0.97\frac{gr}{cc}$	$\rho_{ST} = 0.97\frac{gr}{cc}$	$\rho_{CIP} = 7.87\frac{gr}{cc}$
Material D (Dragon Skin)	-	90%, 97.2gr	5%, 4.9gr	5%, 4.9gr	-
MRE A	65%, 67.6gr	-	5%, 4.9gr	5%, 4.9gr	25%, 196.8gr
MRE B	55%, 57.2gr	-	5%, 4.9gr	5%, 4.9gr	35%, 275.5gr
MRE C	45%, 46.8gr	-	5%, 4.9gr	5%, 4.9gr	45%, 354.2gr

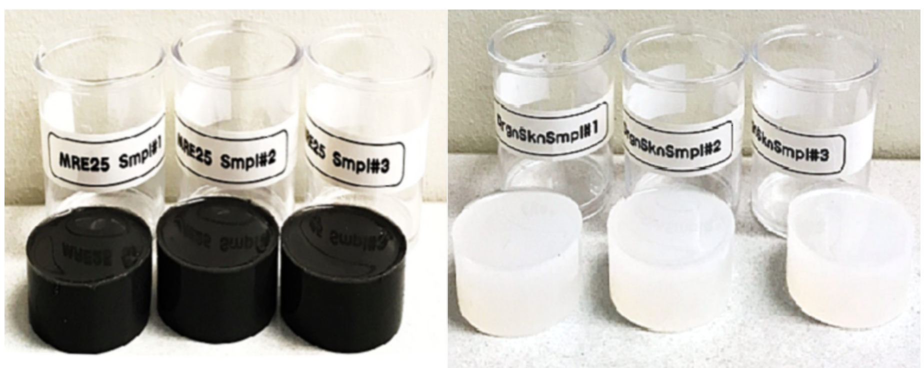

(a)

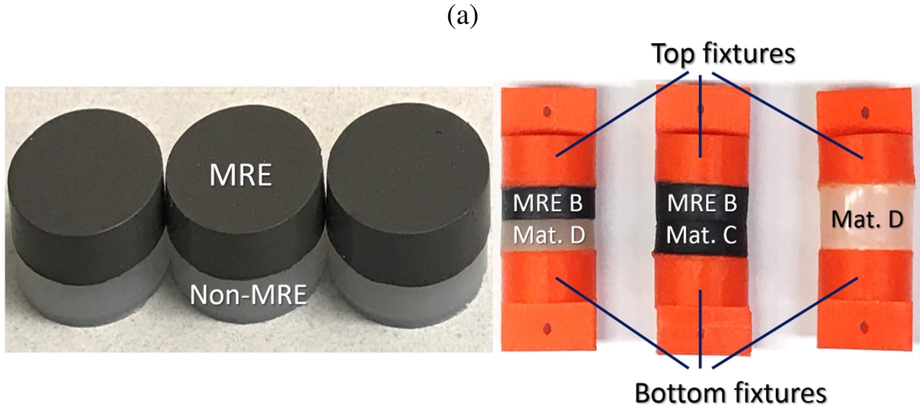

(b)

Figure 2.4: (a) left: mono-layer MRE B, right: Material D samples and (b) left: bi-layer MRE-non-MRE samples, and right: samples attached to the test fixtures.

The elastomer mixtures were poured into three identical molds, i.e. $25cc$-beakers, with $29mm$ diameter, upto the $12.5cc$ indicator. Dimension of the molds were selected in compliance with the sample dimensions suggested in ISO 7743 for compression test [63]. In order to free the entrapped air bubbles in the mixtures, molds were placed in a vacuum chamber (Best Value Vacs, IL, USA) and maintained at 29inHg vaccum pressure for 5 minutes. Afterwards, the molded elastomers were cured in room temperature for 24 hours. The dimensions of the cured samples were 28.8 ± 0.26mm in diameter and 12.4 ± 0.42mm in height. The recorded dimensions were in compliance with the geometrical tolerances mandated in [63]. Fig. 2.4 (a) shows an example of cured MRE and non-MRE samples.

2.2.4 Fabrication of composites

In order to study the properties of bi-layer MRE composites, combining MRE A, B, C, and Material D, six groups of composites were fabricated. The composites were labeled as A-B, A-C, A-D, B-C, B-D, and C-D, to represent the constituent components of each. Three samples per each group were prepared. The composites were prepared by attaching two layers of different materials using glue (Gorilla Super Glue, Gorilla Glue, Inc., Ohio, USA) at the interface. Elastomers used in the composites were fabricated following the method presented in Sec. 2.2.3; however the height of the fabricated layers were half of those previously molded. The reason was to achieve the same total thickness as recommended by ISO 7743, i.e. 12.5 ± 0.5mm. The bi-layer samples were afterward rested for 24 hours for the glue to dry. Fig. 2.4 (b) depicts MRE-non-MRE and MRE-MRE samples.

2.2.5 Test protocol and setup

The single- and bi-layer MREs were tested in quasi-static compression. The reason was that a surgeon's palpation normally has a low strain-rate and is in compression [9]. The compression test protocol was adopted from ISO 7743 [63].

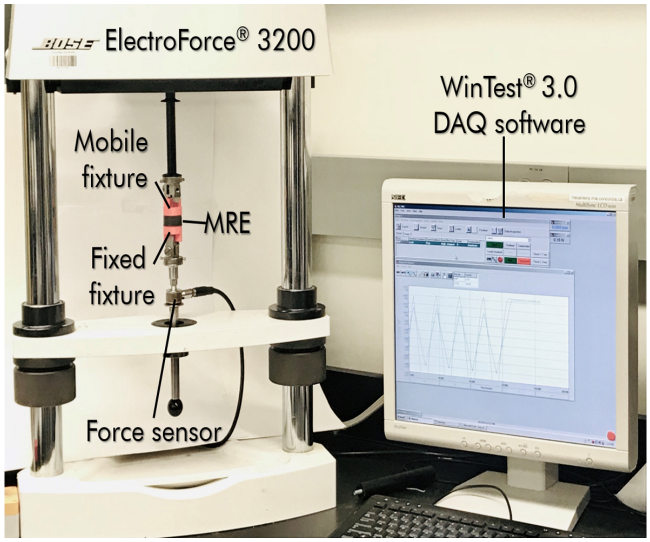

(a)

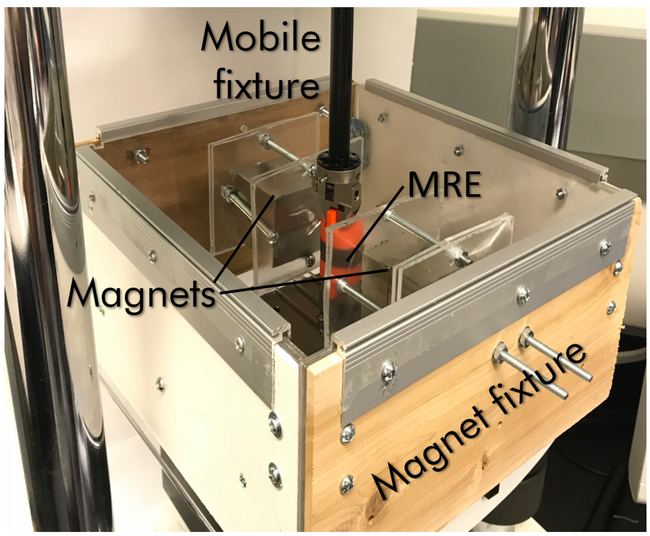

(b)

Figure 2.5: (a) mechanical testing machine and compressive test setup and (b) placement of MREs and magnets in the testing machine.

Each sample was attached to two 3D-printed plastic fixtures (Fig. 2.4 (b)) to be attached to the mobile and fixed fixtures of the universal testing machine (ElectroForce 3200, TA Instruments, DE, USA). The samples were subjected to four cycles of 0.1Hz triangular compressive displacements between 0.625mm (5% strain) and 3.125mm (25% strain). Meanwhile, the compressive force was recorded. Fig. 2.5 (a) and (b) depict the mechanical test setup without and with magnetic field.

2.2.6 Post-processing and analysis

After obtaining the force-displacement curve of each sample, the engineering stress and strain were estimated using Eq. 10-11.

$$\sigma = \frac{F}{A_\circ}, \tag{10}$$

where, σ, F, and $A_\circ$ were the engineering stress, compressive force, and undeformed cross-sectional area of samples. Also,

$$\epsilon = \frac{\delta}{t_\circ}, \tag{11}$$

where, ε, δ, and $t_\circ$ were the engineering strain, compressive displacement, and undeformed thickness of samples. Afterward, the secant modulus at 10%, $S_{10\%}$ and at 20%, $S_{20\%}$ strains were determined as described in Fig. 2.6.

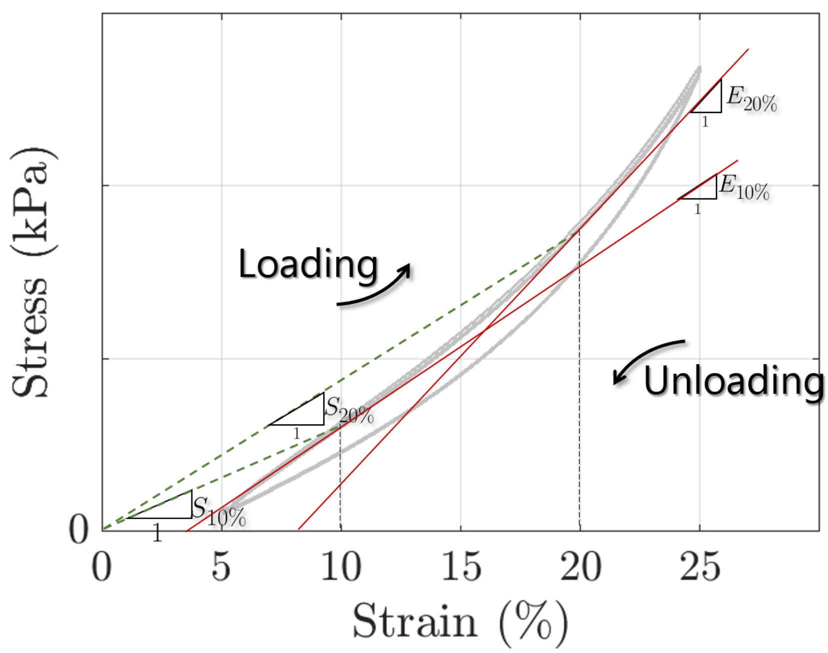

Figure 2.6: A typical stress-strain curve for samples under compressive loading and unloading. Secant modulus, S of each sample were calculated at 10% and 20% as described in ISO 7743.

Finally, the elastic modulus at 10%, $E_{10\%}$ and at 20%, $E_{20\%}$ were estimated using Eq. 12 [63]. In the end, the average elastic modulus at zero magnetic field, $\bar{E}_\circ$, and at 365mT, $\bar{E}_{365}$, absolute MR-effect, $\Delta\bar{E}_{abs}$, and percentage of relative MR-effect, $\Delta\bar{E}_{rel}$ were estimated for further comparison.

$$E_{10\%,20\%} = \frac{S_{10\%,20\%}}{A + B\xi^n}, \tag{12}$$

$$\Delta\bar{E}_{abs} = \bar{E}_{365} - \bar{E}_{\circ}, \tag{13}$$

$$\Delta\bar{E}_{rel} = \frac{\bar{E}_{365} - \bar{E}_{\circ}}{\bar{E}_{\circ}} \tag{14}$$

where A and B were two fitting parameters set as 1 and 0.012 [63], respectively, n was a material-dependent non-linearity heuristic set as 2 for silicon-rubber [63], and ξ was the shape factor of samples defined as:

$$\xi = \frac{d_{\circ}}{4t_{\circ}} = \frac{29\text{mm}}{4 \times 12.5\text{mm}} = 0.58, \tag{15}$$

where $d_{\circ}$ and $t_{\circ}$ were the undeformed diameter and thickness of each sample.

2.3 Results and Discussions

2.3.1 Stress-strain characteristics

As mandated by ISO 7743, three compressive tests were performed for each sample. In each test, four consecutive loading and unloading cycles were applied. For the characterization analysis, the first cycle was excluded and considered as the pre-conditioning cycle. Three samples of nine different MREs (A, B, C, A-B, A-C, A-D, B-C,B-D, and C-D) were each tested under seven different magnetic fields ($0, 143, 157, 189, 224, 287,$ and 365mT). Also, three similar compression tests were performed on the non-MRE material D; resulting in a total of 192 compression tests (3×9×7 for MREs and 3 for Material D). The average force-displacement curve of the three similar samples of each material was used to create the average stress-strain curves. Fig. 2.7 and Fig. 2.8 show the average stress-strain curve of each mono- and bi-layered materials, respectively. Also, Table 2.4 summarizes the mechanical elastic moduli of all materials at zero and 365mT.

The elastic modulus of the bi-layer MREs at all magnetic fields was between the elastic moduli of their constituents. For example, at zero magnetic field, the elastic modulus of MRE C-D was 388, while elastic moduli of MRE C and elastomer D were 281, and 3635kPa, respectively. Similarly, at 365mT, the elastic modulus was 1370kPa for C-D, while it was 873, and 3635kPa for MRE C and elastomer D. This finding was in accordance to the theoretical prediction of Eq. 8. The same trend was observed in all bi-layer MREs.

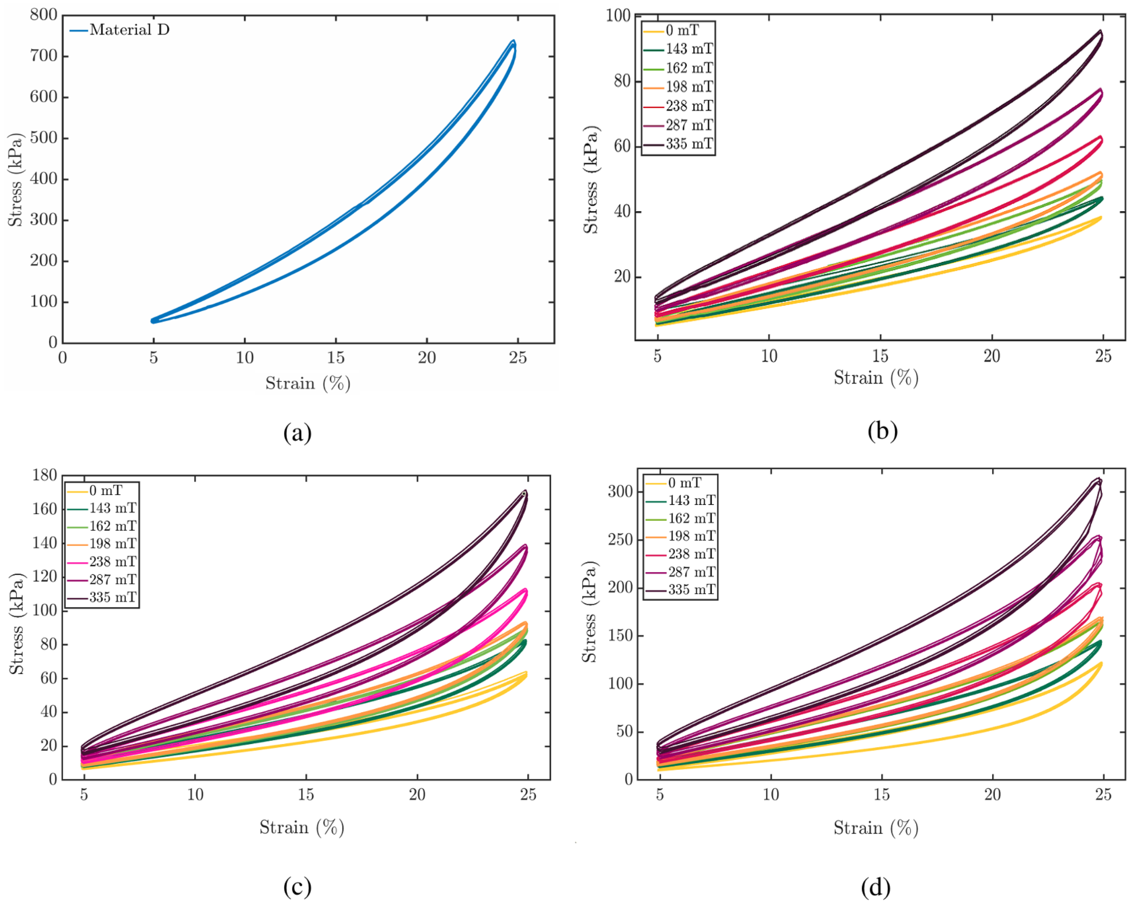

Figure 2.7: Stress-strain curves for compression under various magnetic fields: (a) Material D, (b) MRE A, (c) MRE B, (d) MRE C

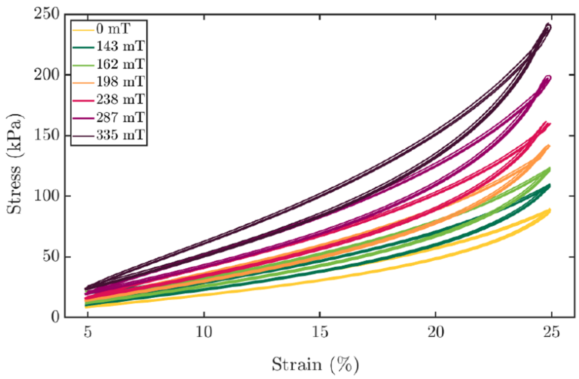

(a)

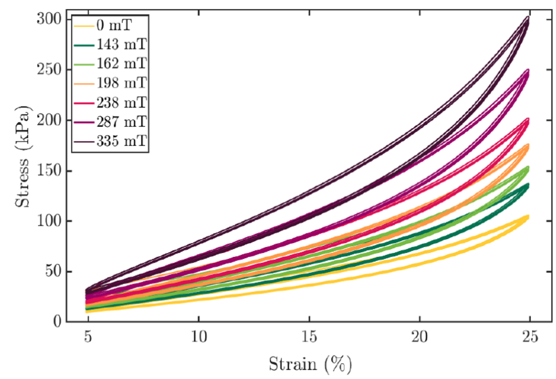

(b)

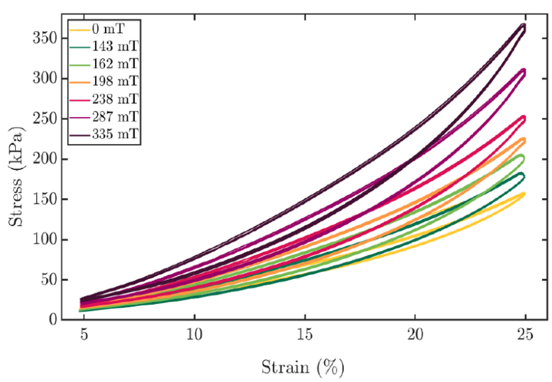

(c)

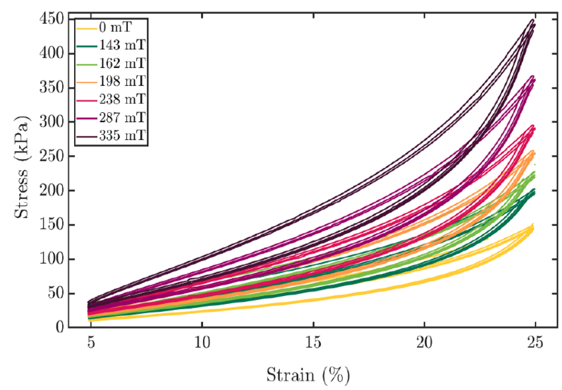

(d)

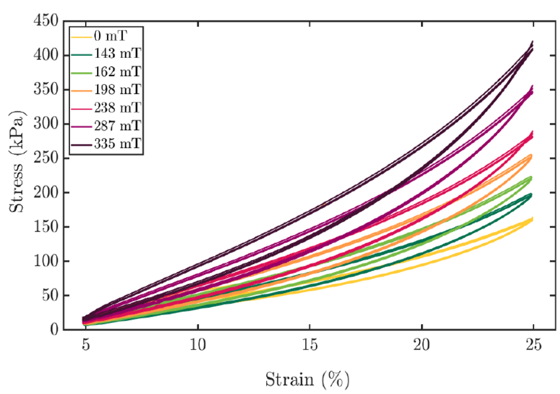

(e)

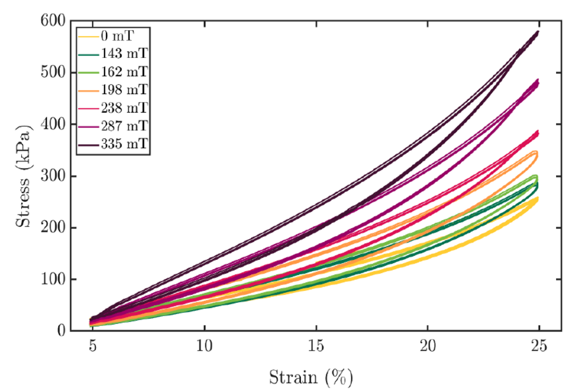

(f)

Figure 2.8: Stress-strain curves for compression under various magnetic fields for composite: (a) A-B, (b) A-C, (c) A-D, (d) B-C, (e) B-D, and (f) C-D.

Table 2.4: Summary of the average elastic moduli at zero and 365mT fields, absolute- and relative MR-effect, and the change in MR-effect due to the bi-layer composition.

Material	Particle content (%)	0 mT $E_{10\%}$ (kPa)	0 mT $E_{20\%}$ (kPa)	0 mT $\bar{E}_{\circ}$ (kPa)	365 mT $E_{10\%}$ (kPa)	365 mT $E_{20\%}$ (kPa)	365 mT $\bar{E}_{365}$ (kPa)	$\Delta\bar{E}_{abs}$ (kPa)	$\Delta\bar{E}_{rel}$ (%)	Change in MR-effect (%)
Material D (Dragon Skin)	0	2495	4775	3635	-	-	-	0.00	0	-
MRE A	25	74	88	81	190	232	211	130	160	-
MRE B	35	174	192	183	469	579	524	341	187	-
MRE C	45	254	308	281	785	961	873	592	211	-
MRE A-B	25-35*	111	124	117	302	349	326	209	179	-8
MRE A-C	25-45*	124	155	140	359	441	400	260	186	-25
MRE A-D	25-0*	153	194	172	431	535	483	311	181	+21
MRE B-C	35-45*	209	238	223	647	713	680	457	205	-6
MRE B-D	35-0*	271	311	291	819	933	876	585	201	+24
MRE C-D	45-0*	346	431	388	1218	1522	1370	982	253	+42

*: bi-layer composite.

2.3.2 Effect of magnetic field

As reflected in Table 2.4, magnetic field showed positive effect in increasing the elastic moduli of all single- and bi-layer sample. Also at all magnetic fields, the MR-effect was higher for MREs with higher volume fraction of CIPs. The same trend was observed in both single- and bi-layer MREs.

It was also observed that the single-layer MREs showed an initial strain-softening effect under magnetic field and at strains below 10% followed by strain-stiffening at higher strains. Bi-layer MREs and material D, however, did not show such an initial softening effect. Nevertheless, single-layered MREs did not exhibit the softening effect without a magnetic field. For example, Fig. 2.9 compares the stress-strain curve of MRE C at zero and 365mT magnetic fields.

For a magnetic field parallel to the mechanical loading, Han *et al.* [77] have associated the strain softening of MREs to the increment of the inter-particle distances in shear and tensile tests. Their findings suggest that in compression, as the particle distance decrease along the magnetic field, only strain-stiffening is expected.

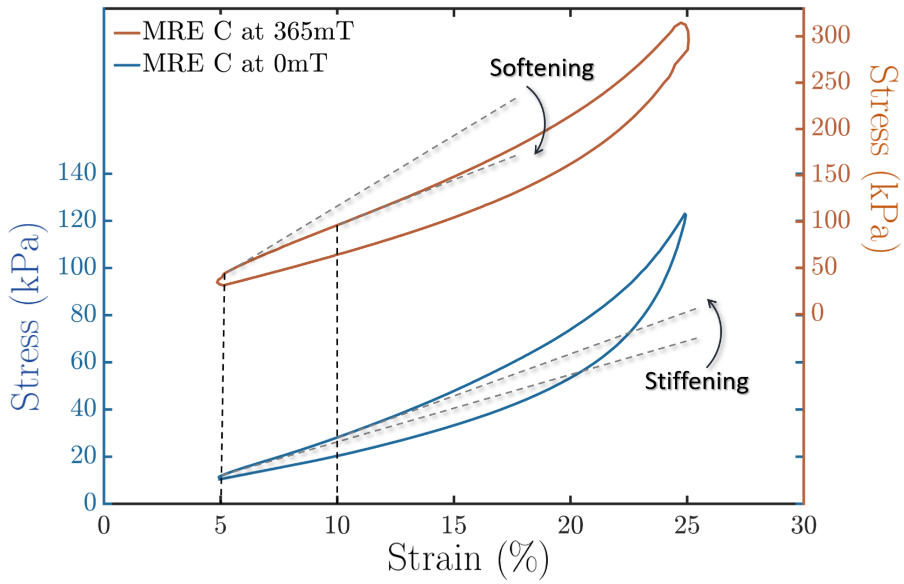

Figure 2.9: Exhibition of the initial strain-softening in MRE C in the presence of magnetic field.

In this study, the magnetic field was perpendicular to compression. It is believed that the initial softening effect might have been related to the increment in the inter-particle distances in the transverse plane to the load, as the samples bulge laterally under the compression. Since the magnetic field is also applied in the transverse plane, low strains cause CIPs to be pushed laterally into more powerful magnetic field, which further softens the material. At higher strains, however, compaction of elastomer matrix as well as decreasing inter-particle distances between CIPs dominate the effects of lateral expansion and causes the stiffening effect. Supported by the evidence in Fig. 2.9, it is considered that the initial softening effect as an exclusive result of transversal application of the magnetic field.

The minimum and maximum observed MR-effect were for MRE A, and MRE C-D with 160% and 253% at 365mT, respectively. The maximum MR-effect observed in this study was approximately half of findings with similar MREs in [25]. For example, a similar MRE to MRE A (ecoflex 00-20+25% CIP) demonstrated 301% of MR-effect in [25], while its MR-effect was 160% in this study. Also, MRE B and C showed 187% and 211% of MR-effect in this study, while similar MREs showed approximately 245% and 450% in [25]. From the comparison, it is believed that the weaker

MR-effect in this study was mainly due to the transverse application of magnetic field. This finding showed that the MREs would exhibit weaker (almost half) the MR-effects along the perpendicular axis to the direction of magnetic field; thus, confirms the need for a compensation mechanism, e.g. bi-layer configuration.

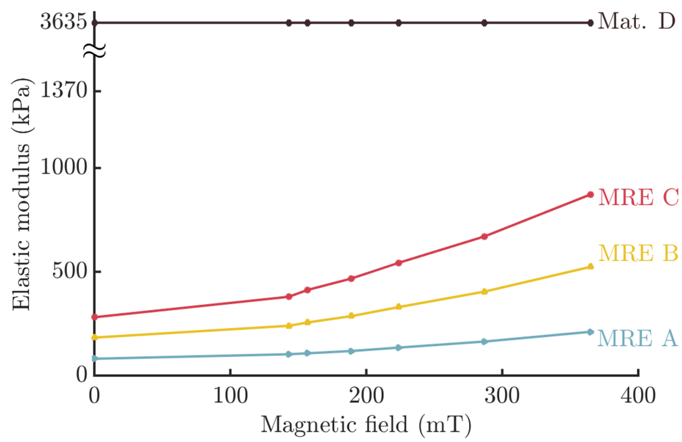

(a)

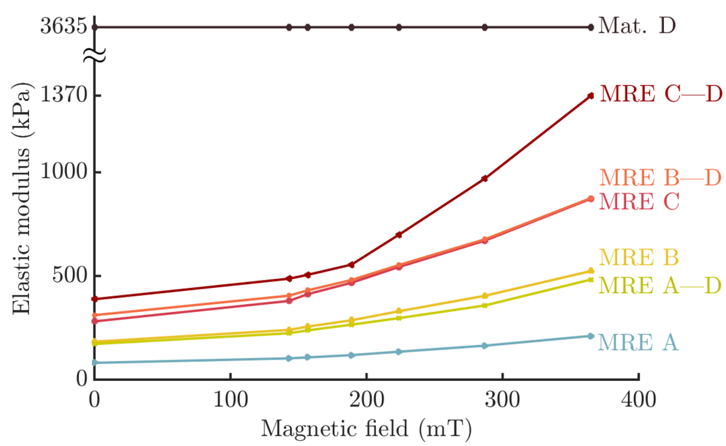

(b)

Figure 2.10: Variation of modulus of elasticity of MREs with respect to the change in magnetic field for (a) single-layer MREs, (b) MRE-non-MRE composites.

In addition, it was observed that in MRE-MRE composites, bi-layer configuration not only did not enhance the MR-effect, but also did decrease it with respect to the stronger MRE e.g. MRE A-B, A-C, B-C. For example, single layer MRE C showed 211% of MR-effect, while MRE B-C

had 205% of MR-effect. The maximum decrease in MR-effect in MRE-MRE composites was for MRE A-C, in which MR-effect decreased 25% from 211% (single-layer MRE C) to 186%.
Furthermore, MRE-non-MRE composites show higher elastic moduli at zero magnetic field compared to their MRE components; however, all MRE-non-MRE composites showed enhanced MR-effects compared to the MR-effect of their MRE component. The maximum enhancement was in MRE C-D, in which MR-effect increased 42% from 211% (single layer MRE C) to 253%. Also, MRE B-D and MRE A-D showed increment in MR-effect of 24% and 21%, respectively. These findings are in agreement with the theoretical explanation in Sec2.2.2 where a non-MRE with high-enough elastic modulus would be necessary for enhancing the MR-effect in an MRE-non-MRE composite. Fig. 2.10 (b) shows the variation of the elastic moduli of single- MREs and bi-layer MREs made with a material D layer.
As depicted in Fig. 2.10, MRE A-D and MRE B-D exhibited elastic moduli similar to moduli of MRE B and MRE C, respectively. This finding, shows that attaining elastic modulus and MR-effect similar to those of an MRE with higher CIP content is possible through MRE-non-MRE composition.

2.4 Conclusions

In this study, first an MRE-based haptic display system was conceptualized. Moreover, the requirements of such haptic display were reviewed and different options for a haptic display were compared. By the comparison, it was inferred that MREs are amongst the best options for developing a haptic display. However, from a practical points of view, the magnetic field would be necessary to be applied on the transverse plane to the touch (loading) direction. Therefore, the first objective of this study was to investigate the MR-effects on MREs when magnetic field was perpendicular to the loading. From the theoretical point of view, it was also predicted that MR-effect would be less when the magnetic field is in the transverse direction. Therefore and to compensate the loss, it was found a necessary condition for a composite bi-layer MRE-non-MRE when a composite would show more MR-effect than its MRE component.
The two hypotheses of this study were examined through a series of experiments. The experiments designed to resemble the use-case of haptic display (quasi-static compression test). Also, the composition of MREs and composites were selected according to the available literature for the sake of comparison. Results revealed that MREs exhibit less (approximately half) MR-effect when the

magnetic field is applied in transverse direction. Also in the presence of a magnetic field, single-layered MREs showed an initial strain softening in compression. This finding was unprecedented in other studies and was deemed related to the transverse application of the field. Also in this study, the MR-effect of MREs with 25%, 35%, and 45% CIP were enhanced by up to 42% in a composite structure. Such enhancement could be considered as a partial compensation of the lost MR-effects with a transverse magnetic field.

Moreover, incorporation of different non-MREs in an MRE-non-MRE composite enables researchers to decide on the initial modulus of elasticity of the composite selectively. This finding is utile in applications such as a haptic display, where various types of MREs can be fabricated for mimicking mechanical properties of different biologic tissue. To further demonstrate the feasibility of an MRE-based haptic display, Table 2.5 summarizes the range of elastic moduli of five biologic tissues and the candidate MREs of this study.

Table 2.5: Elastic modulus of sample biologic tissues

Biologic tissue	Elastic modulus (kPa)	Material for haptic display
Breast tissue [78, 79]	300 - 900	MRE B-D
Forearm skin [80]	420 - 850	MRE C-D
Facial skin [81]	130 - 260	MRE A-B
Cornea [82]	300 - 800	MRE B-D
Heart tissue[83]	110-300	MRE A-B

In this study, only Dragon Skin elastomer was used for feasibility purposes; however, in future studies researchers could explore more elastomers to investigate its effects on the enhancement of MR-effect. Also, theoretical feasibility of such enhancement when magnetic field is in the direction of compression could be studied. Furthermore, more accurate hyper-elastic material models e.g. 2 or 3-term Mooney-Rivlin, could be used to derive a (semi-) analytical minimum necessary elastic modulus for MR-effect enhancement. Nevertheless, instead of compositing an MRE with one high-stiff non-MRE, researchers could investigate the feasibility of decreasing the effective modulus of MRE through sandwiching it with soft (non-) MREs and further composition of the sandwich with a moderate stiff non-MRE.

Chapter 3

Development and Assessment of a Stiffness Display System for Minimally Invasive Surgery based on Smart Magneto-rheological Elastomers

Abstract

In this study, a solution to address the clinical need for stiffness display during manual and robotic minimally invasive surgery was investigated. To this end, a magneto-rheological elastomer-based stiffness display, *MiTouch* , was designed, developed, and analyzed. The mechanical properties of the MRE and system parameters were identified experimentally; based on which, the force-field-stiffness response surface of the smart MRE was characterized. Based on the response surface, a stiffness controller was designed and verified for a set of performance requirements. A heart-beat simulation experiment showed the capability of the system for replicating desired tactile forces through stiffness control. Also, the system successfully attained an arbitrarily selected stiffness ($4{}^{N}/{}_{mm}$) and maintained it within a bounded range ($4.07 \pm 0.41{}^{N}/{}_{mm}$). Comparison of the system performance with current literature validated its applicability for the proposed medical application.

3.1 Introduction

3.1.1 Rationale and Motivation

Minimally invasive surgery (MIS) is a surgical approach during which long, and often flexible, surgical instruments are inserted and maneuvered inside a patient's body. In contrast to the open approach, a surgeon cannot directly touch an internal organ or tissue in the MIS approach. Therefore, surgeon's tactile perception is based on limited tactile cues transferred through the hand-held instruments.

Tactile information is even more limited in case of the robotic MIS (RMIS). RMIS systems consist of a master (console) and slave (robot) units. A surgeon controls maneuvers of the instruments at slave unit through remote controls on the master unit. Fig.3.1 depicts a typical master-slave configuration for RMIS. Such remote master-slave configuration totally diminishes the transfer of tactile information to surgeon. Tactile information is crucial for surgeons for accurate diagnosis and effective treatment[9, 66].

To alleviate this problem, researchers have proposed tactile displays. A tactile display is a medium with controllable bulk and/or surface properties, e.g. stiffness, roughness, texture, etc[9]. Tactile displays have been developed using various principles, i.e. DC-motors[9], pneumatics[22, 21], electro-active polymers (EAP)[24], shape memory alloys (SMA)[67], and magnetorheological fluids (MRF)[12, 13, 14].

From practical considerations, a tactile display is desirable to possess a non-zero passive stiffness so that changing its stiffness to a lower and higher stiffness is possible with low power-consumption. If a tactile display posses a zero passive stiffness, it will need constant power consumption for maintaining a 'base' stiffness. For example, MRFs, due to their fluidic state do not possess a non-zero passive stiffness.

Furthermore from a user safety perspective, electrical passivity of the variable stiffness medium is favorable. Nevertheless, fast response, low power consumption, simplicity of design and working principle, slim profile, and high dynamic stiffness range are amongst other criteria desired in tactile displays. More importantly, a tactile display for RMIS application must be disinfectable and sterilizable to comply with infection control procedures in hospitals. With this perspective, Table 3.1 compares the representative studies on novel tactile displays in the literature.

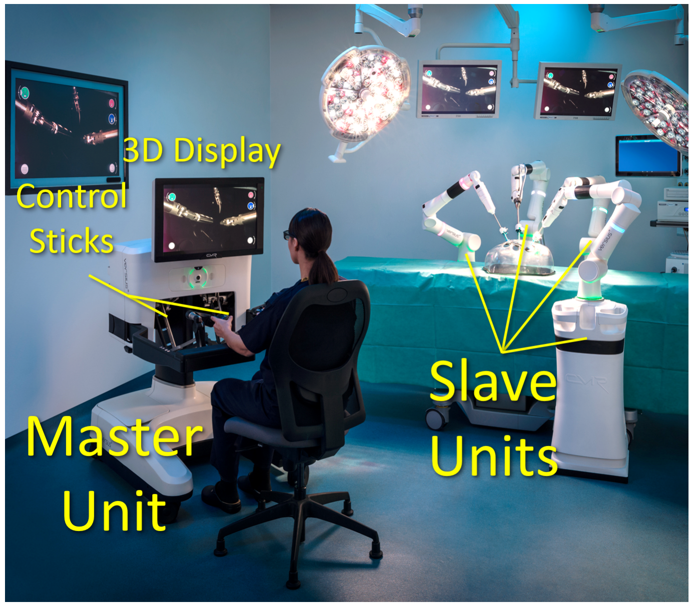

Figure 3.1: Typical master-slave configuration for robotic surgery systems (Versius, courtesy of CMR Surgical Ltd., Cambridge, UK.)

3.1.2 Literature review

MREs are a class of smart materials with controllable mechanical properties, e.g. stiffness. MREs are composed of an elastomeric matrix with dispersed ferromagnetic iron particles. Upon application of an external magnetic field, iron particles align with the field while attached to the elastomeric matrix. The physical alignment of particle with the field incurs internal strains in the matrix; thus, changes the internal strain energy density of the MRE, [84]. The extent of particle aligning with the field depends on the volume fraction of particles, their intrinsic magnetism, and the strength of magnetic field [49, 50].

MREs, thanks to their solid state, intrinsically possess non-zero passive stiffness. Also, MREs are fast in adaptation to the external magnetic field for real-time applications[85]. On the dynamic stiffness range, a recent study have shown up to 1672% of increase in the elastic modulus for MREs[25]. Furthermore, slim profiles are possible through proper molding and cutting of MRE sheets. Nevertheless, recently novel MREs, e.g. PDMS-based MREs, have been introduced for medical and cellular intervention which are bio-compatible and sterilizable[86]. Therefore, MREs are a fitting candidate for developing a tactile display for MIS and RMIS applications.

Table 3.1: Comparison of representative studies proposing novel tactile displays for MIS and RMIS.

Study	Tactile cue	Principle	Advantages	Limitation
Culjat *et al.* [21] (2008)	Stiffness	Pneumatic	MR-safe, dynamic range, simple, low profile	Zero passive stiffness, specific for da Vinci robot
Dargahi *et al.* [9, 87] (2012,2016)	Stiffness	DC motor	Fast, cheap, simple	Dynamic range, not MRI-safe, electrically active
Oh *et al.* [12, 13] (2013)	Stiffness	MRF*	Passive stiffness, simple, dynamic range	Electrically active, not MRI-safe
Han *et al.* [24] (2018)	Stiffness	EAP†	MRI-safe, passive stiffness	Complex, electrically active
Kanjanapas *et al.* (2019)[22]	Texture	Pneumatic	MRI-safe, dynamic range	Complex, zero passive stiffness
Yanatori *et al.* [67] (2019)	Stiffness	SMA‡	Passive stiffness, simple	Electrically active, not MRI-safe, dynamic range
Mazursky *et al.* [14] (2019)	Stiffness	MRF	Passive stiffness, simple, dynamic range, low profile	Electrically active, not MRI-safe
This study	Stiffness	MRE	Passive stiffness, simple, dynamic range, low profile electrically passive	not MRI-safe

*MRF: Magneto-rheological fluid †EAP: electro-active polymer ‡SMA: shape-memory alloy

MREs have been widely investigated under wide range of magnetic fields, i.e. 0-1600mT [38, 68, 30, 25]. Also, MREs have been characterized under quasi-static and dynamic strains [50, 31, 32, 33]. In an early effort, Li *et al.* [65] used a four-parameter linear visco-elastic model to model MREs. Their model was fairly accurate in predicting hysteresis and incorporated the magnetic field as a parameter. However, their model was a behaviorologic model and was accurate only at the trained range of frequency and magnetic field; thus, needed extensive test data for more general predictions. Also the model parameters were of no physical attribution. In another effort, Yang *et al.* [52] used a Bouc-Wen model to model the behavior of MREs in shear. They tested MREs at various frequencies, i.e. 0.1-4.0Hz and strain amplitudes, i.e. 8-32%. However, the model parameters in their studies varied with both magnetic field and strain amplitude; thus, lacked the generality. Similar limitation was also reported by Behrooz *et al.* in [88].

Nguyen *et al.* [26] also proposed a fuzzy-control framework based on a Zener solid model with a variable stiffness spring and coulombian friction. Their model was fairly accurate in predictions; however, its numerical foundation would not allow for derivation of a closed form contact stiffness formula to be exploited for stiffness control. Hybrid models have also been proposed to model the mechanical properties of MREs. Kumar *et al.* [60] proposed a hybrid Kelvin-Voit-Bouc-Wen model for MREs. Despite the accuracy of such models, high number of model parameters necessitated numerous training tests and yet the physical plausibility of the model parameters is to be elaborated. In a recent study, Dargahi *et al.* [25] proposed a ten-parameter Prandtl-Ishlinskii model with stop-operator to model MREs. Their model incorporated the volume-fraction of iron particles, magnetic field, and strain rate as inputs. They have reported a goodness-of-fit of 98% in predicting the MRE behavior under shear. However, high number of model parameters and its non-physical nature were its prime limitations.

In contrast to the behaviorologic models above, constitutive models generally are based on a continuum description of the energetic interactions of MRE with the environment. Such models have been developed based on microscopic [89, 90, 91, 92, 93, 94] and macroscopic structure of MREs [95, 96, 97]. A recent study showed a fair agreement between the predictions of macroscopic and microscopic models as well as 2D and 3D models[98]. Because of the large deformation of MREs, inherited by their elastomeric component, Mooney-Rivlin (MR)[99], Ogden Model[96], and Neo-Hookean solid Model[98], have been proposed for fitting the stress-stretch behavior of MREs. Also, thanks to the continuum nature of such models, stiffness, defined as the derivative of force with respect to the indentation depth, has been derived accordingly.

Despite, the physical plausibility and accuracy, derivation of a continuum-based contact stiffness necessitates employment of highly nonlinear contact mechanics of soft materials. Based on the literature review, no study has investigated the contact mechanics of MREs in particular. A number of studies, however, have focused on contact mechanics of hyperelastic materials in general. For example, Briscoe *et al.* [100] adopted the Hookean elasticity notation and presented a similar contact force-indentation and stress-stretch relationships. Their findings have been validated in [101, 102]. In another study, Lin *et al.* [103] provided a generalized closed form formulation for contact of a sphere and Mooney-Rivlin, Neo-Hookean, reduced polynomial, Ogden, Fung, Van der Waals(Kilian), Gaylord-Douglas, and Tschoegl-Gurer hyperelastic materials. Their proposed formulation incorporated a similar notation to the classical Hertzian contact, yet was fairly accurate in predicting contact force and indentation for hyperelastic large deformations.

In summary, the continuum-based studies reviewed above heavily depend on the model constants and solution techniques that are either cumbersome to determine for MREs or are computationally expensive to implement for real-time applications.

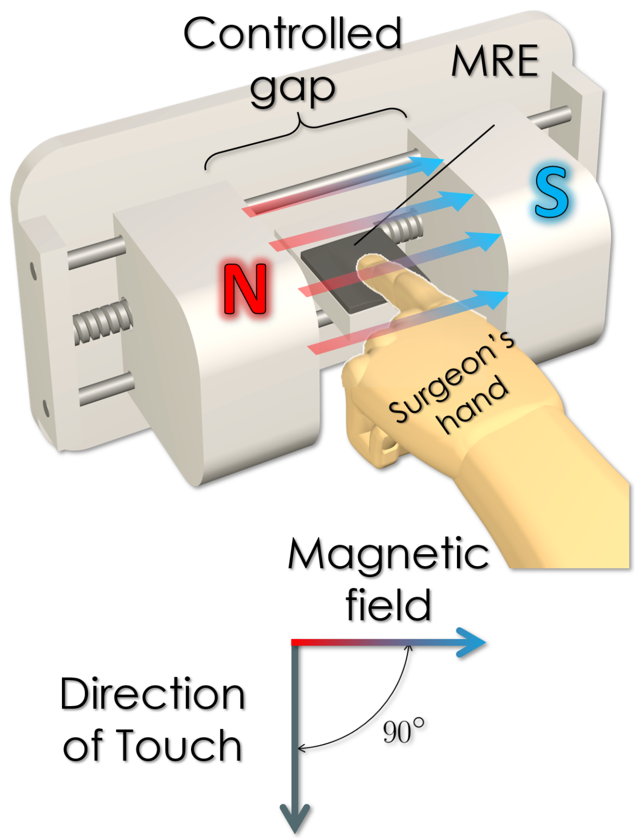

Figure 3.2: Schematic view of the proposed MRE-based stiffness display, *MiTouch* . The magnetic field on the MRE changes as the gap between the permanent magnets changes. Consequently, the stiffness of the MRE adapts to the strength of the magnetic field between the pair of permanent magnets.

To alleviate the limitations above, this study proposes a novel stiffness display, *MiTouch* , using rubber-based bi-layer composite magnetorheological elastomer (MRE). The proposed system is depicted in Fig.3.2.

MiTouch principally was designed based on the control of magnetic field on the MRE. To this end, a pair of permanent magnets were used. Such a use of magnets has been frequently employed in other studies, e.g. [25, 69, 25, 84, 59]. Moreover, a slim sheet of composite MRE placed at the midspan of two permanent magnets. Two DC motors coupled with worm-gears, were used for controlling the magnetic field via changing the gap distance between the magnets. Also, a force sensor was used to measure the touch force in real-time. Afterward, a closed-loop PID stiffness controller was designed and implemented incorporating an empirical force-magnetic field-stiffness surface.
In the following, the detailed design of *MiTouch* , at system- and module-level, is described. Moreover, the methods and results of the design and assessment of the control system as well as the identification and verification experiments are presented. Afterwards, Sec.3.3 presents the results and discussion for the validation tests performed to showcase the feasibility of stiffness control using the proposed system. In the end, the concluding remarks and future directions are discussed in Sec.3.4.

3.2 Material and Methods

In this section, the design and prototyping of the proposed stiffness display are presented. Afterwards, the fabrication of MRE composites, and design of the PID controller is described along with its experimental performance assessment. Also, the method used for testing and acquisition of the empirical force-magnetic field-stiffness surface is explored. Finally, the test apparatus and methods of representative experiments for assessing the performance of the display are discussed.

3.2.1 System Design

The proposed stiffness display, *MiTouch* , was designed as a software-hardware integrated system. The main subsystems of *MiTouch* were the mechanical, electrical, and software modules. Fig.3.3 depicts the system design and components used in *MiTouch* .

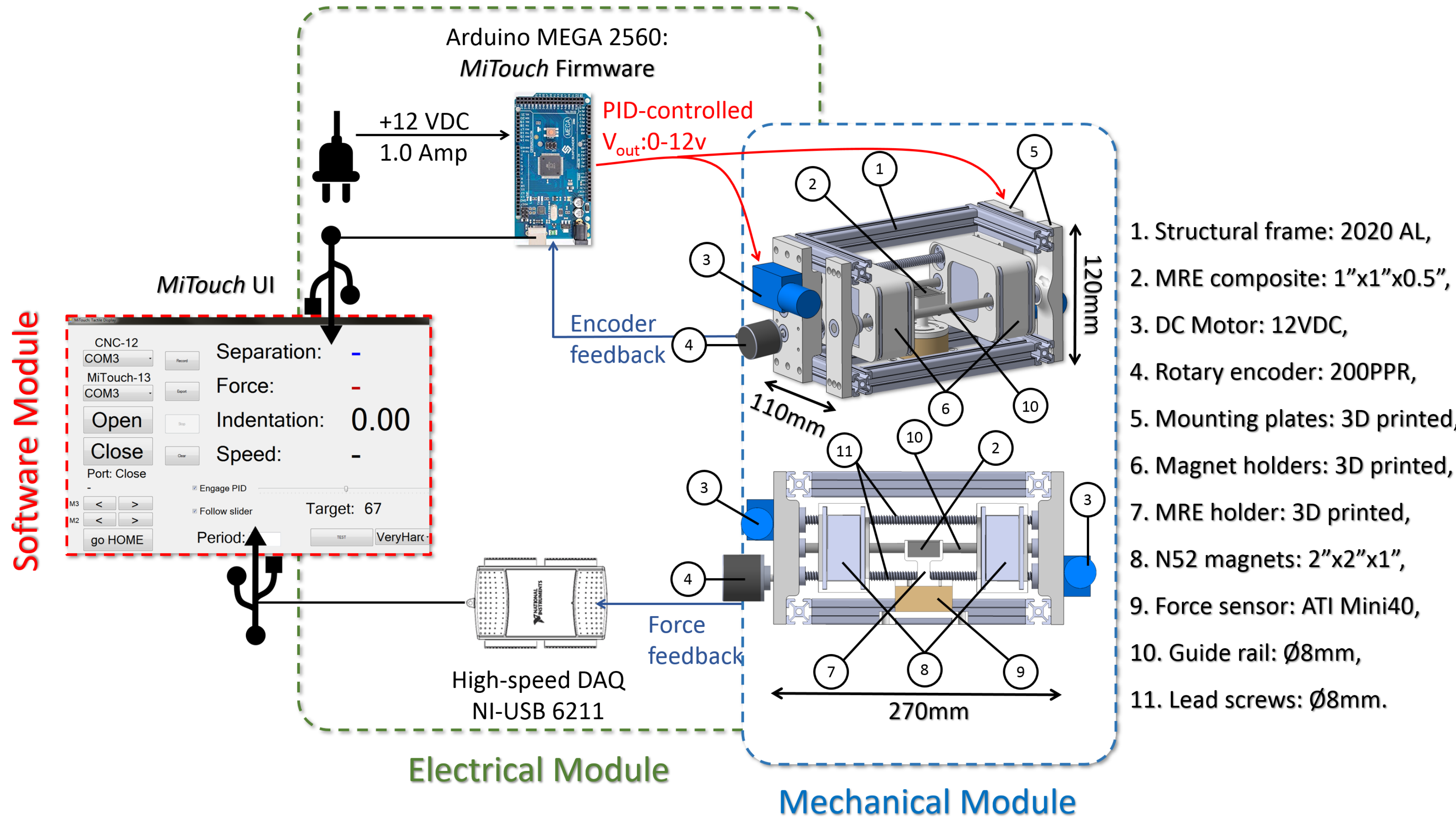

Figure 3.3: High-level system design and inter-connectivity of the subsystems in *MiTouch* .

3.2.1.1 Mechanical module

The mechanical module consisted of a structural frame made of 20mm×20mm aluminum extrusions, which provided a base frame for anchoring other mechanical components. Two Neodymium N52 magnets ($2'' \times 2'' \times 1''$, CMS Magnetics, Inc., Texas, USA) with coercive force of 875$^{kA}/_{m}$ and remanence of 1.45T were used to provide a homogeneous magnetic field.

Each magnet was secured in a custom-designed 3D-printed magnet holder (110mm×70mm×40mm), using two $^{1}/_{4}$mm-acrylic sheets at its left and right. The magnet holders housed two linear bushes for facilitating the passage of the front and rear linear guides. Another linear bush was anchored in the holder to facilitate the passage of non-engaging leading screw while a leading nut (M10-L10mm, 10mm-pitch) was used to engage with the other leading screw. Each leading screw was coupled with one of the DC motors (JGY370-12V, BringSmart Intelligent Tech. Co. Ltd., Fujian, China) using a flexible shaft coupler(ϕ8×6mm-L15mm).

The shaft speed of each motor was reduced with a 1:60 reduction worm gear resulting in a maximum shaft speed of 150RPM. Utilization of worm gears enabled the system to be self-locking against the pull force between the two magnets and served as a safety measure. Also, the self-locking would enable the system to hold the magnets at a desired separation through passive resistance and without power-consumption.

To obtain the position of the magnet holders, the end of one of the leading screws was coupled with a 400 pulse-per-revolution incremental rotary encoder (SEN0230, DFRobot Co., Shanghai, China). Each clockwise revolution of the leading screw would result in 400 pulse of the encoder and would represent +10mm of displacement of the each magnet holder, and +20mm increment of the gap separation. Due to the symmetry in the system configuration, and similarity of the magnets, leading screws, motors and gears, only one encoder was used for the sake of simplicity. The following equation was used to measure the current gap separation, s between the magnets.

$$s = s_{\circ} + \frac{2 \times 10 \times P}{400} (\text{mm}), \tag{16}$$

where s is the gap separation between the two magnets, $s_{\circ}$ is the initial gap separation, and P is the count of pulses from the encoder. Factor 10 converts the number of revolutions, $^{P}/_{400}$ to the moved distance of one magnet on the leading screw and factor 2 is doubles the moved distance to count for symmetric driving of both magnet holders. With this design, each motor would control the motion of one magnet holder, while the holder was supported with the front and rear guide rails and the non-engaging leading screw. The maximum gap separation of 95mm and minimum gap separation of 45mm were reachable with the current design. Fig.3.4 depicts the design of a magnet holder in details.

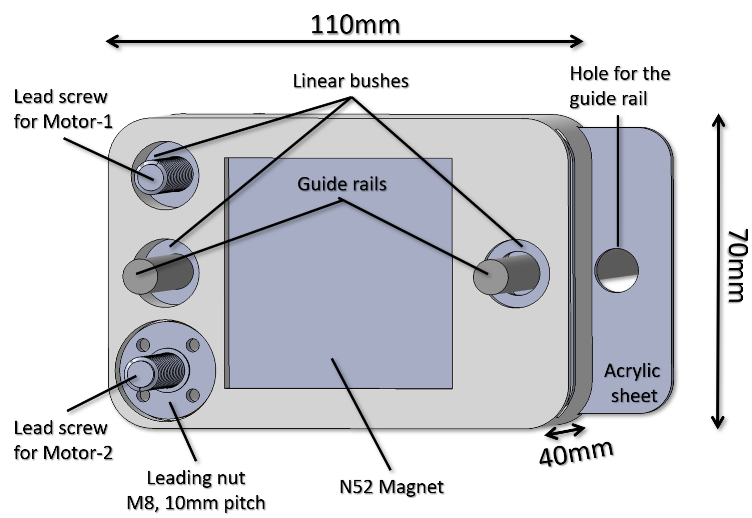

Figure 3.4: Detail-view of the designed magnet holder used in *MiTouch* prototype.

In order to find the relationship between the magnetic field at the center of MRE and the separation, s, the magnets were manually set to 21 random distances, while reading the magnetic field on the MRE with a Gaussmeter (GM2, AlphaLab Inc., PA, USA). Fig.3.5 shows the results of the Gaussmetry. Eq.17 represents the fitting of magnetic field, B and separation, s based on the Gaussmetry test results (R^2=0.97, RMSE=5.76mT).

$$B = 43770s^{-1.413}(\text{mT}) \equiv h(s), \quad 45 \leq s \leq 95 \tag{17}$$

where $h(s)$ is the function defined representing the equation.

3.2.1.2 Electrical module

As depicted in Fig.3.3, the electrical module included a 12-volt DC power-supply with 1.0Amp maximum current for driving the motors, an Arduino embedded board (MEGA 2560, Arduino Co., MA, USA) powered through a USB connection to PC, a pre-calibrated ATI-Mini40 force-torque sensor(SI-20-1, ATI Industrial Automation Inc., NC, USA), with a force resolution of 0.01N, and a high-speed USB data-acquisition (DAQ) board (NI USB 6211, National Instruments Corp., TX, USA).

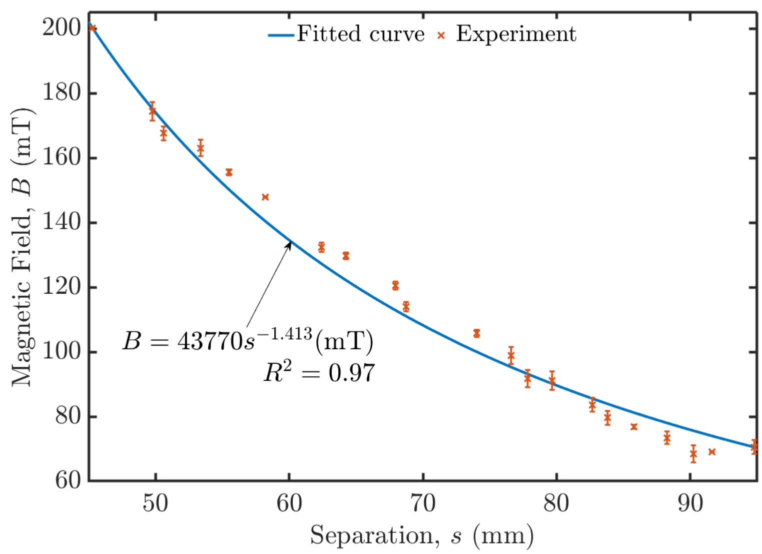

Figure 3.5: Variation of the magnetic field on the MRE with respect to the gap separation between the magnets.

The Arduino board was uploaded with the *MiTouch* firmware to acquire the real-time gap separation feedback, implement the PID controller, and relay/receive data to/from the *MiTouch* user interface (UI). All the USB serial connections were through USB-3.0 ports.
Motors were synchronously controlled through pulse-width-modulation (PWM). PWM is a digital-to-analog modulation technique, where a high-frequency(64kHz) alternation between 0v and +12V with ON-periods between 0-100% would result in corresponding 0-12V RMS voltage on motors.

3.2.1.3 Software module

The software module was comprised of two independent codes, i.e. *MiTouch* firmware and *MiTouch* user interface (UI). Fig.3.6 depicts the software design architecture proposed and implemented in this study. The PID control of the gap separation was implemented in the firmware; where, Arduino board was constantly maintaining the latest received target separation command. Using Eq.16, the embedded board would compare the current separation with the latest command and drive motors respectively. At the end of each loop, the firmware would relay the current separation back to the UI based on the latest feedback from encoder. For the sake of synchronization, the refresh-rate of firmware was set to 100Hz.

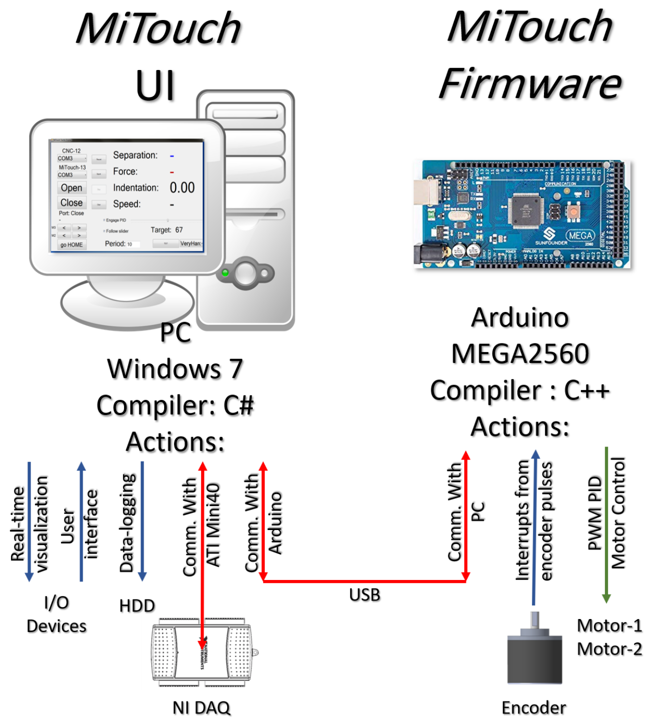

Figure 3.6: Software design architecture implemented in this study.

On the other hand, to achieve real-time performance, i.e. >30Hz[9, 66], the UI was parallelized for the communications with ATI Mini40 DAQ and firmware, user interfacing, and data-logging. Same as the firmware, the refresh-rate of ATI Mini40 DAQ, data-logging, user-interface and PID set-point corrections were programmatically set to 100Hz. ATI Mini40 DAQ was originally running at 1kHz refresh-rate; therefore, a ten-data averaging was implemented in the ATI Mini40 DAQ parallel thread. Fig.3.7 shows the final assembly of the developed system.

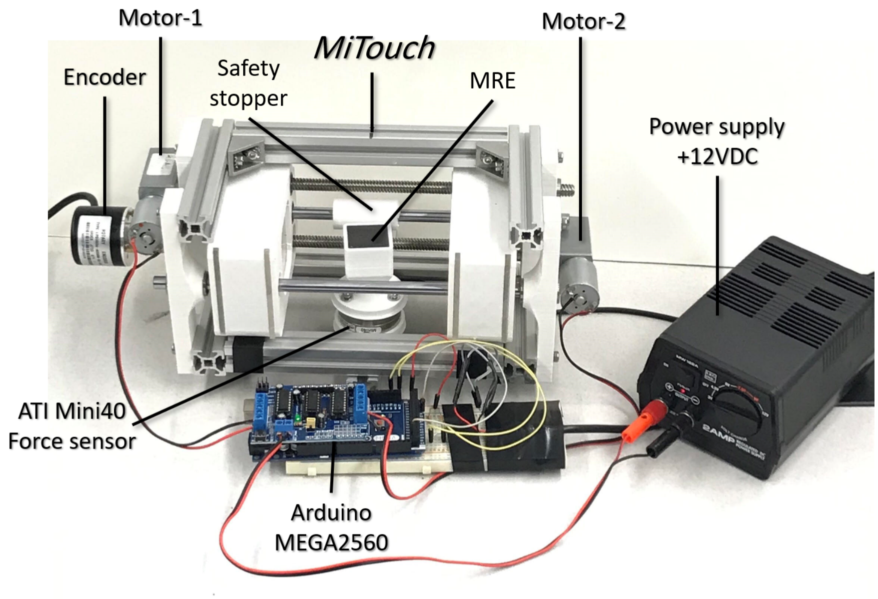

Figure 3.7: Final assembly of *MiTouch* . The front top horizontal Aluminum extrusion is removed intentionally for better visibility.

3.2.2 MRE Selection and Fabrication

For the MRE, the recent fabrication method reported by Dargahi *et al.* [25] was adopted. Also, our recent findings in [104] (see Appendix A for our previous work) validated the reproducibility of the MREs and showed enhanced magneto-rheological (MR-)effect with a bi-layer MRE composite. The maximum MR-effect was achieved using a composite made of a layer of silicon-rubber-based MRE (EcoFlex 00-20, Smooth On Inc., PA, USA) with 45% volume iron particle content and a non-MRE layer (DragonSkin™30, Smooth On Inc., PA, USA). The reason to choose this composition was to achieve the highest dynamic range of stiffness.

On this basis, the constituent of the fabricated MRE composite was adopted from [104] and are summarized in Table 3.2. The weight composition of silicon-rubber, CIPs, slacker, and thinner per 100cc of total volume of each material were calculated using:

$$m_Y = \rho_Y \nu_Y V_{total}, \tag{18}$$

where, Y was, silicon-rubber, slacker, silicone thinner, CIPs, or DragonSkin; while, m was mass, ρ was density, ν was volume fraction, and V_{total} was 100cc.

Table 3.2: Density, ρ_X, volume fraction, ν_X and mass, m_X of the contents in the fabricated elastomers.

Material	Contents ν_Y, m_Y				
	Silicone rubber	DragonSkin	Slacker	Silicone thinner	CIPs
	$\rho_{SR} = 1.04\frac{gr}{cc}$	ρ_{DS} =1.08$\frac{gr}{cc}$	ρ_{SL}=0.97$\frac{gr}{cc}$	ρ_{ST} =0.97$\frac{gr}{cc}$	ρ_{CIP} =7.87$\frac{gr}{cc}$
non-MRE Material (DragonSkin)	-	90%, 97.2gr	5%, 4.9gr	5%, 4.9gr	-
MRE Material (EcoFlex 00-20)	45%, 46.8gr	-	5%, 4.9gr	5%, 4.9gr	45%, 354.2gr

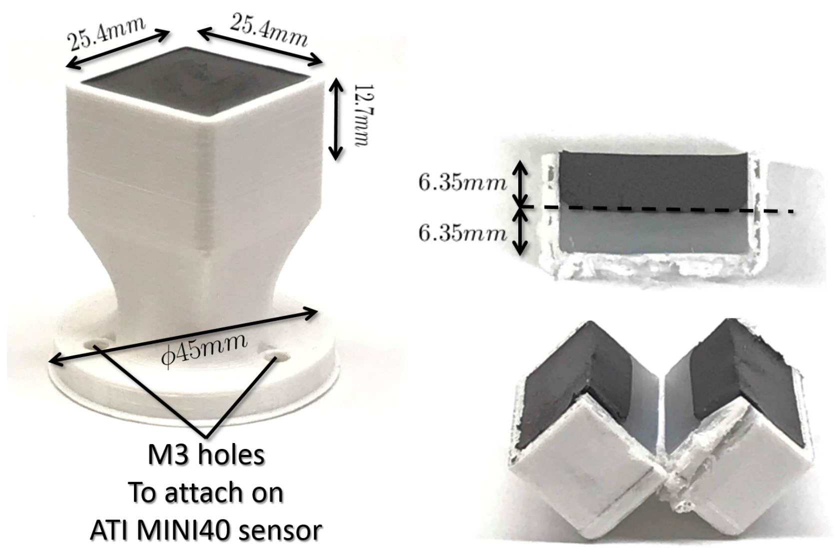

(a) (b)

Figure 3.8: (a) Final cured MRE composite in the 3D-printed mold, (b) cross-sectional views of the MRE composite showing two layers bonding at the intersection.

For molding, initially the non-MRE mixtures was poured into a 3D-printed mold with $25.4mm$ $\times 25.4mm$ surface area resulting in a first layer with $6.35mm$ depth. The half-filled mold was placed in a vacuum chamber (Best Value Vacs, IL, USA) and maintained at 29inHg vacuum pressure for 5 minutes to obtain a bubble-free layer. Finally, the mold was cured at rest in room temperature for 24 hours.

The same process was repeated with MRE mixture to form the MRE layer on top of the non-MRE cured layer. With this method, limited natural dispersion of top layer into bottom layer occurred and the two layers were fused physically without a need for gluing. Fig.3.8 shows the final cured MRE composite in model along with its cross-sectional view.

3.2.3 Force-Magnetic Field-Stiffness Surface

Previous studies have shown that an MRE exhibits different force-displacement curves, and consequently different stiffness, when exposed to different magnetic fields, e.g.[104, 25, 69]. In order to obtain the stiffness behavior of the MRE under contacting with surgeon's finger and at various magnetic fields, a total of 21 indentation tests were performed, i.e. 7 magnetic fields and 3 repetitions. The tests were performed at seven gap separation, i.e. 95, 90, 85, 75, 65, 55, and 45mm. The corresponding magnetic field feedback based on the actual separation at *MiTouch* were 70, 76, 86, 98, 127, 154, and 199mT, respectively.

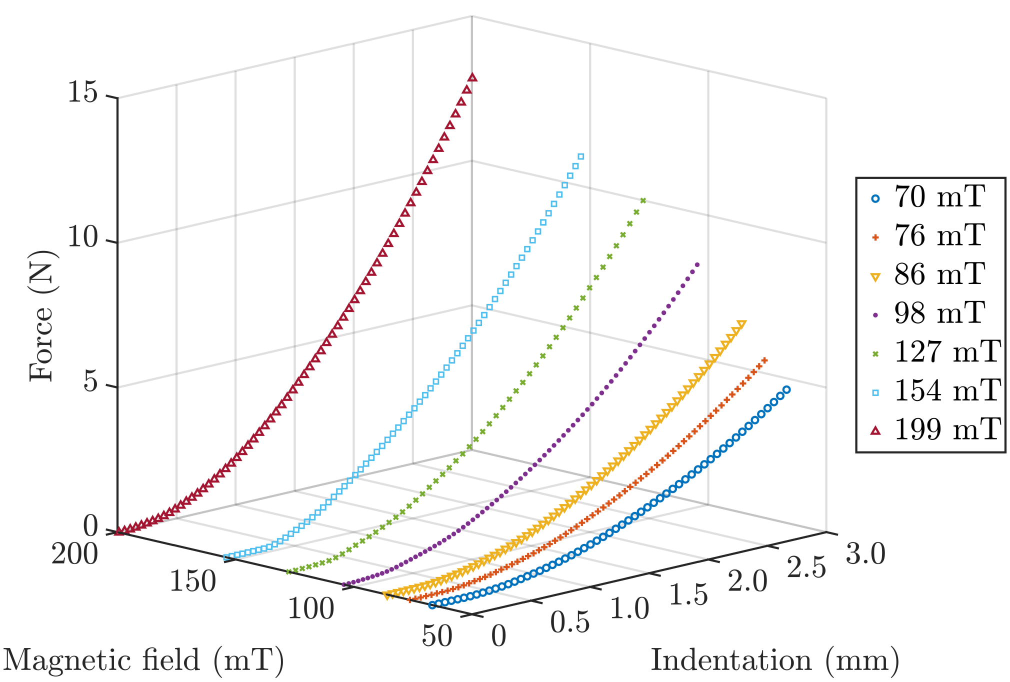

(a)

Figure 3.9: (a) average force-indentation, (b) average stiffness-force curves of the MRE at seven different magnetic fields, and (c) fitted stiffness surface with marked experimental data-points. Contours indicate the iso-stiffness curves on the surface *(cont.)*.

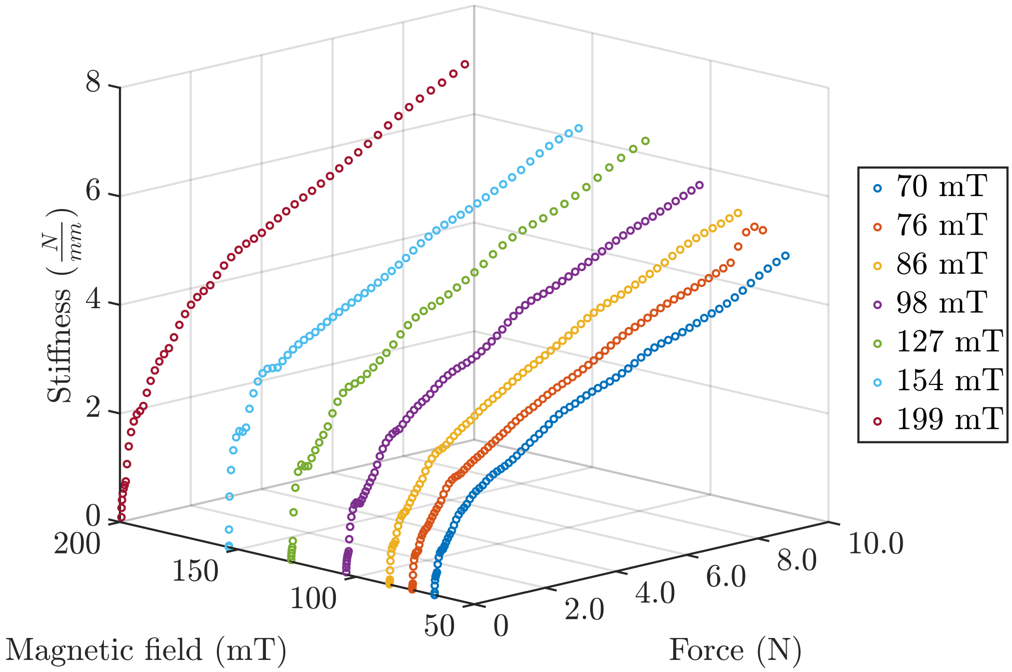

(b)

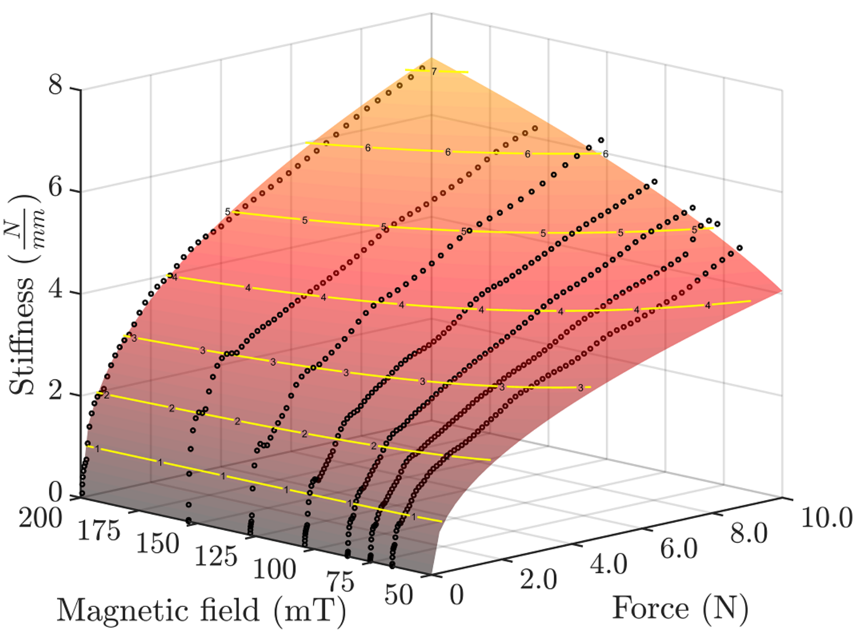

(c)

Figure 3.9: (a) average force-indentation, (b) average stiffness-force curves of the MRE at seven different magnetic fields, and (c) fitted stiffness surface with marked experimental data-points. Contours indicate the iso-stiffness curves on the surface.

The tests were performed using a phantom index finger. The finger was 3D-printed and used to replicate the surgeon's finger. The finger was 20mm in diameter and 72mm in length. The anthropometric dimensions of the index finger were adopted from Blackstone *et al.* [105]. The finger was secured on a home-made three-axis desktop computer numeric controlled (CNC) machine. The CNC machine had $\pm$0.05mm precision in linear position control and was controlled through a macro code on the *MiTouch* UI. Prior to each test,the CNC machine was manually maneuvered until the finger would align center with the MRE and come to contact with it, i.e. contact force more than 0.05N. Afterwards, the finger was moved vertically up until the contact force would return to 0N.
In each test, the finger was indented into the MRE with a rate of 0.33$^{mm}/_{sec}$ until the indentation reached 3mm. This rate was previously shown to discard the stress-relaxation effect in the same MRE, yet is slow-enough not to induce rate-dependency effects[104]. The force-indentation data were obtained for the three repetitions and averaged. Fig.3.9 depicts the average force-indentation curves on the MRE for the indentations up to 3mm.
As depicted in Fig.3.9(a), MRE exhibited strain-stiffening behavior as indentation was applied. The contact force increased with increasing the magnetic fields. For example, at the indentation of 3mm, contact force was 4.60N with 70mT magnetic field while it increased to 12.87N at 199mT (MR-effect=180%). This finding is in agreement with our previous findings in [104]. Afterwards, the average force-indentation graphs for each magnetic field were differentiated with respect to indentation,δ to obtain the contact stiffness. Fig.3.9(b) represents the variation of contact stiffness with respect to the contact force at seven different magnetic fields.

It is important to note that the tactile stiffness felt by the surgeon is the contact stiffness between her/his finger and the tactile medium [9, 66], i.e. MRE. Therefore, an empirical stiffness-magnetic field-force surface was obtained by optimizing the unknown coefficients of Eq.19:

$$k = aF_c^p B^q \equiv f(F_c, B), \tag{19}$$

where, $f(F_c, B)$ is the function representing the equation, a, p, q were the fitting parameters, and k, F_c, B were the contact stiffness, contact force, and magnetic field, respectively. The surface fitting was performed in Curve-Fitting Toolbox of Matlab (R2019a, Mathworks Inc., MA, USA). Table3.3 shows the optimized parameters and Fig.3.9(c) represents the fitted surface and the experimental data-points. The horizontal contours on the surface shows the iso-stiffness lines, on which the controller shall control the magnetic field to keep a specific stiffness. The choice of contact force for the fitting variable was based on:

(1) the contact force was available in real-time through direct measurement,

(2) it eliminated the need for a contact mechanics-base constitutive model for the estimation of the indentation depth,

(3) the viscoelastic stress-relaxation of MRE, which happens under slow loading conditions, would affect the force not the displacement; thus, PID controller would respond to force and compensate for such nonlinear effects.

Table 3.3: Optimized fitting parameters for stiffness-magnetic field-force surface.

Parameter	Value	95% Confidence interval
a	0.3103	(0.3034, 0.3172)
p	0.4266	(0.4244, 0.4288)
q	0.4063	(0.4016, 0.4110)

3.2.4 Stiffness Control System

In order to maintain or follow a desired stiffness, $k^\star$ during the touch (compression), the tactile display must adaptively change the external magnetic field according to the contact force. Due to the strain-stiffening behavior of MRE (Fig.3.9(a)), the surgeon would feel more stiffness with more indentation of finger into the MRE. Therefore, the control system must accordingly decrease the stiffness of MRE through decreasing the magnetic field. With this logic, although the contact force tends to increase as the surgeon's finger indents more into MRE, the controller regulates (decrease) the force through decreasing the stiffness via decreasing the magnetic field.

3.2.4.1 Controller design

To control the stiffness, a closed-loop control system was designed as depicted in Fig.3.10. In the proposed system, a desired stiffness $k^\star$ is set as the input through the UI. Using inverse function $f^{-1}(F_c, k^\star)$, a desired magnetic field $B^\star$ is obtained. Accordingly, the inverse function $h^{-1}(B^\star)$ estimates a desired gap separation $s^\star$ which is fed forward as the set-point of the discrete PID control loop.

To find a proper set of PID coefficients, $k_{P,I,D}$, motor and transmission transfer functions were necessary to obtain. To this end, the symmetric step response of motors were obtained for a step pulse input of ± 12V with a pause of 1.5sec. For better identification, the separation between magnets, s was considered as the output and voltage on the motor as the input. Fig.3.11 shows the average step response of the motors. System Identification Toolbox of Matlab was used to fit a third-order discrete transfer function (Eq.20) to the symmetric step response. The third-order transfer function was chosen to directly model the gap separation with respect to the voltage without a need for integrating velocity.

$$M(z) = \frac{-0.107}{1 - 0.942z^{-1} - 0.483z^{-2} + 0.425z^{-3}}, \tag{20}$$

where, $M(z)$ is the transfer function of motors in $z-$domain.

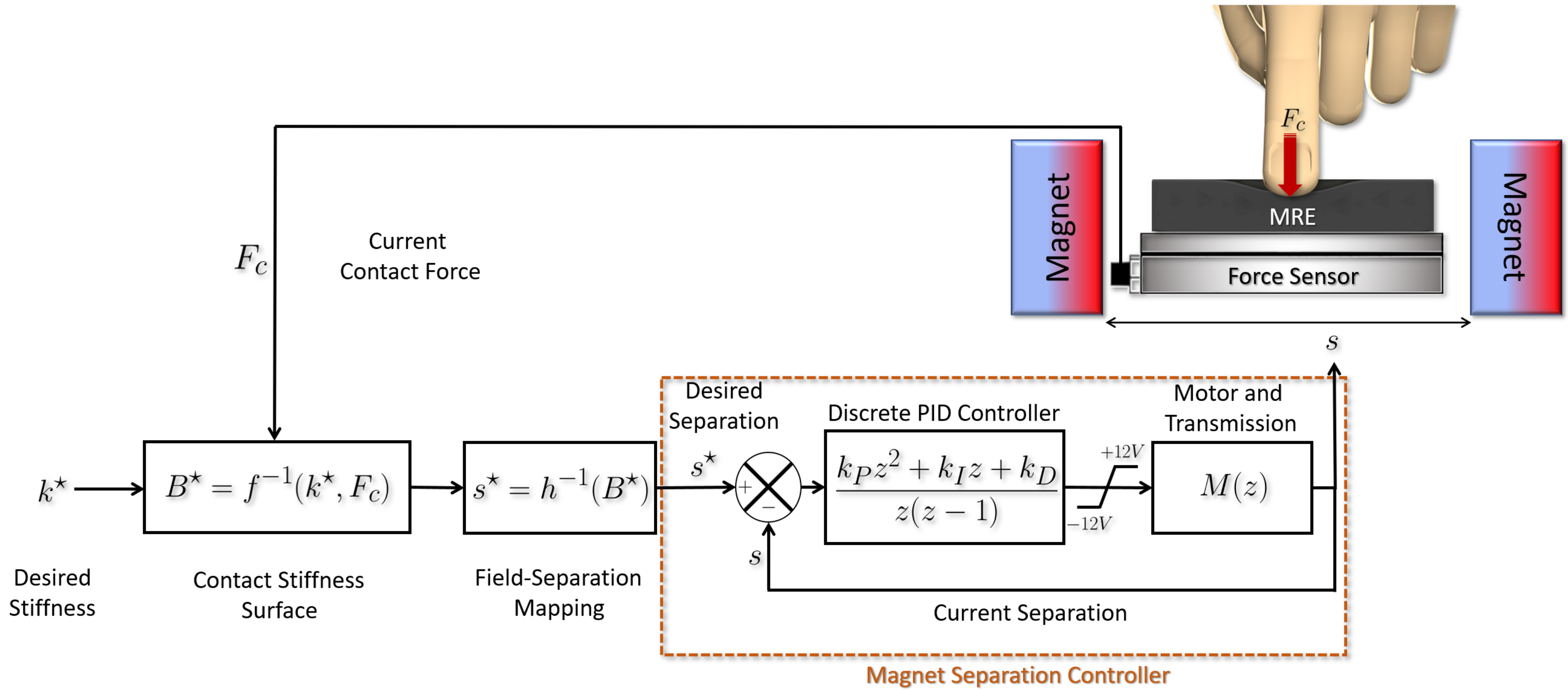

Figure 3.10: Proposed feedback loop for controlling stiffness of MRE for realtime stiffness adaptation in tactile display.

3.2.4.2 Controller assessment

Using $M(z)$, the magnet separation controller was modeled in Matlab Simulink environment and PID Tuner was used to obtain $k_{P,I,D}$. Table3.4 summarizes the PID coefficients, requirements for the system response, model predictions and the actual performance of the system for unit step input with reversal. As summarized in Table3.4, the response of *MiTouch* control system met the requirements set on rise-time, settling-time, error and overshoot. Although, the rise-time of the actual system was larger than the model, it resulted in less overshoot and less steady-state error. The relatively slower response of the system could be related to the uncaptured factors in the assembled system, e.g pulling force from magnets, and friction.

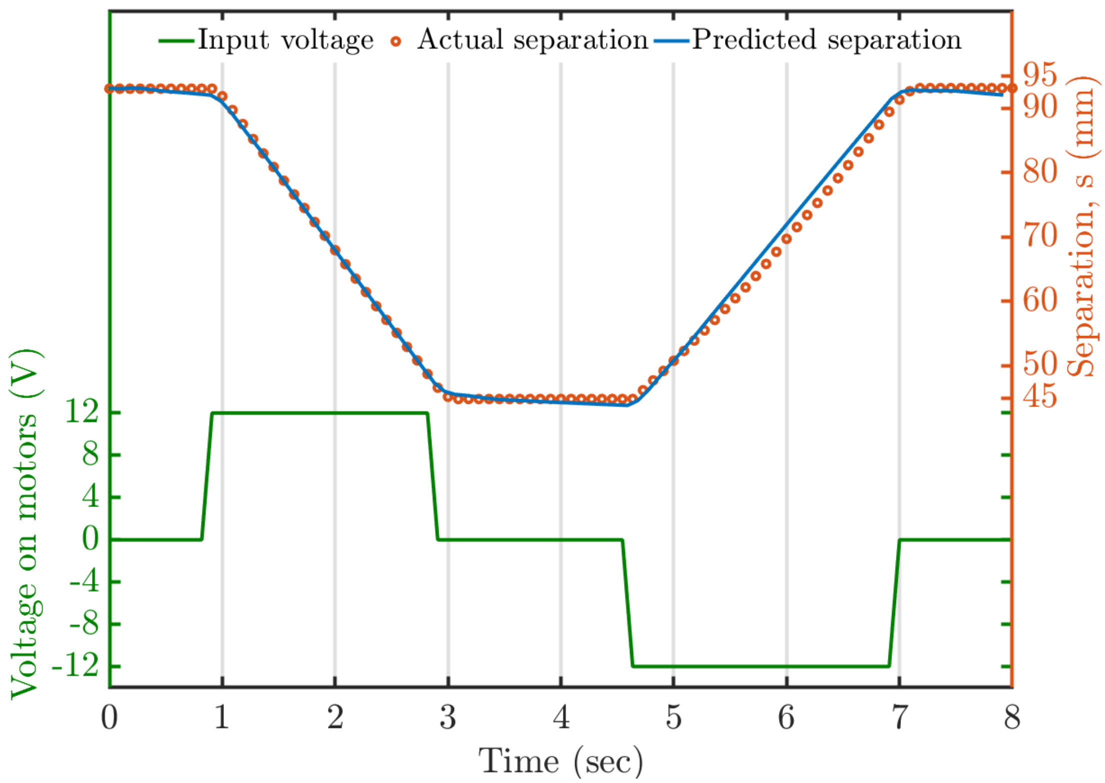

(a)

Figure 3.11: (a) Comparison of the step response of motors and the fitted discrete model (R^2=96%), (b) step response of the motors with PID controller *(cont.)*.

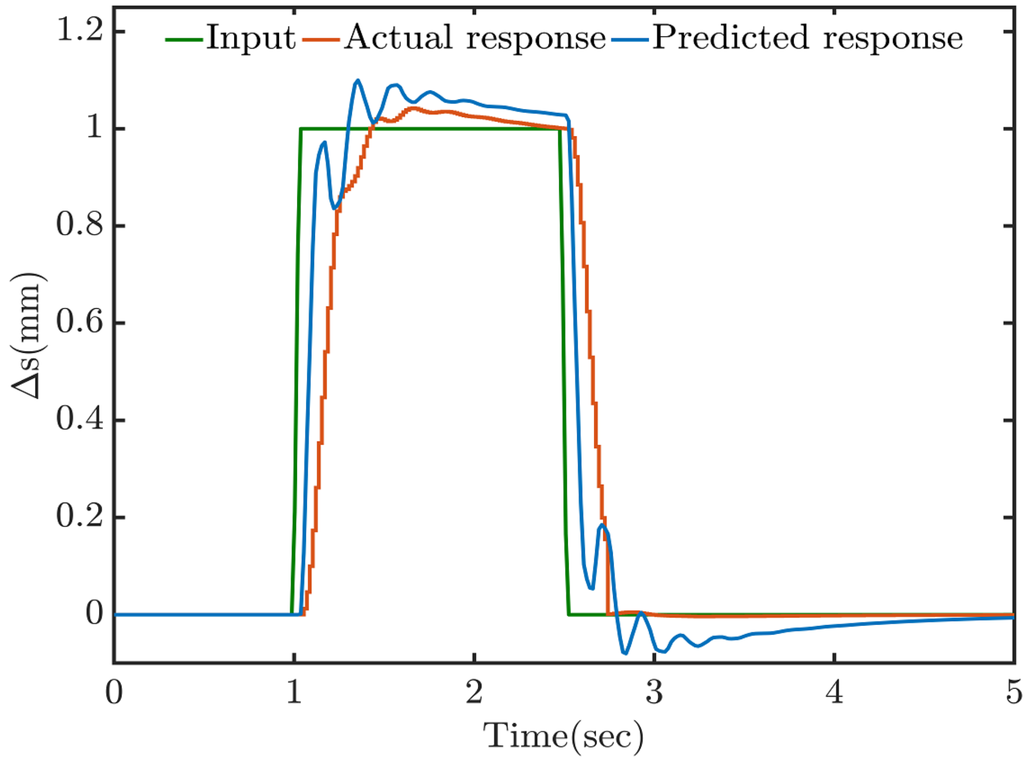

(b)

Figure 3.11: (a) Comparison of the step response of motors and the fitted discrete model (R^2=96%), (b) step response of the motors with PID controller.

With this design, the set-point stiffness could possibly be obtained through either tactile sensors embedded at the tip of surgical robots, e.g. [106, 107, 108] or from a contact mechanics model, e.g. [109]. A detailed review of both approaches can also be found in [66].

The proposed control system uses the stiffness-magnetic field-force surface defined by Eq.19 and does not require *a priori* knowledge of the material model of MRE.

Table 3.4: Selected PID coefficients and system response for a unit step input with reversal. T_r:rise time, $T_{5\%}$:settling time to 5%-band, PO:overshoot, e_{ss}:steady-state error.

k_P=2.751, k_I=2.771, k_D=0.193

	Required	Predicted	Actual	Passed
T_r	$\leq$0.3sec	0.12	0.24	✓
$T_{5\%}$	$\leq$0.5sec	1.02	0.34	✓
PO	$\leq$5%	9.3%	4.2%	✓
e_{ss}	$\leq$2%	2.8%	0.0%	✓

3.3 System Validation

In order to assess and validate the performance of developed system, two experiments were performed. The first experiment was to simulate the tactile forces during manual arterial pulse examination and the second experiment was to maintain a constant stiffness during an indentation with the phantom finger. The test was performed using the setup depicted in Fig.3.13 and each test was repeated for five times.

3.3.1 Pulsation experiment

In the first validation, a pulsation replication experiment was performed. Studies have shown that during a manual arterial pulse examination, an examiner feels the pulsation of blood with a tactile force in the range of 0.5-2N, depending on the examiner's finger pressure on the skin[110, 111]. Also during manual surgery, surgeons often manually check an unknown tissue for pulsation; so they would avoid cutting an artery[9]. Such use-case is of high practical importance for robotic MIS where direct touch on the organ is not possible.

In this experiment, the phantom finger was indented 1.5mm into the MRE. Afterward, the separation was decreased monotonically from 55mm(154mT) to 45mm(199mT) and returned to 55mm with a frequency of 1Hz. This frequency was chosen to resemble the frequency of a normal heart-beat. The cycle was continued for five consecutive repetitions, while the finger was kept at position. This experiment was aimed to showcase an application of the developed device for a real clinical need.

Fig.3.12 shows the result of the pulsation experiment. Results showed synchrony in the variation of contact force with the magnetic field. In the initial phase, contact force increased nonlinearly from 0 to 3.2N as a result of 1.5mm indentation. Afterward, contact force varied in a pulsatile form and in a range of 0.6N while its mean exponentially decreasing to 2.3N. The exponential decrease was due to the viscoelastic stress-relaxation of the MRE and the variations were merely due to the variation of magnetic field.

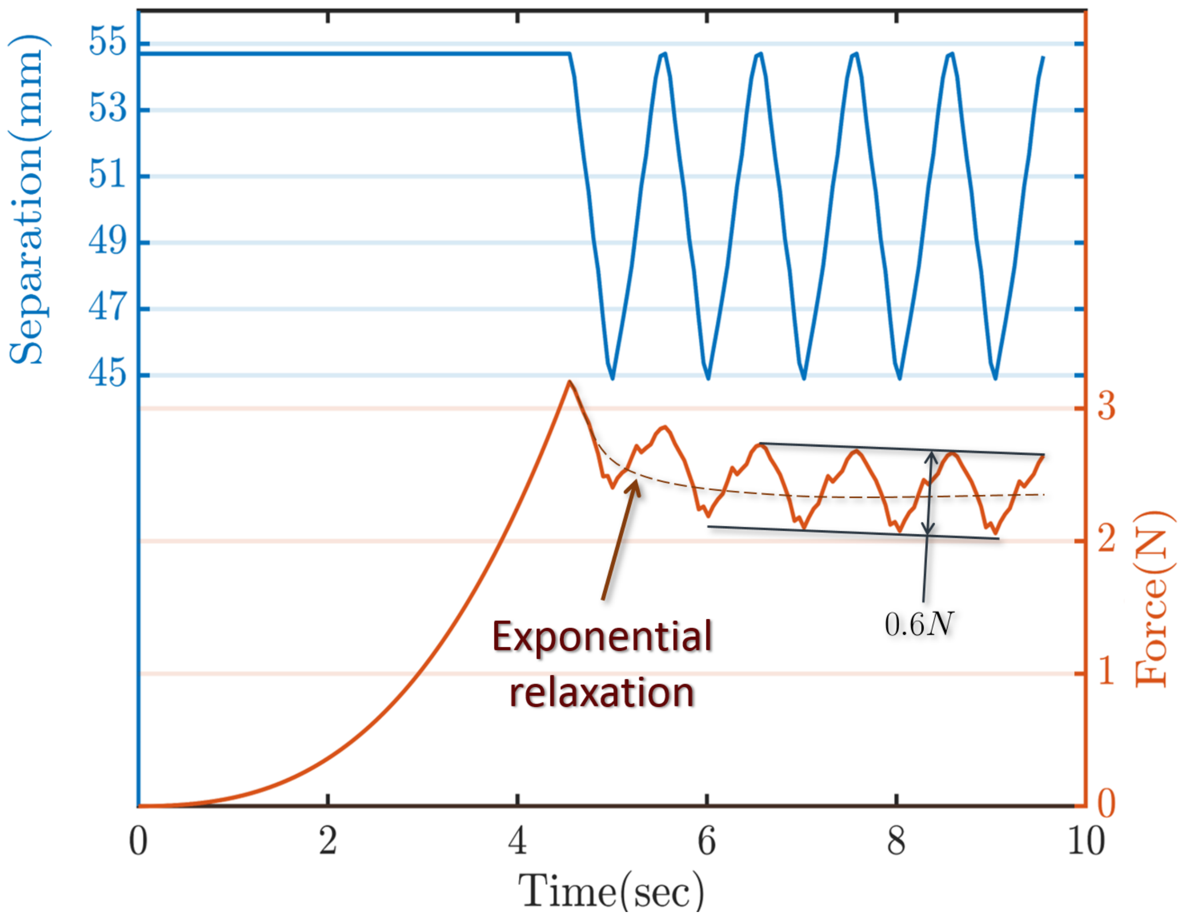

Figure 3.12: Pulsatile variation of contact force as a result of variable magnetic field with the phantom finger at constant indentation depth of 1.5mm.

Higher amplitude for pulsatile force could also be achieved with more variation of magnetic field and/or deeper indentation depth. However, since the amplitude of variation in contact force (±0.3N) was in accordance within the range of reported literature, i.e. 0.5-2.0N, this application was considered valid with *MiTouch* .

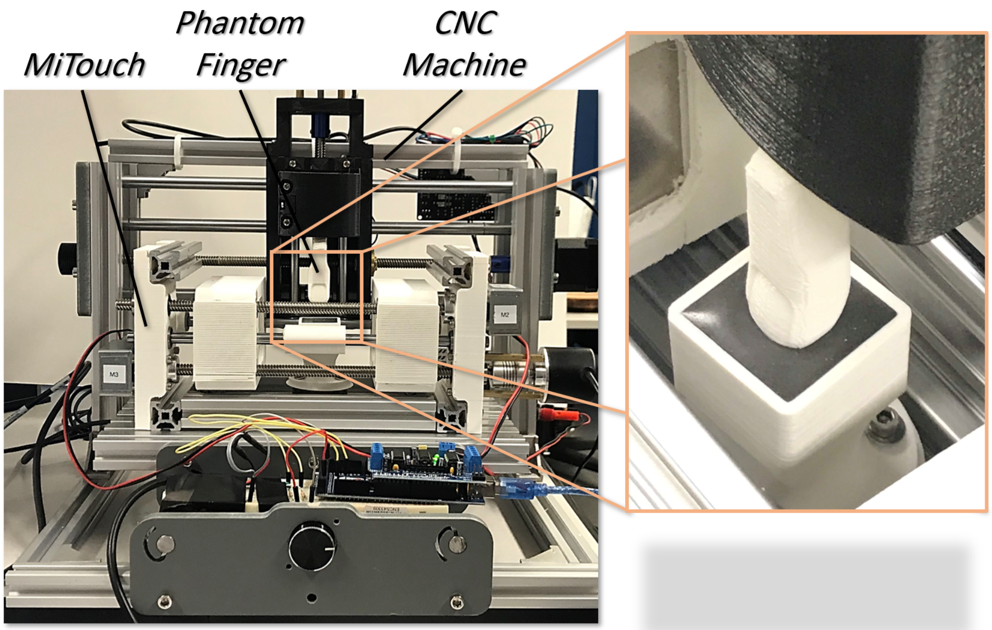

Figure 3.13: Test setup used for the stiffness identification and validation tests.

3.3.2 Constant stiffness experiment

The second experiment was to test the capability of the device in maintaining a constant stiffness during the indentation. Considering the iso-stiffness contours in Fig.3.9(c), the experiment was to maintain a stiffness of $4^{N}/_{mm}$ throughout a an indentation up to 10N of force. The indentation was applied with the rate of $0.33^{mm}/_{sec}$. To comply with the initial conditions on the corresponding contour to $4^{N}/_{mm}$ the magnets were placed at 45mm separation before the start of the test. Our previous study [104] showed that the composite MRE used in *MiTouch* has a similar range of elastic modulus to human skin, i.e. 420-850kPa [80]. On the other hand, since the size of the phantom finger used in this study resembles a median adult (male and female), the feasible stiffness 4 was deemed as feasible for a manual skin indentation.

Fig.3.14(a) shows the average force-indentation diagram and Fig.3.14(b) depicts the variation of average stiffness for the five repetitions. As indicated on the graph, the largest feasible working domain of the system was between the force-indentation graphs related to the minimum and maximum magnetic fields. Results showed that the system '*hopped*' on the next feasible force-indentation graph corresponding to a lower magnetic field when the stiffness was passing higher than $4^{N}/_{mm}$.

The sudden decreasing of the magnetic field decreased the stiffness of MRE, thus causing the contact force to drop. The system kept the feasible magnetic field level until the stiffness would pass higher than $4 {}^{N}\!/_{mm}$. This adaptation continued until the system could not find a feasible solution for magnetic field, i.e. maximum separation was reached at about 95mm.

The results of five repetitions showed the system maintained stiffness at an average of $4.07 \pm 0.41 {}^{N}\!/_{mm}$. The control-active interval indicated of Fig.3.14(b) shows the range of force-magnetic field where the system could find a feasible solution for the separation, i.e. between 95-45mm.
Fig.3.14(c) depicts the trajectory of the average experimental stiffness on the force-magnetic field-stiffness surface. As depicted on the graph, since the system was initially at maximum magnetic field (45mm), the stiffness increased similar to MRE at maximum field (green line) until it approaches $4 {}^{N}\!/_{mm}$ contour at 2.25N (trajectory 1). Afterwards, the consecutive changes in the magnetic field keep the stiffness at $4.07 \pm 0.41 {}^{N}\!/_{mm}$. With further indentation, the system reaches the end of feasible domain at the force of 7.12N (trajectory 2) and out of the feasible domain, force follows the MRE behavior at the minimum magnetic field (blue line, trajectory 3).
The average absolute error between the experimental stiffness and the stiffness surface for five repetitions was 0.08 ± 0.03, 0.45 ± 0.12, and $0.04 \pm 0.01 {}^{N}\!/_{mm}$ for trajectory 1, 2 and 3, respectively. The higher error in trajectory 2 was mainly due to the higher changes of stiffness due to the effects of controller and error accumulation in curve fitting for stiffness surface and separation-field. During the experiment, the average refresh-rate of the set-point separation was 63Hz in UI, while the refresh-rate of PID controller was 100Hz. The reason of slower response of UI, was due to the computational surplus of Newton-Raphson solution for estimating the desired magnetic field $B^{\star}$ (7msec) and desired separation s* (9msec).

3.4 Conclusions

In this study, a solution to address the clinical need for stiffness display during minimally invasive surgery was investigated. To this end, initially a comparison between the previously proposed modalities based on a set of clinical and technical requirements was performed. The survey showed that MRE-based stiffness display would comply with the requirements; therefore, an MRE-based stiffness display was proposed, designed, prototyped and tested. The composite MRE chosen in this

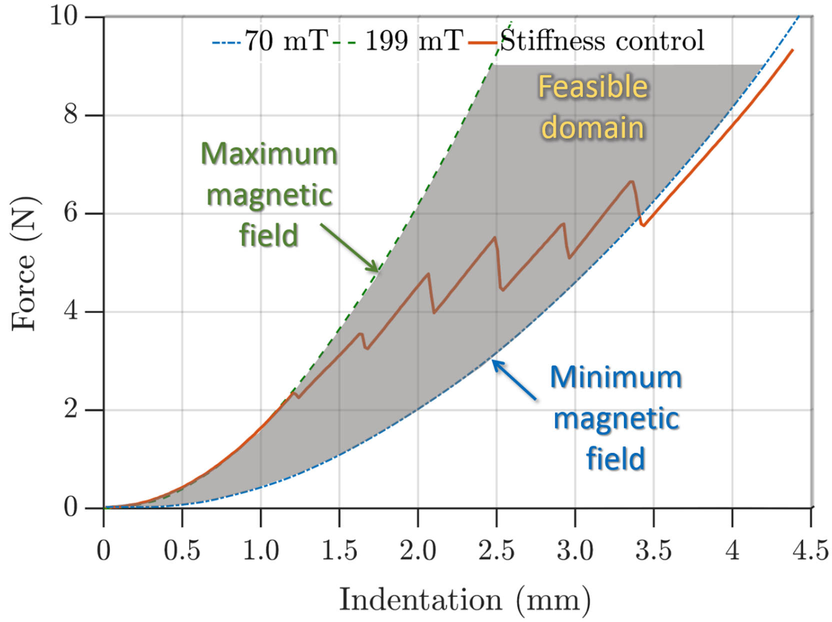

(a)

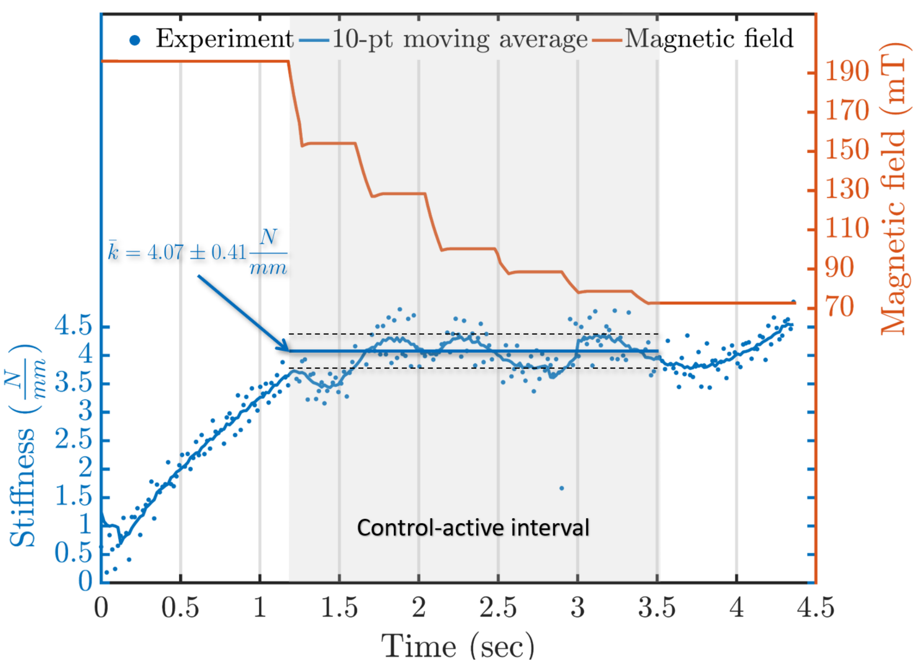

(b)

Figure 3.14: (a) average force-indentation graph with controlled magnetic field, (b) temporal variation of the magnetic field and stiffness, (c) variation of the stiffness with respect to the force-magnetic field-stiffness surface as the reference for control *(cont.)*..

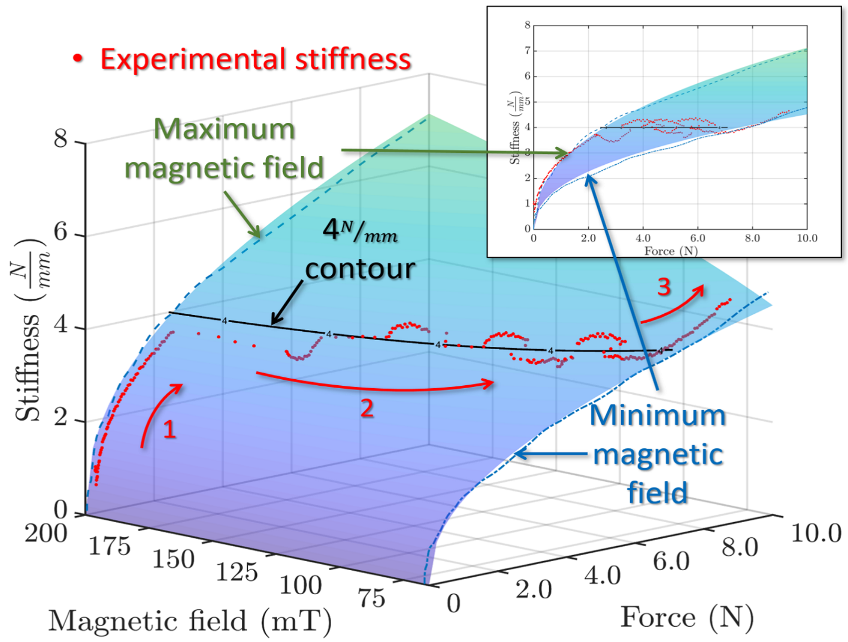

(c)

Figure 3.14: (a) average force-indentation graph with controlled magnetic field, (b) temporal variation of the magnetic field and stiffness, (c) variation of the stiffness with respect to the force-magnetic field-stiffness surface as the reference for control.

study had enhanced MR-effect based on the author's findings in [104]. The system design requirements and specifications were reported and verified for system and subsystem levels.

Based on the literature review, this study was the first to report an MRE-based stiffness display for the minimally invasive surgery. Also, the results of pulsation validation experiment successfully showcased a potential application of *MiTouch* system. The demonstrated range of tactile forces and stiffness demonstrated in the experiments were within the reported range in the literature, e.g. [13]. The system performance of *MiTouch* was comparable to the previously published studies. Table 3.5 compares the error and variation of the controlled force in this study with other studies. As presented in the table, the average error percentage for stiffness control experiment (11±3%) was within the range of representative studies (8-16%) also the maximum error (14%) was among the lowest in comparison.

Similarity of the tactile force and stiffness demonstrated by *MiTouch* to the range of force and stiffness reported in the literature shows the applicability of *MiTouch* for practical medical use-cases.

Table 3.5: Comparison of the error in stiffness control for the proposed system versus representative studies.

Study	Average error ($\frac{\Sigma\lvert k^\star - k\rvert}{nk^\star} \times 100\%$)	Maximum error
Xie *et al.* [112]	8±6%	14%
Son *et al.* [113]	8±8%	16%
Arbatani *et al.* [87]	16±8%	24%
This study	11±3%	14%

The simplicity and independence of the proposed control system from continuum-based constitutive models resulted in high refresh-rate of the control system (63Hz). Another contributing factor to the high refresh-rate of the system was the maximal parallelization in software architecture and data acquisition.

Relative low error between the desired stiffness and the experimental stiffness, verified the hypothesis of this study and showed the feasibility of an MRE-based stiffness display. However, the stiffness control experiment was performed for a specific stiffness, i.e. $4^N/_{mm}$. Stiffness of up to $7^N/_{mm}$ were also possible to achieve, however the feasible domain would become small.

In future works, as a limitation of the current system the magnetic field generated by the device can be increased by using using multiple magnet couples, optimizing the configuration of multiple magnets or utilization of coil magnets. Nevertheless, such modifications would consequently require mechanical and electrical changes in the system. Also, researchers could investigate the feasibility of stiffness control utilizing a hybrid tactile medium, e.g. MRF and MRE, to improve higher ranges of stiffness.

Moreover, the experiments were performed at quasi-static conditions; therefore, rate-dependency of the MRE did not contribute to the force. Exploitation of the rate-dependent (viscous) forces in MRE could also be another possible future study.

Chapter 4

Conclusions and Future Works

4.1 Conclusions

This thesis presents the change of mechanical properties of MREs and composite MREs due to the transverse magnetic field. Moreover, it provides the tactile display based on composite MREs. Major conclusions of this research are listed below:

(i) The experimental results of the mechanical properties of MREs revealed that single-layer MREs would exhibit less MR-effect when the magnetic field is perpendicular to applied force. Furthermore, the composite MREs demonstrated an increase of the MR-effect up to 42%.

(ii) An MRE-based tactile display was proposed to have horizontal applied magnetic fields and composite MREs.

(iii) Based on the survey on previous tactile displays, the proposed MRE-based tactile display would conform the functional requirements needed for tactile display systems. Therefore, the proposed system was designed, developed, and tested.

(iv) The pulse validation results showed that *MiTouch* system could effectively be used in medical applications.

(v) The average error of the proposed tactile system (11±3%) was in the range of other studies (8-16%). In addition, the maximum error in this study (14%) was the lowest compared to other representative studies.

(vi) The relative small error between the desired and experimental stiffness demonstrated the applicability of MRE-based stiffness displays.

4.2 Future Studies

For future works, researchers could employ different approaches for MREs to be used in tactile display systems. The recommendations for future studies are listed below:

(i) Investigate different elastomers, rather than the DragonSkin used in this study, in composite MREs to examine their effects on enhancing the MR-effect.

(ii) Study the use of composite MREs in compression test with parallel magnetic field.

(iii) Investigate the MR-effect by sandwiching MRE between two rubber layers.

(iv) Examine the utilization of anisotropic MREs in composite samples to find the enhancement of MR-effect.

(v) For the proposed tactile system only two magnets were utilized, researchers could use multiple permanent magnets or coil magnets.

(vi) Investigate the use of hybrid tactile display based on MRE-MRF.

(vii) Study the rate-dependency of composite MREs in compression with perpendicular magnetic field.

4.3 Contributions

The main contribution of this research is to develop and assess a tactile display based on composite magnetorheological elastomers to be used in minimally invasive surgeries. The contributions of this thesis can be summarized as:

(i) Testing single- and double-layer magnetorheological elastomers in a quasi-static compression test with transverse magnetic field.

(ii) MR-effects of magnetorheological elastomers were improved by the utilization of bi-layer MRE-no-MRE samples.

(iii) Enhancement of MR-effects via bi-layer configurations was equivalent to the effect of magnifying the iron particles in the studied MREs.

(iv) A tactile display system based on smart magnetorheological elastomers was designed, developed, and verified.

(v) The proposed system was successful in attaining and maintaining a desired stiffness.

(vi) The tactile display system was successful in simulating a heartbeat examination through applying a desired pulse force to a phantom finger.

Appendix A

Enhancement of MR-effect in Magnetorheological Elastomers through Bi-layer Composition: Theory and Validation

Abstract In this study, an MRE-non-MRE bi-layer composition approach was postulated for enhancement of the MR-effect in magneto-rheological elastomers. To this end, a constitutionally necessary condition was derived for enhancing the MR-effect. Both single and bi-layer MREs were tested under compression with a transverse magnetic field. Experimental results validated the hypothesis and showed enhanced MR-effect in bi-layer MREs up to 42%.

Introduction

Magnetorheological elastomers (MREs) are a class of smart materials with controllable mechanical properties. MREs are composed of ferrous particles diffused in a rubber medium. Interaction of the ferrous particles with the magnetic field and the elastomeric host matrix determines the mechanical properties of an MRE (Asadi Khanouki *et al.* , 2019). Studies have shown that the volume fraction of iron particles and type of the elastomeric matrix affect the MR-effect, i.e. change in the elastic modulus of MREs (Dargahi *et al.* , 2019). Studies have reported a positive correlation between iron particle content with the MR-effect in MREs. However, experimental results have shown a saturation volume fraction (40-45%) for iron particles. Therefore, the saturation is a barrier to achieving further MR-effect. Higher MR-effect is also desirable for better adaptability of

MRE-based structures. In this study, a bi-layer MRE-non-MRE composite configuration was proposed and assumed to have a higher MR-effect than its constituent MRE. Afterward, a necessary constitutive condition was found for the elastic modulus of non-MRE component that necessarily would enhance the MR-effect in the composite.

Material and Methods

To study the feasibility of enhancing MR-effect in an MRE through bi-layer composition, MRE (A), non-MRE material (B), and bi-layer composite (C) were assumed to exhibit a power-law stress-strain relationship (Eq. **??**). This assumption could further be specified to an Ogden or Mooney-Rivlin solid. Also, it was assumed that initial shear modulus and absolute MR-effect of MRE A are a priori knowledge.

$$\sigma_{A,B,C} = \mu_{A,B,C}\lambda^{\alpha}_{A,B.C} \tag{21}$$

Where, μ, α, σ, and λ were the fitting parameters, engineering stress and, stretch ratio. Previous studies have postulated and validated α=1.3 for EcoFlex silicone-based rubbers in compression. Also, the required condition for the enhanced MR-effect was defined as:

$$\mu^{'}_{C} - \mu_{C} > \mu^{'}_{A} - \mu_{A} \tag{22}$$

where, μ_A and μ_C were the initial shear moduli of MRE A and bi-layer composite at zero magnetic field, while $\mu^{'}_{A}$ and $\mu^{'}_{C}$ were the elastic moduli of elastomers under magnetic field. Considering the structure of composite as depicted in Figure 1, the effective initial and final shear modulus of composite C was obtained:

$$\mu_C = 2^{\alpha}\left(\mu_D^{\frac{-1}{\alpha}} + \mu_X^{\frac{-1}{\alpha}}\right)^{-\alpha}, \tag{23}$$

$$\mu'_C = 2^{\alpha}\left(\mu_D^{\frac{-1}{\alpha}} + \mu_X'^{\frac{-1}{\alpha}}\right)^{-\alpha}, \tag{24}$$

Therefore, substituting Eq. 23 and Eq. 24 in Eq. 22, and the explicit form of the necessary

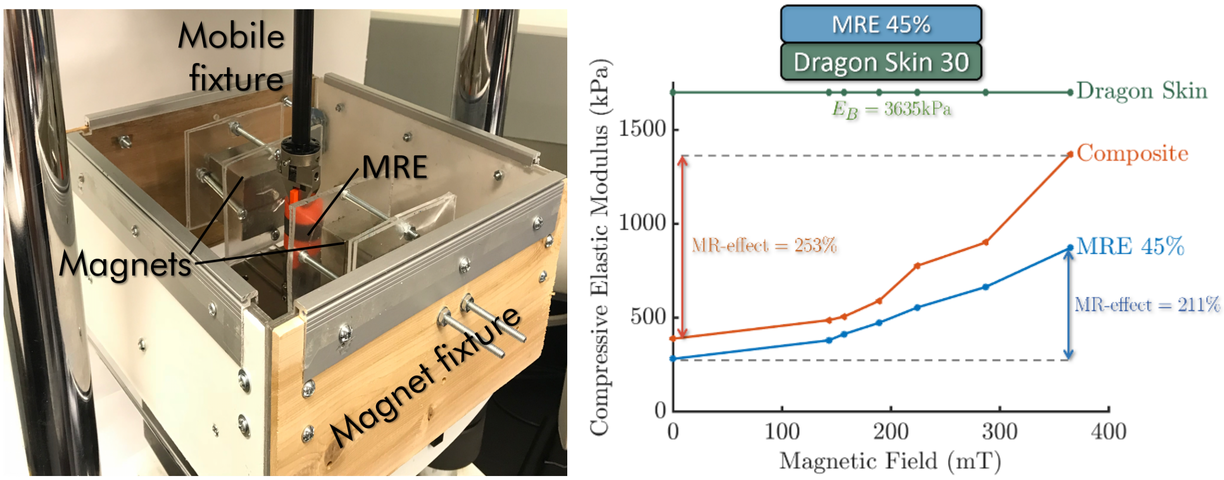

(a) (b)

Figure A.1: (a) Schematic illustration of samples under a compression test. (b) variation of elastic modulus of samples versus magnetic field.

condition was derived:

$$\left(\mu_X^{\frac{-1}{\alpha}} + \mu_D^{\frac{-1}{\alpha}}\right)^{\alpha} - \left(\mu_X'^{\frac{-1}{\alpha}} + \mu_D^{\frac{-1}{\alpha}}\right)^{\alpha} - (\mu_X' - \mu_X) \times \left(\frac{\left(\mu_X'^{\frac{-1}{\alpha}} + \mu_D^{\frac{-1}{\alpha}}\right)\left(\mu_X^{\frac{-1}{\alpha}} + \mu_D^{\frac{-1}{\alpha}}\right)}{2}\right)^{\alpha} > 0 \tag{25}$$

Numerical analysis showed that there exists a unique minimum μ_B which ensures the satisfaction of the condition.

Results

From the stress strain-curve, the compressive elastic modulus of elastomer B was found to be 3635kPa. Substituting μ_B =1211kPa in Eq. 5 Also, elastic moduli of MRE A and composite C were 281kPa and 388kPa at zero magnetic field, and 873kPa and 1370kPa at 365mT. Therefore, MRE C exhibited an MR-effect of 253%, while its MR component, MRE A only showed an MR-effect of 211%. Fig.1(b) depicts variation of compressive elastic moduli of MRE A, elastomer B and composite C. MR-effects were approximately half as reported in (Dargahi *et al.* , 2019), the reason might be due to the transverse application of the magnetic field.

Conclusion

In this study, a bi-layer MRE-non-MRE composite structure was postulated and validated. Surpassing the minimum required elastic modulus for the non-MRE component was theoretically predicted and experimental results validated the hypothesis. Although the MRE component of the composite in this study was saturated with CIPs, the MR-effect was successfully enhanced through the bi-layer composition.

References

(i) Asadi Khanouki M., Sedaghati R. and Hemmatian M. (2019) Characterization of Magneto-Mechanical Properties and Quasi-Static Physical Modelling of MR Elastomers. In AIAA Scitech 2019 Forum (p. 1114).

(ii) Dargahi A., Sedaghati R. and Rakheja S. (2019) On the properties of magnetorheological elastomers in shear mode: Design, fabrication and characterization. Composites Part B: Engineering, 159, pp.269-283.

(iii) ISO 7743:2017 (2017) Rubber, vulcanized or thermoplastic – Determination of compression stress-strain properties.

(iv) Steck, D., Qu, J., Kordmahale, S. B., Tscharnuter, D., Muliana, A., and Kameoka, J. (2019). Mechanical responses of Ecoflex silicone rubber: Compressible and incompressible behaviors. Journal of Applied Polymer Science, 136(5), 47025.

Appendix B

Technical Characteristics of Materials

PRODUCT DESCRIPTION

This powerful neodymium block magnet measures 2" in length, 2" in width, and 1" in thickness and is made of a grade N52 neodymium, iron, and boron magnetic alloy blend. This magnetic blend is patent licensed and made under the ISO 9001 quality control systems and are plated in a nickel-copper-nickel triple layer coating for a shiny corrosion resistant finish. This magnet is great for holding purposes such as holding objects to magnetic surfaces. Moreover, this magnet is versatile and robust; applications range from industrial use to personal projects.

Please note that all neodymium rare earth magnets are fragile and require extreme caution when handling due to their brittle nature and to avoid injury due to pinching.

- **Material:** Sintered NdFeB. Grade N52
- **Gauss Rating:** 14,400 Gauss
- **Pulling Force:** 250 lbs
- **Pole Orientation:** Magnetized through the thickness, the poles are on the 2" x 2" surfaces.
- **Coating:** Ni+Cu+Ni 3 layer coating, the best available.
- **Tolerance:** The tolerances of all the dimensions are +/-0.002in with coating.

PLEASE NOTE:

- All magnets may chip and shatter, but if used correctly can last a lifetime.
- Keep away from pacemakers.
- Not for children, parental supervision required.
- If damaged please dispose of completely. Shards are still magnetized and if swallowed can inflict serious damage if magnets join inside the digestive tract.

Figure B.1: Technical properties of N52 magnets

Ecoflex™ Series

Super-Soft, Addition Cure Silicone Rubbers

LAB TESTED SKIN SAFE CERTIFIED

SMOOTH-ON

www.smooth-on.com

Cured Material Certified Skin Safe!

PRODUCT OVERVIEW

Ecoflex™ rubbers are platinum-catalyzed silicones that are versatile and easy to use. **Ecoflex™** rubbers are mixed 1A:1B by weight or volume and cured at room temperature with negligible shrinkage. Low viscosity ensures easy mixing and de-airing, or you can choose to mix and dispense using our convenient dispensing cartridges. Cured rubber is very soft, very strong and very "stretchy", stretching many times its original size without tearing and will rebound to its original form without distortion. **Ecoflex™** rubbers are water white translucent and can be color pigmented with Silc Pig™ pigments for creating a variety of color effects. You can also add Smooth-On's Silicone Thinner™ to further lower the viscosity. THI-VEX™ silicone thickener can be added by weight to Ecoflex™ silicones for brushable applications.

Soft, Softer, Softest . . . Ecoflex™ rubbers are based on Smooth-On's Dragon Skin™ technology and are currently available in many different hardnesses: Shore A-5, Shore 00-10, 00-20, 00-30 and 00-50. They are suitable for a variety of applications including making prosthetic appliances, cushioning for orthotics and special effects applications (especially in animatronics where repetitive motion is required). **Ecoflex™ 5** has a pot life of 1 minute and a demold time of 5 minutes – Available only in dispensing cartridges. **Ecoflex™ 00-33 AF** is an **anti-fungal** silicone suitable for making a variety of skin-safe cushioning device configurations that resist fungi for orthopedic and orthotic applications. Cured Ecoflex™ is skin safe and certified by an independent laboratory.

Note: Ecoflex™ 00-10 cures with a "tacky" surface.

TECHNICAL OVERVIEW

	Mixed Viscosity (ASTM D-2393)	Specific Gravity (g/cc) (ASTM D-1475)	Specific Volume (cu. in./lb.) (ASTM D-1475)	Pot Life (ASTM D-2471)	Cure Time	Shore Hardness (ASTM D-2240)	Tensile Strength (ASTM D-412)	100% Modulus (ASTM D-412)	Elongation at Break % (ASTM D-412)	Die B Tear Strength (ASTM D-624)	Shrinkage (in./in.) (ASTM D-2566)
Ecoflex™ 5	13,000 cps	1.07	25.8	1 min.	5 min.	5A	350 psi	15 psi	1000%	75 pli	< .001 in./in.
Ecoflex™ 00-50	8,000 cps	1.07	25.9	18 min.	3 hours	00-50	315 psi	12 psi	980%	50 pli	< .001 in./in.
Ecoflex™ 00-30	3,000 cps	1.07	26.0	45 min.	4 hours	00-30	200 psi	10 psi	900%	38 pli	< .001 in./in.
Ecoflex™ 00-33 AF	3,000 cps	1.07	26.0	45 min.	4 hours	00-33	200 psi	10 psi	900%	38 pli	< .001 in./in.
Ecoflex™ 00-20	3,000 cps	1.07	26.0	30 min.	4 hours	00-20	160 psi	8 psi	845%	30 pli	< .001 in./in.
Ecoflex™ 00-10	14,000 cps	1.04	26.6	30 min.	4 hours	00-10	120 psi	8 psi	800%	22 pli	< .001 in./in.

*All values measured after 7 days at 73°F/23°C

Mix Ratio: 1A:1B by volume or weight
Color: Translucent
Useful Temperature Range: -65°F to 450°F (-53°C to 232°C)
Dielectric Strength (ASTM D-147-97a)**:** >350 volts/mil

PROCESSING RECOMMENDATIONS

PREPARATION... ***Safety*** – Use in a properly ventilated area ("room size" ventilation). Wear safety glasses, long sleeves and rubber gloves to minimize contamination risk. Wear vinyl gloves only. Latex gloves will inhibit the cure of the rubber.

Store and use material at room temperature (73°F/23°C). Warmer temperatures will drastically reduce working time and cure time. Storing material at warmer temperatures will also reduce the usable shelf life of unused material. These products have a limited shelf life and should be used as soon as possible. Mixing containers should have straight sides and a flat bottom. Mixing sticks should be flat and stiff with defined edges for scraping the sides and bottom of your mixing container.

Cure Inhibition – Addition-cure silicone rubber may be inhibited by certain contaminants in or on the pattern to be molded resulting in tackiness at the pattern interface or a total lack of cure throughout the mold. Latex, tin-cure silicone, sulfur clays, certain wood surfaces, newly cast polyester, epoxy, tin cure silicone rubber or urethane rubber may cause inhibition. If compatibility between the rubber and the surface is a concern, a small-scale test is recommended. Apply a small amount of rubber onto a non-critical area of the pattern. Inhibition has occurred if the rubber is gummy or uncured after the recommended cure time has passed.

Because no two applications are quite the same, a small test application to determine suitability for your project is recommended if performance of this material is in question.

Figure B.2: Technical bulletin of silicone rubber page 1

Safety First!

The Material Safety Data Sheet (MSDS) for this or any Smooth-On product should be read prior to use and is available upon request from Smooth-On. All Smooth-On products are safe to use if directions are read and followed carefully.

Keep Out of Reach of Children

Be careful. Use only with adequate ventilation. Contact with skin and eyes may cause irritation. Flush eyes with water for 15 minutes and seek immediate medical attention. Remove from skin with waterless hand cleaner followed by soap and water.

Important: The information contained in this bulletin is considered accurate. However, no warranty is expressed or implied regarding the accuracy of the data, the results to be obtained from the use thereof, or that any such use will not infringe upon a patent. User shall determine the suitability of the product for the intended application and assume all risk and liability whatsoever in connection therewith.

To prevent inhibition, one or more coatings of a clear acrylic lacquer applied to the model surface is usually effective. Allow any sealer to thoroughly dry before applying rubber. Note: Even with a sealer, platinum silicones will not work with modeling clays containing heavy amounts of sulfur. Do a small scale test for compatibility before using on your project.

Applying A Release Agent - Although not usually necessary, a release agent will make demolding easier when pouring into or over most surfaces. Ease Release™ 200 is a proven release agent for use with silicone rubber. Mann Ease Release™ products are available from Smooth-On or your Smooth-On distributor.

IMPORTANT: To ensure thorough coverage, lightly brush the release agent with a soft brush over all surfaces of the model. Follow with a light mist coating and let the release agent dry for 30 minutes.

If there is any question about the effectiveness of a sealer/release agent combination, a small-scale test should be made on an identical surface for trial.

MEASURING & MIXING...

Stir Part A and Part B thoroughly before dispensing. After dispensing required amounts of Parts A and B into mixing container (1A:1B by volume or weight), **mix thoroughly for 3 minutes making sure that you scrape the sides and bottom of the mixing container several times.** After mixing parts A and B, vacuum degassing is recommended to eliminate any entrapped air. Vacuum material for 2-3 minutes (29 inches of mercury), making sure that you leave enough room in container for product volume expansion.

POURING, CURING & MOLD PERFORMANCE...

For best results, pour your mixture in a single spot at the lowest point of the containment field. Let the rubber seek its level up and over the model. **A uniform flow will help minimize entrapped air.** The liquid rubber should level off at least 1/2" (1.3 cm) over the highest point of the model surface.

Curing / Post Curing - Allow rubber to cure as prescribed at room temperature (73°F/23°C) before demolding. Do not cure rubber where temperature is less than 65°F/18°C. **Optional:** Post curing the mold will aid in quickly attaining maximum physical and performance properties. After curing at room temperature, expose the rubber to 176°F/80°C for 2 hours and 212°F/100°C for one hour. Allow mold to cool to room temperature before using.

If Using As A Mold - When first cast, silicone rubber molds exhibit natural release characteristics. Depending on what is being cast into the mold, mold lubricity may be depleted over time and parts will begin to stick. No release agent is necessary when casting wax or gypsum. Applying a release agent such as Ease Release™ 200 (available from Smooth-On) prior to casting polyurethane, polyester and epoxy resins is recommended to prevent mold degradation.

Thickening Ecoflex™ Silicones - THI-VEX™ is made especially for thickening Smooth-On's silicones for vertical surface application (making brush-on molds). Different viscosities can be attained by varying the amount of THI-VEX™. See the **THI-VEX™ technical bulletin** (available from Smooth-On or your Smooth-On distributor) for full details.

Thinning Ecoflex™ Silicones - Smooth-On's Silicone Thinner™ will lower the viscosity of Ecoflex™ silicones for easier pouring and vacuum degassing. A **disadvantage** is that ultimate tear and tensile are reduced in proportion to the amount of Silicone Thinner™ added. ***It is not recommended to exceed 10% by weight of total system (A+B).*** See the Silicone Thinner™ technical bulletin (available from Smooth-On or your Smooth-On distributor) for full details.

Mold Performance & Storage - The physical life of the mold depends on how you use it (materials cast, frequency, etc.). Casting abrasive materials such as concrete can quickly erode mold detail, while casting non-abrasive materials (wax) will not affect mold detail. Before storing, the mold should be cleaned with a soap solution and wiped fully dry. Two part (or more) molds should be assembled. Molds should be stored on a level surface in a cool, dry environment.

SMOOTH-ON

Call Us Anytime With Questions About Your Application.
Toll-free: **(800) 381-1733** Fax: **(610) 252-6200**

The new www.smooth-on.com is loaded with information about mold making, casting and more.

122018-JR

Figure B.2: Technical bulletin of silicone rubber page 2

Dragon Skin™ Series

Addition Cure Silicone Rubber Compounds

SKIN SAFE LAB TESTED CERTIFIED

SMOOTH-ON

www.smooth-on.com

Cured Material Certified Skin Safe!

PRODUCT OVERVIEW

Dragon Skin™ silicones are high performance platinum cure liquid silicone compounds that are used for a variety of applications ranging from creating skin effects and other movie special effects to making production molds for casting a variety of materials. Because of the **superior physical properties** and flexibility of Dragon Skin™ rubbers, they are also used for medical prosthetics and cushioning applications. Dragon Skin™ rubbers are also used for a variety of industrial applications and have a service temperature range of a constant -65°F to +450°F (-53°C to +232°C).

Great for Making Molds for a Variety of Applications - Available in **Shore 10A, 20A and 30A**, Dragon Skin™ silicones can be used to make exceptionally strong and tear resistant molds for casting plaster, wax, concrete (limited production run), resins and other materials. **Dragon Skin™ 10 AF** is an **anti-fungal** silicone suitable for making a variety of skin-safe cushioning device configurations that resist fungi for orthopedic and orthotic applications.

Time Tested, Versatile Special Effects Material – Soft, super-strong and stretchy, Dragon Skin™ 10 (**Very Fast, Fast, Medium and Slow speeds**) is used around the world to make spectacular skin and creature effects. An infinite number of color effects can be achieved by adding Silc Pig™ silicone pigments or Cast Magic™ effects powders. Cured rubber can also be painted with the Psycho Paint™ system. Cured material is skin safe and certified by an independent laboratory.

Easy To Use – Dragon Skin™ silicones are mixed 1A:1B by weight or volume. Liquid rubber can be thinned with Silicone Thinner™ or thickened with THI-VEX™. Rubber cures at room temperature (73°F/23°C) with negligible shrinkage. ***Vacuum degassing is recommended to minimize air bubbles in cured rubber.***

TECHNICAL OVERVIEW

	Mixed Viscosity (ASTM D-2393)	Specific Gravity (g/cc) (ASTM D-1475)	Specific Volume (cu. in./lb) (ASTM D-1475)	Pot Life (ASTM D-2471)	Cure Time	Shore A Hardness (ASTM D-2240)	Tensile Strength (ASTM D-412)	100% Modulus (ASTM D-412)	Elongation at Break % (ASTM D-412)	Die B Tear Strength (ASTM D-624)	Shrinkage (in./in.) (ASTM D-2566)
Dragon Skin™ 10 Very Fast	23,000 cps	1.07	25.8	4 min.	30 min.	10A	475 psi	22 psi	1000%	102 pli	< .001 in./in.
Dragon Skin™ 10 Fast	23,000 cps	1.07	25.8	8 min.	75 min.	10A	475 psi	22 psi	1000%	102 pli	< .001 in./in.
Dragon Skin™ 10 Medium	23,000 cps	1.07	25.8	20 min.	5 hours	10A	475 psi	22 psi	1000%	102 pli	< .001 in./in.
Dragon Skin™ 10 Slow	23,000 cps	1.07	25.8	45 min.	7 hours	10A	475 psi	22 psi	1000%	102 pli	< .001 in./in.
Dragon Skin™ 10 AF	23,000 cps	1.07	25.8	20 min.	5 hours	10A	475 psi	22 psi	1000%	102 pli	< .001 in./in.
Dragon Skin™ 20	20,000 cps	1.08	25.6	25 min.	4 hours	20A	550 psi	49 psi	620%	120 pli	< .001 in./in.
Dragon Skin™ 30	20,000 cps	1.08	25.7	45 min.	16 hours	30A	500 psi	86 psi	364%	108 pli	< .001 in./in.

Mix Ratio: 1A:1B by volume or weight
Color: Translucent
Useful Temperature Range: -65°F to +450°F (-53°C to +232°C)
Dielectric Strength (ASTM D-147-97a)***:*** >350 volts/mil

PROCESSING RECOMMENDATIONS

*All values measured after 7 days at 73°F/23°C

PREPARATION... Safety – Use in a properly ventilated area ("room size" ventilation). Wear safety glasses, long sleeves and rubber gloves to minimize contamination risk. Wear vinyl gloves only. Latex gloves will inhibit the cure of the rubber.

Store and use material at room temperature (73°F/23°C). Warmer temperatures will drastically reduce working time and cure time. Storing material at warmer temperatures will also reduce the usable shelf life of unused material. These products have a limited shelf life and should be used as soon as possible. Mixing containers should have straight sides and a flat bottom. Mixing sticks should be flat and stiff with defined edges for scraping the sides and bottom of your mixing container.

Cure Inhibition – Addition-cure silicone rubber may be inhibited by certain contaminants in or on the pattern to be molded resulting in tackiness at the pattern interface or a total lack of cure throughout the mold. Latex, tin-cure silicone, sulfur clays, certain wood surfaces, newly cast polyester, epoxy, tin cure silicone rubber or urethane rubber may cause inhibition. If compatibility between the rubber and the surface is a concern, a small-scale test is recommended. Apply a small amount of rubber onto a non-critical area of the pattern. Inhibition has occurred if the rubber is gummy or uncured after the recommended cure time has passed.

Because no two applications are quite the same, a small test application to determine suitability for your project is recommended if performance of this material is in question.

Figure B.3: Technical bulletin of dargon skin page 1

Safety First!

The Material Safety Data Sheet (MSDS) for this or any Smooth-On product should be read prior to use and is available upon request from Smooth-On. All Smooth-On products are safe to use if directions are read and followed carefully.

Keep Out of Reach of Children

Be careful. Use only with adequate ventilation. Contact with skin and eyes may cause irritation. Flush eyes with water for 15 minutes and seek immediate medical attention. Remove from skin with waterless hand cleaner followed by soap and water.

Important: The information contained in this bulletin is considered accurate. However, no warranty is expressed or implied regarding the accuracy of the data, the results to be obtained from the use thereof, or that any such use will not infringe upon a patent. User shall determine the suitability of the product for the intended application and assume all risk and liability whatsoever in connection therewith.

Cure Inhibition – To prevent inhibition, one or more coatings of a clear acrylic lacquer applied to the model surface is usually effective. Allow any sealer to thoroughly dry before applying rubber. Note: Even with a sealer, platinum silicones will not work with modeling clays containing heavy amounts of sulfur. Do a small scale test for compatibility before using on your project.

Applying A Release Agent - Although not usually necessary, a release agent will make demolding easier when pouring into or over most surfaces. Ease Release™ 200 is a proven release agent for making molds with silicone rubber. Mann Ease Release™ products are available from Smooth-On or your Smooth-On distributor.

IMPORTANT: To ensure thorough coverage, lightly brush the release agent with a soft brush over all surfaces of the model. Follow with a light mist coating and let the release agent dry for 30 minutes.

If there is any question about the effectiveness of a sealer/release agent combination, a small-scale test should be made on an identical surface for trial.

MEASURING & MIXING...

Stir Part A and Part B thoroughly before dispensing. After dispensing required amounts of Parts A and B into mixing container (1A:1B by volume or weight), **mix thoroughly for 3 minutes making sure that you scrape the sides and bottom of the mixing container several times.** After mixing parts A and B, vacuum degassing is recommended to eliminate any entrapped air. Vacuum material for 2-3 minutes (29 inches of mercury), making sure that you leave enough room in container for product volume expansion.

POURING, CURING & MOLD PERFORMANCE...

For best results, pour your mixture in a single spot at the lowest point of the containment field. Let the rubber seek its level up and over the model. **A uniform flow will help minimize entrapped air.** The liquid rubber should level off at least 1/2" (1.3 cm) over the highest point of the model surface.

Curing / Post Curing - Allow rubber to cure as prescribed at room temperature (73°F/23°C) before demolding. Do not cure rubber where temperature is less than 65°F/18°C. **Optional:** Post curing the mold will aid in quickly attaining maximum physical and performance properties. After curing at room temperature, expose the rubber to 176°F/80°C for 2 hours and 212°F/100°C for one hour. Allow mold to cool to room temperature before using.

If Using As A Mold - When first cast, silicone rubber molds exhibit natural release characteristics. Depending on what is being cast into the mold, mold lubricity may be depleted over time and parts will begin to stick. No release agent is necessary when casting wax or gypsum. Applying a release agent such as Ease Release™ 200 (available from Smooth-On) prior to casting polyurethane, polyester and epoxy resins is recommended to prevent mold degradation.

Thickening Dragon Skin™ Silicones - **THI-VEX™** is made especially for thickening Smooth-On's silicones for vertical surface application (making brush-on molds). Different viscosities can be attained by varying the amount of THI-VEX™. See the **THI-VEX™ technical bulletin** (available from Smooth-On or your Smooth-On distributor) for full details.

Thinning Dragon Skin™ Silicones - Smooth-On's **Silicone Thinner™** will lower the viscosity of Dragon Skin™ for easier pouring and vacuum degassing. **A disadvantage** is that ultimate tear and tensile are reduced in proportion to the amount of **Silicone Thinner™** added. ***It is not recommended to exceed 10% by weight of total system (A+B).*** See the **Silicone Thinner™ technical bulletin** (available from Smooth-On or your Smooth-On distributor) for full details.

Mold Performance & Storage - The physical life of the mold depends on how you use it (materials cast, frequency, etc.). Casting abrasive materials such as concrete can quickly erode mold detail, while casting non-abrasive materials (wax) will not affect mold detail. Before storing, the mold should be cleaned with a soap solution and wiped fully dry. Two part (or more) molds should be assembled. Molds should be stored on a level surface in a cool, dry environment.

SMOOTH-ON

Call Us Anytime With Questions About Your Application.

Toll-free: **(800) 381-1733** Fax: **(610) 252-6200**

The new www.smooth-on.com is loaded with information about mold making, casting and more.

122018-JR

Figure B.3: Technical bulletin of dargon skin page 2

Silicone Thinner®

Silicone Rubber Thinning Fluid

SMOOTH-ON

www.smooth-on.com

Silicone Thinner® is a non-reactive silicone fluid that will lower the mixed viscosity of tin cure (condensation) or platinum cure (addition) silicone rubber products.

Silicone Thinner® offers the following advantages:

- A lower mixed viscosity (A+B) means that the rubber will de-air faster when vacuuming.
- Mixed rubber (A+B) will flow better over intricate model detail.
- Silicone Thinner® will lower the ultimate shore hardness (durometer) of cured silicone rubber.
- Pot life (working time) is increased in proportion to the amount of Silicone Thinner® used.

Disadvantage: Ultimate tear and tensile strength are reduced in proportion to the amount of Silicone Thinner® added, however knotty tear properties of the Mold Max® series rubbers are unaffected. The following test data is offered as an example of the effects of Silicone Thinner® on Mold Max® 30 silicone rubber (your results may vary):

Value	Mold Max® 30 0% Silicone Thinner*	Mold Max® 30 5% Silicone Thinner*	Mold Max® 30 10% Silicone Thinner*
Mixed Viscosity (A+B)	25,000 cps	19,000 cps	13,800 cps
Shore Hardness (after 7 days)	30 A	26 A	23 A
Tensile Strength (after 7 days)	400 psi	350 psi	330 psi
Tear Strength (Die B) (after 7 days)	130 pli	115 pli	110 pli

Directions: Materials should be stored and used in a warm environment (73° F / 23° C). This material has a limited shelf life and should be used as soon as possible. Wear safety glasses, long sleeves and rubber gloves to minimize contamination risk.

Silicone Thinner® is added as a percentage of the total Part A+Part B rubber system. An accurate gram scale must be used. Weigh out and pre-mix required amount of Silicone Thinner® with Part A of silicone rubber before adding Part B.** Mix all components thoroughly and vacuum as directed on mold rubber technical bulletin. ***It is not recommended to exceed 10% by weight of total system (A+B).

Because no two applications are quite the same, a small test application to determine suitability for your project is recommended if performance of this material is in question.

Safety First!

The material safety data sheet (MSDS) for this or any Smooth-On product should be read before using and is available on request or on our website at www.smooth-on.com. All Smooth-On products are safe to use if directions are read and followed carefully. ***Keep Out of Reach Of Children.*** ***IMPORTANT*** - The information contained in this bulletin is considered accurate. However, no warranty is expressed or implied regarding the accuracy of the data, the results to be obtained from the use thereof, or that any such use will not infringe a copyright or patent. User shall determine suitability of the product for the intended application and assume all associated risks and liability.

SMOOTH-ON

Call Us Anytime With Questions About Your Application.

Toll-free: **(800) 762-0744** Fax: **(610) 252-6200**

The new **www.smooth-on.com** is loaded with information about mold making, casting and more.

22510 - JR

Figure B.4: Technical bulletin of silicone thinner

Slacker®

Silicone Tactile Mutator

SMOOTH-ON

www.smooth-on.com

PRODUCT OVERVIEW

Slacker® is one component translucent clear fluid that is added to our translucent **platinum-cure silicones** such as Dragon Skin® and Ecoflex® products. **Slacker®** will change the "feel" of the silicone rubber to a softer and more "flesh-like" material. It also alters the rebound properties of the silicone, making it feel more like human tissue.

Slacker® allows the user to vary the degree of tackiness to the cured silicone, allowing for the creation of self-sticking silicone appliances. The amount of tackiness is in direct proportion to the amount of **Slacker®** added. Pieces created with **Slacker® will not exude silicone oil,** eliminating a common problem with other softening methods.

Slacker® can be added in larger proportions to Smooth-On's super soft and stretchy platinum silicones (for example, Dragon Skin® FX-Pro®) to make silicone gel that can be used to create gel-filled silicone prosthetic appliances. Gel-filled appliances will flex, bend, and even wrinkle like human flesh. Silicone gels created with **Slacker®** can also be used to create **cushioning materials** for medical applications (anaplastology). ***Use Skin Tite® adhesive to temporarily, but securely, adhere silicone appliances to the skin.***

PROCESSING RECOMMENDATIONS

PREPARATION...

Temperature - Store and use all products at room temperature (73°F / 23°C). This product has a limited shelf life and should be used as soon as possible. Wear safety glasses, long sleeves and vinyl gloves to minimize contamination risk.

MEASURING & MIXING...

Measuring Is Done By Volume Or Weight – Whether using an Ecoflex® product or a Dragon Skin® product, the proper mix ratio is 100 Parts A + 100 Part B + X Parts Slacker®. Everyone's application and desired level of stickiness or "tack" will vary. The following chart should be used as a reference for you to achieve your own desired effect.

1 Part A + 1 Part B + **1 Part Slacker®** **Result -** "Tacky"	1 Part A + 1 Part B + **2 Parts Slacker®** **Result -** "Very Tacky"
1 Part A + 1 Part B + **3 Parts Slacker®** **Result -** "Extremely Tacky / Gel-like"	1 Part A + 1 Part B + **4 Parts Slacker®** **Result -** "Super Soft Tacky Silicone Gel"

Example - 50 grams Dragon Skin® FX-Pro® part A + 50 grams Dragon Skin® FX-Pro® part B + 150 grams Slacker® (3 parts) will give you an "Extremely Tacky / Gel-like" result.

USING SLACKER® WITH DRAGON SKIN® OR ECOFLEX® PRODUCTS...

Adding Color - Silc Pig ® silicone pigments can be added and mixed thoroughly into the silicone rubber prior to adding Slacker® for matching a specific skin tone, etc.

Mixing – Ecoflex® or Dragon Skin® silicones with Slacker® added can be hand mixed. Aggressively hand mix for 3 minutes, making sure that you scrape the sides and bottom of your mixing container several times.

Release Agent - When using a platinum silicone mold, Ease Release® 200 should be used. **If there is any question** about the effectiveness of a release agent combination, a small scale test should be made on an identical surface for trial.

Pouring - For best results, pour your mixture in a single spot at the lowest point of the mold. Let the rubber seek its level in the mold. **A uniform flow will help minimize entrapped air.**

CREATING SILICONE GEL FILLED MAKEUP APPLIANCES...

Using An Encapsulator – When creating a gel-filled appliance, use a platinum silicone as your membrane for best results. Dragon Skin® FX-Pro® works very well as a membrane for gel filled appliances.

Applying A Mold Release – Appliances appliances made with Slacker® can be cast into platinum silicone molds, urethane resin molds (Shell Shock®) or rigid gypsum molds. Ease Release® 200 can be used as a mold release. Another release option is to apply a soap solution (1 part unscented dish soap to 2 parts 99% isopropyl alcohol works well) with a clean brush over all mold surfaces. Allow release to dry for at least 30 minutes.

Figure B.5: Technical bulletin of slacker page 1

Safety First!

The Material Safety Data Sheet (MSDS) for this or any Smooth-On product should be read prior to use and is available upon request from Smooth-On. All Smooth-On products are safe to use if directions are read and followed carefully.

Keep Out of Reach of Children

BE CAREFUL - Avoid contact with eyes. Silicone polymers are generally non-irritating to the eyes however a slight transient irritation is possible. Flush eyes with water for 15 minutes and seek medical attention. Remove from skin with waterless hand cleaner followed by soap and water. Children should not use this product without adult supervision.

IMPORTANT - The information contained in this bulletin is considered accurate. However, no warranty is expressed or implied regarding the accuracy of the data, the results to be obtained from the use thereof, or that any such use will not infringe upon a patent. User shall determine the suitability of the product for the intended application and assume all risk and liability whatsoever in connection therewith.

ADHERING APPLIANCE TO THE SKIN...

After the casting is fully cured, the mold release should be removed. Soap based release can be removed using warm water, Ease Release® 200 can be removed using isopropyl alcohol. Smooth-On's Skin Tite® adhesive can be used to temporarily adhere the piece to the skin. Theatrical makeup can be used to further blend and color the piece. If using Skin Tite® as an adhesive, remove the piece slowly after use. You can use baby oil or makeup remover to assist in removal.

We recommend that you do a small scale test on the back of your hand to ensure that you have no allergic reaction to silicone. If you notice any type of skin reaction, do not use product.

CURING & PERFORMANCE...

Curing - The cure time of the silicone will be lengthened when Slacker® is added. As platinum-cure silicones are heat sensitive, curing can be accelerated by applying heat. Do not cure rubber where temperature is less than 65°F /18°C.

Cure Inhibition - Platinum-cure silicone rubber may be inhibited by certain contaminants in or on the pattern to be molded (such as sulfur based clays, polyesters, certain wood surfaces, epoxies, urethane rubber and tin-cured silicone rubber) resulting in tackiness at the mold interface or a total lack of cure throughout the piece.

If compatibility between the rubber and the mold is a concern, a small-scale test is recommended. Apply a small amount of rubber onto a non-critical area of the mold. Inhibition has occurred if the rubber is uncured after the recommended cure time has passed.

Because no two applications are quite the same, a small test application to determine suitability for your project is recommended if performance of this material is in question

SMOOTH-ON

Call Us Anytime With Questions About Your Application.

Toll-free: **(800) 762-0744** Fax: **(610) 252-6200**

The new www.smooth-on.com is loaded with information about moldmaking, casting and more.

080310-JR

Figure B.5: Technical bulletin of slacker page 2

Bibliography

[1] Michael J Mack. Minimally invasive and robotic surgery. *Jama*, 285(5):568–572, 2001.

[2] Clinical Outcomes of Surgical Therapy Study Group. A comparison of laparoscopically assisted and open colectomy for colon cancer. *New England Journal of Medicine*, 350(20):2050–2059, 2004.

[3] Jim C Hu, Xiangmei Gu, Stuart R Lipsitz, Michael J Barry, Anthony V D'Amico, Aaron C Weinberg, and Nancy L Keating. Comparative effectiveness of minimally invasive vs open radical prostatectomy. *Jama*, 302(14):1557–1564, 2009.

[4] Colon Cancer Laparoscopic or Open Resection Study Group et al. Laparoscopic surgery versus open surgery for colon cancer: short-term outcomes of a randomised trial. *The lancet oncology*, 6(7):477–484, 2005.

[5] Christine Hartzell, Young-Tai Choi, Norman M Wereley, and Thomas JG Leps. Performance of a magnetorheological fluid-based robotic end effector. *Smart Materials and Structures*, 2019.

[6] MD Christie, Shuaishuai Sun, Lei Deng, DH Ning, Haiping Du, SW Zhang, and WH Li. A variable resonance magnetorheological-fluid-based pendulum tuned mass damper for seismic vibration suppression. *Mechanical Systems and Signal Processing*, 116:530–544, 2019.

[7] Amit Pandey, Pranay Singh Thakur, and Aakash Soni. Analysis of magnetorheological fluid brake system and its operation. 2018.

[8] Jie Wu, Hua Li, Xuezheng Jiang, and Jin Yao. Design, simulation and testing of a novel radial multi-pole multi-layer magnetorheological brake. *Smart Materials and Structures*, 27(2):025016, 2018.

[9] Javad Dargahi, Saeed Sokhanvar, Siamak Najarian, and Siamak Arbatani. *Tactile Sensing and Displays: Haptic Feedback for Minimally Invasive Surgery and Robotics*. John Wiley & Sons, 2012.

[10] Yu Zhen Dong, Yongsok Seo, and Hyoung Choi. Recent development of electro-responsive smart electrorheological fluids. *Soft matter*, 2019.

[11] Seung-Woo Cha, Seok-Rae Kang, Yong-Hoon Hwang, Jong-Seok Oh, and Seung-Bok Choi. A controllable tactile device for human-like tissue realization using smart magneto-rheological fluids: Fabrication and modeling. *Smart Materials and Structures*, 27(6):065015, 2018.

[12] Jong Seok Oh, Young Min Han, and Seung Bok Choi. Design and performance evaluation of mr tactile device for medical application. In *Applied Mechanics and Materials*, volume 433, pages 869–872. Trans Tech Publ, 2013.

[13] Jong-Seok Oh, Jin-Kyu Kim, and Seung-Bok Choi. Experimental test of mr fluid based tactile device for minimally invasive surgery. In *Active and Passive Smart Structures and Integrated Systems 2013*, volume 8688, page 86882C. International Society for Optics and Photonics, 2013.

[14] Alex Mazursky, Jeong-Hoi Koo, and Tae-Heon Yang. Design, modeling, and evaluation of a slim haptic actuator based on electrorheological fluid. *Journal of Intelligent Material Systems and Structures*, page 1045389X19836172, 2019.

[15] Jacob Mingear, Bing Zhang, Darren Hartl, and Alaa Elwany. Effect of process parameters and electropolishing on the surface roughness of interior channels in additively manufactured nickel titanium shape memory alloy actuators. *Additive Manufacturing*, 2019.

[16] Ernur Karadoğan. Probabilistic evaluation of the one-dimensional brinson model's sensitivity to uncertainty in input parameters. *Journal of Intelligent Material Systems and Structures*, 30(7):1070–1083, 2019.

[17] Pierre-Antoine Gédouin, Laurent Pino, Shabnam Arbab Chirani, Sylvain Calloch, Emmanuel Delaleau, and Jean-Matthieu Bourgeot. R-phase shape memory alloy helical spring based actuators: Modeling and experiments. *Sensors and Actuators A: Physical*, 289:65–76, 2019.

[18] Parris S Wellman, William J Peine, Gregg Favalora, and Robert D Howe. Mechanical design and control of a high-bandwidth shape memory alloy tactile display. In *Experimental robotics V*, pages 56–66. Springer, 1998.

[19] Fuminobu Kimura, Akio Yamamoto, and Toshiro Higuchi. Development of a 2-dof softness feeling display for tactile tele-presentation of deformable surfaces. In *Robotics and Automation (ICRA), 2010 IEEE International Conference on*, pages 1822–1827. IEEE, 2010.

[20] Kinya Fujita and Hisayuki Ohmori. A new softness display interface by dynamic fingertip contact area control. In *5th World Multiconference on Systemics, Cybernetics and Informatics*, pages 78–82, 2001.

[21] Martin Culjat, Chih-Hung King, Miguel Franco, James Bisley, Warren Grundfest, and Erik Dutson. Pneumatic balloon actuators for tactile feedback in robotic surgery. *Industrial Robot: An International Journal*, 35(5):449–455, 2008.

[22] Smita Kanjanapas, Cara M Nunez, Sophia R Williams, Allison M Okamura, and Ming Luo. Design and analysis of pneumatic 2-dof soft haptic devices for shear display. *IEEE Robotics and Automation Letters*, 4(2):1365–1371, 2019.

[23] Yoseph Bar-Cohen and Iain A Anderson. Electroactive polymer (eap) actuators—background review. *Mechanics of Soft Materials*, 1(1):5, 2019.

[24] Amy Kyungwon Han, Jung Hwa Bae, Katerina C Gregoriou, Christopher J Ploch, Roger E Goldman, Gary H Glover, Bruce L Daniel, and Mark R Cutkosky. Mr-compatible haptic display of membrane puncture in robot-assisted needle procedures. *IEEE transactions on haptics*, 11(3):443–454, 2018.

[25] Ashkan Dargahi, Ramin Sedaghati, and Subhash Rakheja. On the properties of magnetorheological elastomers in shear mode: Design, fabrication and characterization. *Composites Part B: Engineering*, 159:269–283, 2019.

[26] Xuan Bao Nguyen, Toshihiko Komatsuzaki, Yoshio Iwata, and Haruhiko Asanuma. Modeling and semi-active fuzzy control of magnetorheological elastomer-based isolator for seismic response reduction. *Mechanical Systems and Signal Processing*, 101:449–466, 2018.

[27] Y Hu, YL Wang, XL Gong, XQ Gong, XZ Zhang, WQ Jiang, PQ Zhang, and ZY Chen. New magnetorheological elastomers based on polyurethane/si-rubber hybrid. *Polymer testing*, 24(3):324–329, 2005.

[28] Hua-xia Deng, Xing-long Gong, and Lian-hua Wang. Development of an adaptive tuned vibration absorber with magnetorheological elastomer. *Smart materials and structures*, 15(5):N111, 2006.

[29] Ngoc Thien Lai, Hanafi Ismail, Mohd Khalil Abdullah, and Raa Khimi Shuib. Optimization of pre-structuring parameters in fabrication of magnetorheological elastomer. *Archives of Civil and Mechanical Engineering*, 19(2):557–568, 2019.

[30] Kyriaki Sapouna, YP Xiong, and RA Shenoi. Dynamic mechanical properties of isotropic/anisotropic silicon magnetorheological elastomer composites. *Smart Materials and Structures*, 26(11):115010, 2017.

[31] Lin Chen, Xing-long Gong, Wan-quan Jiang, Jing-jing Yao, Hua-xia Deng, and Wei-hua Li. Investigation on magnetorheological elastomers based on natural rubber. *Journal of Materials Science*, 42(14):5483–5489, 2007.

[32] Ioan Bica, Eugen M Anitas, Madalin Bunoiu, Boris Vatzulik, and Iulius Juganaru. Hybrid magnetorheological elastomer: influence of magnetic field and compression pressure on its electrical conductivity. *Journal of Industrial and Engineering Chemistry*, 20(6):3994–3999, 2014.

[33] Anna Boczkowska, Stefan F Awietjan, and Rafal Wroblewski. Microstructure–property relationships of urethane magnetorheological elastomers. *Smart Materials and Structures*, 16(5):1924, 2007.

[34] Holger Böse, Raman Rabindranath, and Johannes Ehrlich. Soft magnetorheological elastomers as new actuators for valves. *Journal of Intelligent Material Systems and Structures*, 23(9):989–994, 2012.

[35] Guoliang Hu, Miao Guo, Weihua Li, Haiping Du, and Gursel Alici. Experimental investigation of the vibration characteristics of a magnetorheological elastomer sandwich beam under

non-homogeneous small magnetic fields. *Smart materials and structures*, 20(12):127001, 2011.

[36] Mahmood Norouzi, Seyed Masoud Sajjadi Alehashem, Hossein Vatandoost, Yi Qing Ni, and Mohammad Mohsen Shahmardan. A new approach for modeling of magnetorheological elastomers. *Journal of Intelligent Material Systems and Structures*, 27(8):1121–1135, 2016.

[37] Xincheng Song, Wenju Wang, Fufeng Yang, Guoping Wang, and Xiaoting Rui. Study on dynamic mechanical properties of magnetorheological elastomers based on natural rubber/thermoplastic elastomer hybrid matrix. *Materials Research Express*, 5(11):115705, 2018.

[38] Zhirong Yang, Chunyun Qin, Zhushi Rao, Na Ta, and Xinglong Gong. Design and analyses of axial semi-active dynamic vibration absorbers based on magnetorheological elastomers. *Journal of Intelligent Material Systems and Structures*, 25(17):2199–2207, 2014.

[39] CY Yang, J Fu, M Yu, X Zheng, and BX Ju. A new magnetorheological elastomer isolator in shear–compression mixed mode. *Journal of Intelligent Material Systems and Structures*, 26(10):1290–1300, 2015.

[40] John M Ginder, Mark E Nichols, Larry D Elie, and Seamus M Clark. Controllable-stiffness components based on magnetorheological elastomers. In *Smart structures and materials 2000: smart structures and integrated systems*, volume 3985, pages 418–426. International Society for Optics and Photonics, 2000.

[41] A Albanese Lerner and KA Cunefare. Performance of mre-based vibration absorbers. *Journal of Intelligent Material Systems and Structures*, 19(5):551–563, 2008.

[42] SS Sun, Ying Chen, Jian Yang, TF Tian, HX Deng, WH Li, Haiping Du, and Gursel Alici. The development of an adaptive tuned magnetorheological elastomer absorber working in squeeze mode. *Smart Materials and Structures*, 23(7):075009, 2014.

[43] Weihua Li and Xianzhou Zhang. Research and applications of mr elastomers. *Recent Patents on Mechanical Engineering*, 1(3):161–166, 2008.

[44] WH Li, XZ Zhang, and H Du. Magnetorheological elastomers and their applications. In *Advances in Elastomers I*, pages 357–374. Springer, 2013.

[45] Mattias Lokander and Bengt Stenberg. Performance of isotropic magnetorheological rubber materials. *Polymer Testing*, 22(3):245–251, 2003.

[46] LC Davis. Model of magnetorheological elastomers. *Journal of Applied Physics*, 85(6):3348–3351, 1999.

[47] Marke Kallio. *The elastic and damping properties of magnetorheological elastomers*. VTT, 2005.

[48] J David Carlson and Mark R Jolly. Mr fluid, foam and elastomer devices. *mechatronics*, 10(4-5):555–569, 2000.

[49] Lin Chen, XL Gong, and WH Li. Effect of carbon black on the mechanical performances of magnetorheological elastomers. *Polymer Testing*, 27(3):340–345, 2008.

[50] Hossein Vatandoost, Mahmood Norouzi, Seyed Masoud Sajjadi Alehashem, and Stoyan K Smoukov. A novel phenomenological model for dynamic behavior of magnetorheological elastomers in tension–compression mode. *Smart Materials and Structures*, 26(6):065011, 2017.

[51] Yancheng Li, Jianchun Li, Weihua Li, and Haiping Du. A state-of-the-art review on magnetorheological elastomer devices. *Smart materials and structures*, 23(12):123001, 2014.

[52] Jian Yang, Haiping Du, Weihua Li, Yancheng Li, Jianchun Li, Shuaishuai Sun, and HX Deng. Experimental study and modeling of a novel magnetorheological elastomer isolator. *Smart Materials and Structures*, 22(11):117001, 2013.

[53] Faramarz Gordaninejad, Xiaojie Wang, and Praveen Mysore. Behavior of thick magnetorheological elastomers. *Journal of Intelligent Material Systems and Structures*, 23(9):1033–1039, 2012.

[54] Anna Boczkowska and Stefan F Awietjan. Smart composites of urethane elastomers with carbonyl iron. *Journal of Materials Science*, 44(15):4104–4111, 2009.

[55] Mohamed Tourab and Salah Aguib. Experimental analysis of the thermal effect of the magneto-mechanical behavior of viscoelastic elastomer. *Journal of Advanced Research in Fluid Mechanics and Thermal Sciences*, 53(1):25–34, 2019.

[56] Maryam Mahdiani, Faezeh Soofivand, Fatemeh Ansari, and Masoud Salavati-Niasari. Grafting of cufe12o19 nanoparticles on cnt and graphene: eco-friendly synthesis, characterization and photocatalytic activity. *Journal of cleaner production*, 176:1185–1197, 2018.

[57] Fatemeh Ansari, Azam Sobhani, and Masoud Salavati-Niasari. Simple sol-gel synthesis and characterization of new cotio3/cofe2o4 nanocomposite by using liquid glucose, maltose and starch as fuel, capping and reducing agents. *Journal of colloid and interface science*, 514:723–732, 2018.

[58] Bhaktha Sandesh, Hegde Sriharsha, U Rao Sathish, and Gandhi Nikhil. Investigation of tensile properties of rtv silicone based isotropic magnetorheological elastomers. In *MATEC Web of Conferences*, volume 144, page 02015. EDP Sciences, 2018.

[59] Jin Yong Lee, Vineet Kumar, and Dong-Joo Lee. Compressive properties of magnetorheological elastomer with different magnetic fields and types of filler. *Polymers for Advanced Technologies*, 30(4):1106–1115, 2019.

[60] Vineet Kumar and Dong-Joo Lee. Mechanical properties and magnetic effect of new magneto-rheological elastomers filled with multi-wall carbon nanotubes and iron particles. *Journal of Magnetism and Magnetic Materials*, 2019.

[61] Yangguang Xu, Xinglong Gong, Shouhu Xuan, Xiaofeng Li, Lijun Qin, and Wanquan Jiang. Creep and recovery behaviors of magnetorheological plastomer and its magnetic-dependent properties. *Soft Matter*, 8(32):8483–8492, 2012.

[62] Song Qi, Miao Yu, Jie Fu, and Mi Zhu. Stress relaxation behavior of magnetorheological elastomer: Experimental and modeling study. *Journal of Intelligent Material Systems and Structures*, 29(2):205–213, 2018.

[63] International Organization for Standardization. *ISO 7743: Rubber, vulcanized or thermoplastic – Determination of compression stress-strain properties*, 10 2017. Edition 5.

[64] HM Yin, LZ Sun, and JS Chen. Micromechanics-based hyperelastic constitutive modeling of magnetostrictive particle-filled elastomers. *Mechanics of materials*, 34(8):505–516, 2002.

[65] WH Li, Yang Zhou, and TF Tian. Viscoelastic properties of mr elastomers under harmonic loading. *Rheologica acta*, 49(7):733–740, 2010.

[66] A Hooshiar, S Najarian, and J Dargahi. Haptic telerobotic cardiovascular intervention: a review of approaches, methods, and future perspectives. *IEEE reviews in biomedical engineering*, 2019.

[67] Hiroshi Yanatori, Kazuki Tsuji, Konomu Abe, Kenji Iwasaki, and Takashi Mineta. Fabrication and characterization of an arrayed shape memory alloy thick film actuator device for planar tactile displays. *IEEJ Transactions on Sensors and Micromachines*, 139(1):15–20, 2019.

[68] H Böse and R Röder. Magnetorheological elastomers with high variability of their mechanical properties. In *Journal of physics: Conference series*, volume 149, page 012090. IOP Publishing, 2009.

[69] Ashkan Dargahi, Subhash Rakheja, and Ramin Sedaghati. Development of a field dependent prandtl-ishlinskii model for magnetorheological elastomers. *Materials & Design*, 166:107608, 2019.

[70] D Meeker. Finite element method magnetics: User's manual, 4th ver, 2004.

[71] Jeong-Hoi Koo, Fazeel Khan, Dong-Doo Jang, and Hyung-Jo Jung. Dynamic characterization and modeling of magneto-rheological elastomers under compressive loadings. *Smart Materials and Structures*, 19(11):117002, 2010.

[72] Majid Behrooz, Xiaojie Wang, and Faramarz Gordaninejad. Performance of a new magnetorheological elastomer isolation system. *Smart Materials and Structures*, 23(4):045014, 2014.

[73] Hossein Darijani and Reza Naghdabadi. Hyperelastic materials behavior modeling using consistent strain energy density functions. *Acta mechanica*, 213(3-4):235–254, 2010.

[74] Mark Alger. *Polymer science dictionary*. Springer Science & Business Media, 1996.

[75] D Steck, J Qu, SB Kordmahale, D Tscharnuter, A Muliana, and J Kameoka. Mechanical responses of ecoflex silicone rubber: Compressible and incompressible behaviors. *Journal of Applied Polymer Science*, 136(5):47025, 2019.

[76] Ahmad Atieh. *Design, Modeling, Fabrication and Testing of a Piezoresistive-Based Tactile Sensor for Minimally Invasive Surgery Applications*. PhD thesis, Concordia University, 2012.

[77] Yi Han, Wei Hong, and LeAnn E Faidley. Field-stiffening effect of magneto-rheological elastomers. *International Journal of Solids and Structures*, 50(14-15):2281–2288, 2013.

[78] Thomas A Krouskop, Thomas M Wheeler, Faouzi Kallel, Brian S Garra, and Timothy Hall. Elastic moduli of breast and prostate tissues under compression. *Ultrasonic imaging*, 20(4):260–274, 1998.

[79] Parris Wellman, Robert D Howe, Edward Dalton, and Kenneth A Kern. Breast tissue stiffness in compression is correlated to histological diagnosis. *Harvard BioRobotics Laboratory Technical Report*, pages 1–15, 1999.

[80] Pierre G Agache, C Monneur, Jean Luc Leveque, and Jean De Rigal. Mechanical properties and young's modulus of human skin in vivo. *Archives of dermatological research*, 269(3):221–232, 1980.

[81] AO Barel, W Courage, and P Clarys. Suction chamber method for measurement of skin mechanics: the new digital version of the cutometer. *Handbook of Noninvasive Methods and the Skin*, pages 583–591, 2006.

[82] A Champa Jayasuriya, Snehasish Ghosh, Jerry I Scheinbeim, Virginia Lubkin, Greg Bennett, and Phillip Kramer. A study of piezoelectric and mechanical anisotropies of the human cornea. *Biosensors and Bioelectronics*, 18(4):381–387, 2003.

[83] William Hiesinger, Matthew J Brukman, Ryan C McCormick, J Raymond Fitzpatrick III, John R Frederick, Elaine C Yang, Jeffrey R Muenzer, Nicole A Marotta, Mark F Berry, Pavan Atluri, et al. Myocardial tissue elastic properties determined by atomic force microscopy after stromal cell–derived factor 1α angiogenic therapy for acute myocardial infarction in a murine model. *The Journal of thoracic and cardiovascular surgery*, 143(4):962–966, 2012.

[84] M Asun Cantera, Majid Behrooz, Ronald F Gibson, and Faramarz Gordaninejad. Modeling of magneto-mechanical response of magnetorheological elastomers (mre) and mre-based systems: a review. *Smart Materials and Structures*, 26(2):023001, 2017.

[85] Seung-Hyun Eem, Jeong-Hoi Koo, and Hyung-Jo Jung. Feasibility study of an adaptive mount system based on magnetorheological elastomer using real-time hybrid simulation. *Journal of Intelligent Material Systems and Structures*, 30(5):701–707, 2019.

[86] Elise Corbin, Alexia Vite, Eliot G Peyster, Myan Bhoopalam, Jeffrey Brandimarto, Xiao Wang, Alexander I Bennett, Andy T Clark, Xuemei Cheng, Kevin T Turner, et al. Tunable and reversible substrate stiffness reveals dynamic mechanosensitivity of cardiomyocytes. *ACS applied materials & interfaces*, 2019.

[87] Siamak Arbatani. *Identification of Mechanical Properties of Nonlinear Materials and Development of Tactile Displays for Robotic Assisted Surgery Applications*. PhD thesis, Concordia University, 2016.

[88] Majid Behrooz, Xiaojie Wang, and Faramarz Gordaninejad. Modeling of a new semi-active/passive magnetorheological elastomer isolator. *Smart Materials and Structures*, 23(4):045013, 2014.

[89] Evan Galipeau and Pedro Ponte Castañeda. The effect of particle shape and distribution on the macroscopic behavior of magnetoelastic composites. *International Journal of Solids and Structures*, 49(1):1–17, 2012.

[90] Evan Galipeau and Pedro Ponte Castañeda. A finite-strain constitutive model for magnetorheological elastomers: magnetic torques and fiber rotations. *Journal of the Mechanics and Physics of Solids*, 61(4):1065–1090, 2013.

[91] A Javili, Georges Chatzigeorgiou, and P Steinmann. Computational homogenization in magneto-mechanics. *International Journal of Solids and Structures*, 50(25-26):4197–4216, 2013.

[92] Karl A Kalina, Philipp Metsch, and Markus Kästner. Microscale modeling and simulation of magnetorheological elastomers at finite strains: a study on the influence of mechanical preloads. *International Journal of Solids and Structures*, 102:286–296, 2016.

[93] KA Kalina, J Brummund, P Metsch, M Kästner, D Yu Borin, JM Linke, and S Odenbach. Modeling of magnetic hystereses in soft mres filled with ndfeb particles. *Smart Materials and Structures*, 26(10):105019, 2017.

[94] Philipp Metsch, Karl A Kalina, Christian Spieler, and Markus Kästner. A numerical study on magnetostrictive phenomena in magnetorheological elastomers. *Computational Materials Science*, 124:364–374, 2016.

[95] SV Kankanala and N Triantafyllidis. On finitely strained magnetorheological elastomers. *Journal of the Mechanics and Physics of Solids*, 52(12):2869–2908, 2004.

[96] A Dorfmann and RW Ogden. Nonlinear magnetoelastic deformations of elastomers. *Acta Mechanica*, 167(1-2):13–28, 2004.

[97] Roger Bustamante. Transversely isotropic nonlinear magneto-active elastomers. *Acta mechanica*, 210(3-4):183–214, 2010.

[98] P Metsch, KA Kalina, J Brummund, and M Kästner. Two-and three-dimensional modeling approaches in magneto-mechanics: a quantitative comparison. *Archive of Applied Mechanics*, 89(1):47–62, 2019.

[99] Nomesh Kumar and V Venkateswara Rao. Hyperelastic mooney-rivlin model: determination and physical interpretation of material constants. *Parameters*, 2(10):01, 2016.

[100] BJ Briscoe, L Fiori, and E Pelillo. Nano-indentation of polymeric surfaces. *Journal of Physics D: Applied Physics*, 31(19):2395, 1998.

[101] Norio Iwashita, Michael V Swain, John S Field, Naoto Ohta, and Shingo Bitoh. Elasto-plastic deformation of glass-like carbons heat-treated at different temperatures. *Carbon*, 39(10):1525–1532, 2001.

[102] Gilles Hochstetter, Armel Jimenez, Jean-Paul Cano, and Eric Felder. An attempt to determine the true stress-strain curves of amorphous polymers by nanoindentation. *Tribology International*, 36(12):973–985, 2003.

[103] David C Lin, David I Shreiber, Emilios K Dimitriadis, and Ferenc Horkay. Spherical indentation of soft matter beyond the hertzian regime: numerical and experimental validation of hyperelastic models. *Biomechanics and modeling in mechanobiology*, 8(5):345, 2009.

[104] Ali Alkhalaf, Amir Hooshiar, and Javad Dargahi. Enhancement of mr-effect in magnetorheological elastomers through bi-layer composition: Theory and validation. In *Proceeding of*

30th International Conference on Adaptive Structures and Technologies, volume 1, pages 1–2. Concordia University, 2019.

[105] Janet M Blackstone. Children and gender-differences in exposure and how anthropometric differences can be incorporated into the design of computer input devices. *Scandinavian Journal of Work, Environment & Health*, page 26, 2007.

[106] Naghmeh M Bandari, Roozbeh Ahmadi, Amir Hooshiar, Javad Dargahi, and Muthukumaran Packirisamy. Hybrid piezoresistive-optical tactile sensor for simultaneous measurement of tissue stiffness and detection of tissue discontinuity in robot-assisted minimally invasive surgery. *Journal of biomedical optics*, 22(7):077002, 2017.

[107] Amin TermehYousefi, Saman Azhari, Amin Khajeh, Mohd Nizar Hamidon, and Hirofumi Tanaka. Development of haptic based piezoresistive artificial fingertip: Toward efficient tactile sensing systems for humanoids. *Materials Science and Engineering: C*, 77:1098–1103, 2017.

[108] Guo-Hua Feng and Wei-Lun Huang. A self-strain feedback tuning-fork-shaped ionic polymer metal composite clamping actuator with soft matter elasticity-detecting capability for biomedical applications. *Materials Science and Engineering: C*, 45:241–249, 2014.

[109] Amir Hooshiar, Masoud Razban, Naghmeh M Bandari, and Javad Dargahi. Sensing principle for real-time characterization of viscoelasticity in the beating myocardial tissue. In *2017 IEEE International Conference on Computational Intelligence and Virtual Environments for Measurement Systems and Applications (CIVEMSA)*, pages 72–77. IEEE, 2017.

[110] M Darcy Driscoll, JM Arnold, and Marvin H Sherebrin. Applied recording force and noninvasive arterial pulses. *Clinical and investigative medicine. Medecine clinique et experimentale*, 18(5):370–379, 1995.

[111] Xiao-Fei Teng and Yuan-Ting Zhang. Theoretical study on the effect of sensor contact force on pulse transit time. *IEEE Transactions on Biomedical Engineering*, 54(8):1490–1498, 2007.

[112] Xin Xie. *High performance micro actuators for tactile displays*. PhD thesis, Northeastern University, 2017.

[113] Jae S Son and RD Nowe. Tactile sensing and stiffness control with multifingered hands. In *Proceedings of IEEE International Conference on Robotics and Automation*, volume 4, pages 3228–3233. IEEE, 1996.